PREPARATION OF NANOFIBERS OF TiO$_2$-LOADED POLYLACTIDE BASED BLENDS FOR USE IN ENVIRONMENTAL AND AGRICULTURAL APPLICATIONS

BY

BUNTHOEUN NIM

A THESIS SUBMITTED IN PARTIAL FULFILLMENT OF THE
REQUIREMENTS FOR THE DEGREE OF
MASTER OF ENGINEERING
SIRINDHORN INTERNATIONAL INSTITUTE OF TECHNOLOGY
THAMMASAT UNIVERSITY
ACADEMIC YEAR 2016

PREPARATION OF NANOFIBERS OF TiO$_2$-LOADED POLYLACTIDE BASED BLENDS FOR USE IN ENVIRONMENTAL AND AGRICULTURAL APPLICATIONS

BY

BUNTHOEUN NIM

A THESIS SUBMITTED IN PARTIAL FULFILLMENT OF THE

REQUIREMENTS FOR THE DEGREE OF

MASTER OF ENGINEERING

SIRINDHORN INTERNATIONAL INSTITUTE OF TECHNOLOGY

THAMMASAT UNIVERSITY

ACADEMIC YEAR 2016

PREPARATION OF NANOFIBERS OF TiO$_2$-LOADED POLYLACTIDE BASED BLENDS FOR USE IN ENVIRONMENTAL AND AGRICULTURAL APPLICATIONS

A Thesis Presented

By

BUNTHOEUN NIM

Submitted to

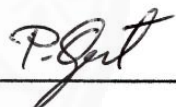Sirindhorn International Institute of Technology

Thammasat University

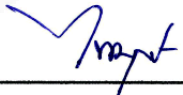In partial fulfillment of the requirements for the degree of

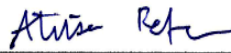MASTER OF ENGINEERING

Approved as to style and content by

Advisor and Chairperson of Thesis Committee _____

(Assoc. Prof. Dr. Pakorn Opaprakasit)

Committee Member and
Chairperson of Examination Committee _____

(Asst. Prof. Dr. Paiboon Sreearunothai)

Committee Member _____

(Dr. Atitsa Petchsuk)

December 2016

Abstract

PREPARATION OF NANOFIBERS OF TiO$_2$-LOADED POLYLACTIDE BASED BLENDS FOR USE IN ENVIRONMENTAL AND AGRICULTURAL APPLICATIONS

by

BUNTHOEUN NIM

Bachelor of Science, Royal University of Phnom Penh, Cambodia, 2014

Master of Engineering (Chemical Engineering), Sirindhorn International Institute of Technology, 2016

Biopolymers composited with nanoparticles are very interesting materials for packaging applications due to their physical, thermal, mechanical and biodegradable properties. This study aims to improve special performance of biopolymers composited with TiO$_2$, which contribute to environmental and agricultural applications, especially as biopolymer plastic packaging.

Nanofibers of polylactide (PLA)/poly(vinylpyrrolidone) (PVP) blends loaded with TiO$_2$ particles have been prepared by an electrospinning technique. TiO$_2$ particles are formed by sol-gel mechanisms from titanium (IV) isopropoxide (TTIP) precursor. Effect of TiO$_2$ formation rate on properties of the fibers are examined by adding isopropyl alcohol (IPPA) to slow down the TiO$_2$ precipitation process. The use of IPPA produces fiber mats consisting of slightly bigger and smoother filaments, but smaller-sized embedded TiO$_2$ particles. Both materials show a distinct UV absorption characteristic of TiO$_2$ at λ_{max} 300 nm, which can be applied in many catalytic applications.

Nanofibers of polylactide (PLA)/poly(vinlylpyrrolidone) (PVP) blends loaded with TiO$_2$ nanoparticles have been prepared by an electrospinning method. The electrospun fiber mats were characterized by ATR-FTIR, X-ray diffraction (XRD), SEM, EDX, and UV-Visible spectroscopy to examine structures, functional groups, crystallinity, surface morphology, and UV absorptivity. It is clearly observed that

TiO$_2$ particles are embedded on the filaments. All PLA-based spun fibers are completely amorphous in nature, in which surface morphology of those blended with PVP are smoother and more uniform than the corresponding samples without PVP. Neat PLA fibers shows a UV absorption band at around 200 nm, whereas the fibers loaded with TiO$_2$nanoparticles show an additional absorption band covering the 200-380 nm region. Photo-degradation of the fiber samples are conducted in phosphate buffer solution (PBS) under UVA light. The results indicate that the PVP component is dissolved into PBS solution, and the PLA matrix is degraded as a function of time. The fibers are then applied as a catalytic system for epoxidation of unsaturated sunflower oil (SFO) for use as additives or plasticizers for biopolymers, employing a performic acid oxidizing agent. The fibers, especially those containing PVP, can effectively enhance the epoxidation yield of oils with a slow rate of undesirable side reactions, which break ester bonds of the triglyceride to generate free fatty acids.

Keywords: Polylactide, Poly(vinylpyrrolidone), Titanium dioxide, Electrospinning, Degradation, Epoxidation Catalyst.

Acknowledgements

Table of Contents

List of Tables

List of Figures

ix

List of Equations

Chapter 1

Introduction

1.1 Background

In recent years, waste pollutants have increased very unpredictable, which caused serious problems to the environment and affected to human health. Water, air, and soil have been polluted by waste from agriculture pesticides and fertilizers, industrial, mining, and household. Serious pollutants include toxic organic substances and inorganic compounds. Organic toxicity covers on chlorinated and nonchlorinated aliphatic, aromatic substances, dyes, detergents, pesticides, insecticides, herbicides, disinfection byproducts, pathogens, fungi, and viruses. Inorganic pollutants contain heavy metals, toxic gases, such as NO_x, SO_x, CO and NH_3. All of these pollutants need to degrade before they are ended-up into the atmosphere and water resource[1].

Many researchers have focused on how to deal with these problems. Discoveries of semiconductor photocatalysis have become one of the effective solutions and successful for environmental decontamination[2]. Several reports have illustrated the ways of catalytic degrade and remove organic and inorganic pollutants in the environmental clean-up. Among these useful photocatalyst, TiO_2 is one of the most attractive that has been applied for environmental remediation today [3, 4]. TiO_2 is used as catalyst for photodegradation of organic contamination in wastewater treatment, drinking water disinfection, and air purification [4, 5]. TiO_2 is a photocatalyst that has high efficiency of photoreaction, inexpensive, non-toxic, stability, high resistant to acid-alkali, and organic solutions [6, 7].

Biopolymers have attracted vast attention, due to their excellent characteristics, such as biodegradable and biocompatibility. These polymers can be degraded by oxidation processes, photodegradation, enzymatic activity, microorganisms, or other living organisms[8]. Biopolymers can be called bio-plastics, as these are synthesized from renewable sources[9]. Some examples of biopolymers which are widely investigated and used are poly(lactic acid) (PLA), poly(glycolic acid) (PLGA), poly(vinyl alcohol) (PVA), polycaprolactone (PCL), silk, gelatin, and chitosan.

1

Composite biopolymer-photocatalyst materials have become an interesting area today[10]. PLA is one of the most promising materials for commercial polymeric products in various applications, e.g. packaging, agriculture, electronic devices, automobiles, textiles, tissue engineering, wound dressing, drug delivery, and anti-microbial materials. PLA is synthesized from abandoned agricultural renewable resources, such as cassava, rice, and corn. These raw materials are major sources of lactic acid, through fermentation using bacteria or fungi [11, 12]. Furthermore, the material is a degradable plastic that possesses many good properties, such as good mechanical properties, thermal plasticity, fabric ability, water resistance, good transparency[13], biocompatibility[14], and degradability [15, 16]. Additionally, combination of TiO_2 with biodegradable polymers of PLA is promising in modern nanotechnology and applications.

1.2 Statement of Problem

Plastics become more important applications in many fields, especially in food packagings and agriculture. However, plastic waste has become one of serious problems to the environment. Plastics usually have low degradability or non-degradability that makes them stay long period in the environment and become risks to the ecosystem. Biopolymers have become more important to replace non-degradable plastics, due to their excellent properties, i.e, biodegradability, biocompatibility, low cost, and synthesis from renewable resources. Significantly, polylactide (PLA), one of biopolymers, becomes more interesting in research and commercial use. TiO_2 is a photocatalyst with high efficiency to degrade organic pollutants. TiO_2 composited with PLA is promising research topic for properties improvement of biopolymers for various applications. In this study, (PLA)/poly (vinylpyrrolidone) (PVP)/ TiO_2 composite will be prepared by an electrospinning method. The efficiency of the PLA/PVP/TiO_2 fibers is examined for self-degradation and sunflower oil (SFO) epoxidation.

1.3 Objectives of the Study

The main objective of this thesis is to prepare PLA/PVP/TiO$_2$ nanofibers via an electrospinning method and use the material as catalyst for photodegradation of organic pollutants in the environmental, agricultural applications, and epoxidation of unsaturated oils. The detailed objectives of this study are:

- Develop electrospinning process to fabricate PLA/PVP/TiO$_2$ nanofibers.
- Study on the self degradation mechanisms of the composite fibers in buffer condition and under UVA light.
- Applying PLA/PVP/TiO$_2$ nanofibers as a catalyst to epoxidize sunflower oils.
- Propose mechanisms of the epoxidation reactions of unsaturated oils based on FTIR-ATR results.

1.4 Significance of Study

This study is aimed to develop polymeric nanofibers from biopolymers composited with TiO$_2$ and contribute to environmental and agricultural applications, especially biopolymeric packagings and epoxidizing catalyst. The resulting PLA/PVP/TiO$_2$ has higher biodegradability property than non-degradable plastics. In addition, using biopolymers can help reducing non-degradable plastics applications and will decrease plastics waste to the environment. Moreover, TiO$_2$ photocatalyst composite with PLA/PVP can be used as catalysts to degrade organic pollutants, specifically photodegradation hazardous organic compounds in wastewaters, drinking water, and air purification. In agricultural applications, PLA/PVP/TiO$_2$ can be applied as food packaging material. The PLA/TiO$_2$ composites can protect food products from bacteria activities, or toxic gases. In fruits packaging applications, this biopolymer material have potential to absorb and convert acetylene gaseous that make fruits ripen. Furthermore, TiO$_2$ composited with PLA is easier to recycle or degrade faster in environmental conditions by enzymatic activities. In addition, PLA/PVP/TiO$_2$ will be applied as catalyst to epoxidize sunflower oils, which can then be used as plasticizer for bioplastics.

1.5 Thesis Structure

3

This research consists of four chapters, starting with background information on several sources and types of serious pollutants. TiO_2 nanoparticals is applied for environmental clean-up. Biodegradable polymers are promising to replace petroleum-based plastics to reduce the amount of non-degradable waste. PLA/TiO_2 nanocomposites fibers and films have been used in wide variety applications.

Chapter 2 focuses on applications of lactic acid and synthesizes methods. This acid is used as raw material for polylactide. This section also clarifies the polymerization techniques, i.e. direct polycondensation and ring-opening polymerization. Additionally, TiO_2 photocatalyst is reported in many applications, such as water treatments, air purifications, antimicrobial activities, and anti-cancer cells. In addition, TiO_2 is used to degrade most of organic pollutants contaminated in the environment. To expand its applications, TiO_2 composite with biopolymers have been developed by many researchers using alternative techniques. Particularly, PLA/TiO_2 nancomposite fibers and films were investigated to further increasing their applications.

Chapter 3 focuses on the methodology of PLA/ PVP/TiO_2 nanocomposite fibers and films preparation. TiO_2 composited with PLA/PVP nanofibers is prepared by using an electrospinning technique. This has been conducted by several researchers to fabricate the nanofiber. To improve the PLA fiber properties, PVP and TiO_2 nanoparticles are added by dissolving in a mixture of two solvents, chloroform and N,N-Dimethyformamide (DMF). Then, the nanofiber characteristic properties are examined by various techniques, i.e. FTIR-ATR measured the spectrum of the components. Scanning electron microscope (SEM) is used to measure the surface morphology of the particles. Energy-dispersive X-ray (EDX) microanalysis is applied to examine the weight percentages. X-ray diffraction (XRD) analysis is used to observe the presence of the crystalline of materials. UV-Vis spectroscopy is applied for absorption behaviors of materials. Photo-degradation of the $PLA/PVP/TiO_2$ nanofibers in phosphate buffer solution pH 7.4 under UVA light irradiation is examined. To investigate the efficiency of these catalysts, $PLA/PVP/TiO_2$ fibers are used in epoxidation of sunflower oils. The products can then be used as plasticizers for many bioplastics.

4

Finally, chapter 4 and 5 covers the results, discussions, and conclusions of these experiments. Following this technique, fine fibers are obtained and have the absorption behavior at UV regions. These fibers show high performance as catalysts for epoxidation of sunflower oils.

Chapter 2
Literature review

2.1 Background on Polylactide

Lactic acid was first found and isolated from sour milk in 1780 by Carl Wilhelm Scheele. After a decade of this discovery, Lavoisier named this milk component as "*acid lactique*" in 1789, which opened the terminology of lactic acid for recent. Until 1857, Pasteur convinced that lactic acid was not a milk component. Pasteur proposed that lactic acid was generated from fermentation metabolite by certain microorganisms. In 1881, Fr´emy, French scientist, used fermentation processes by using microbial to produce lactic acid and become the foundation of industrial production in the United States. Therefore, carbohydrates fermentation by bacteria activities have contributed to the commercial of lactic acid [17]. Since 1990, the annual global lactic acid production has accounted around 40,000 tons and supplied by two manufacturers, CCA Biochem and Sterling Chemicals. CCA Biochem locates in The Netherlands and has subsidiary in Brazil and Spain. Sterling Chemicals locates in Texas City, TX, USA. Archer Daniels Midland (ADM) was a new lactic acid manufacturer and established in early 1990. In 1997, Cargill and Dow Chemical joined forces together and established the Cargill-Dow and supplied polylactic acid polymer. In 2005, NaturalWorks is a well-known subsidiary of Cargill to supply polylactic acid [18].

Around 130,000 to 150,000 tons per year of lactic acid was consumed in 2007 with the commercial prices of food-grade lactic acid between 1.38 US\$kg^{-1} (for 50% purity) and 1.54 US\$kg^{-1} (for 88% purity)[19]. The Global and China Lactic Acid and Derivative Industry Report, 2014-2016 reported that the demanding of lactic acid has been increased rapidly since 2008, and its consumption has reached 800,000 tons in 2013. Among this amount, the United States demanded 31% that is the largest user in 2013. Western Europe is the second largest demanding of lactic acid for consumption in food and beverage industry. The top 3 manufacturers of lactic acid in 2013 were PURAC, Cargill, and Henan Jindan Lactic acid Technology contributed the total capacity of 505,000 tons. In 2013, NaturalWorks was a largest polylactic acid supplier

6

and had an annual capacity of 150,000 tons. Currently, several manufacturers have been established such as Galactic, CCA Biochem, PURAC, Henan Jindan Lactic acid Technology, Musashino Chemical Co. Ltd, NaturalWorks LLC (USA), and other Chinese companies.

Lactic acid has become more popular beneficial in wide range of applications, such as food and beverage, textile, cosmetic, pharmaceutical, biodegradable polymer, and chemical industry[20]. Lactic acid is synthesized from two different techniques such as carbohydrate fermentation (like starch and sugar) or chemical synthesis. Firstly, fermentation of carbohydrates generated the source of lactic acid. Lactic acid or 2-hydroxy propionic acid has an asymmetric carbon's atom with the L (+) and D (-) configurations, as shown in Figure 2.1 . Then lactic acid can be polymerized to form PLA. Lactic acid is possible synthesized from farm and agricultural products like cassava, rice, corn, corncob, vegetable oil that contain the source of lactic acid fermented by bacteria strains, fungi or enzymes[12, 21]. Several types of bacteria and fungi have been developed from biotechnology to produce pure D/or L-lactic acid. For instances, *E. coli*, *G. stearothermophilus*, *R. oryzae* and *R. arrhizus*, *Lactobacillus amylophilus*, *Bacillus coagulans* was fermented on different sources of raw material to produce D/or L-lactic acid, as illustrated in Table 2.1.
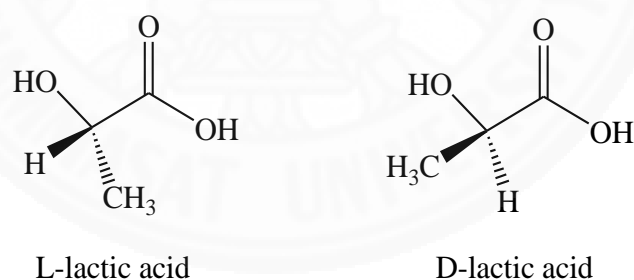
Figure 2.1**:** Lactic acid configurations, L-lactic acid and D-lactic acid.

Table 2.1: Raw materials and microorganisms used for lactic acid production.

Raw material	Bacteria or fungi	Lactic acid yield	Ref
Potato starch	*Rhizopus oryzae* & *Rhizopus arrhizus*	0.85–0.92 g/g substrate	[22]
Wheat bran	*Lactobacillus amylophilus*	18 to 36 g/100g substrate	[23]

7

Cassava bagasse	*Lactobacillus casei*	0.97 g/g substrate	[24]
Rice bran	*Lactobacillus delbrueckii*	100 kg/m^3 rice bran produced 28 kg/m^3 lactic acid	[25]
cassava starch	*Lactobacillus delbrueckii*	0.75–0.95 g/g substrate with productivity 0.48 g l^{-1} h^{-1}	[26]
wheat straw	*Bacillus coagulans*	lime-treated straw (2,706 g) produced lactic acid (711 g)	[27]
Unpolished rice	*Lactobacillus delbrueckii*	731.50 g/kg substrate with production rate of 1.50 g/(l h)	[28]
Corncob	*Lactobacillus brevis*	39.1 g/l lactic acid with yield 0.75 g/g substrate and productivity 0.82 g l^{-1} h^{-1}	[29]
Biomass-derived sugars	*Lactobacillus delbrueckii*	0.83 g/g substrate with productivity 1.01 g l^{-1} h^{-1}	[30]
Corn Stover	*Bacillus sp. strain NL01*	74.5% L-lactic acid with productivity 1.04 g l^{-1} h^{-1}	[31]
Glucose	*Actinobacillus succinogenes*	0.97 g/g substrate with productivity 1.53 g l^{-1} h^{-1}	[32]
Glucose	*Escherichia coli*	126 kg/ ton, yield 97%, optical purity 99.5%, productivity 6 kg ton^{-1} h^{-1}	[33]
Potato starch	*Geobacillus stearothermophilus*	50 g/L raw potato starch produced 37g/L L-lactic acid	[34]

2.1.1 **Lactic acid processing**

Lactic acid synthesis can generate one or two stereoisomers or their racemic mixture depending on different techniques. In Figure **2.2**, chemical synthesis can produce lactic acid in a racemic mixture of DL-lactic acid. Otherwise, microbial fermentation technique from renewable resources or lignocellulosic biomass can generate optically pure L(+)- or D(-)-lactic acid due to selectivity of microbial strains.

8

In fermentation processes, sugar solution was supplied with nutrients and inoculated with the specific microorganism. Furthermore, fermentation conditions are very important to the selected microorganism, such as temperature, pH, aeration, agitation, and other parameters [35].
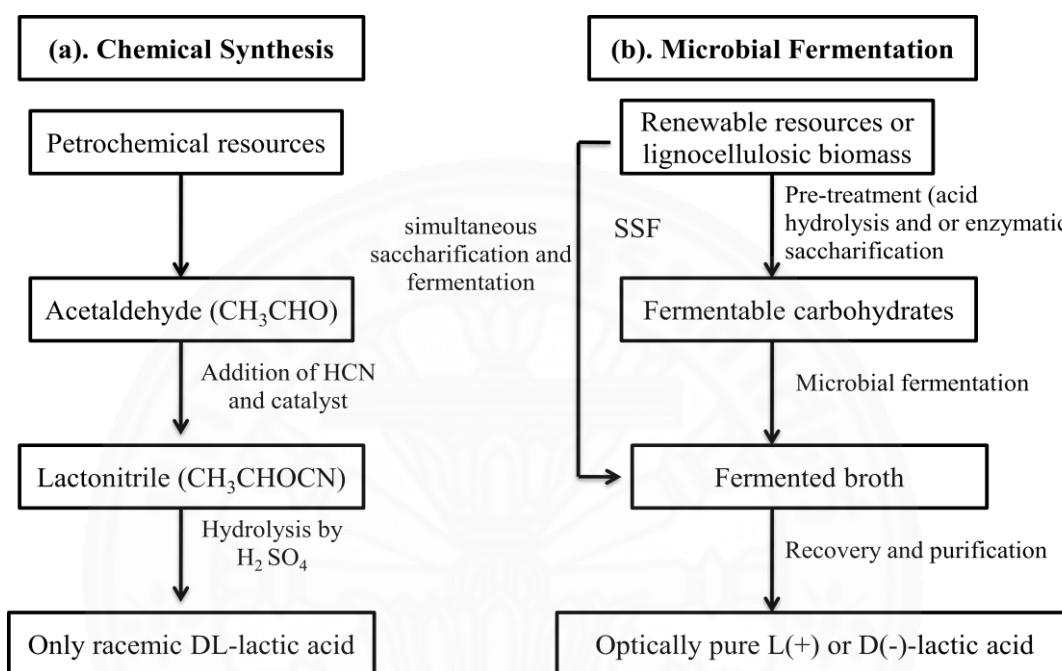
Figure 2.2: Two different methods to synthesize lactic acid: (a) chemical synthesis and (b) microbial fermentation [20].

2.1.1.1 Chemical synthesis processes

Chemical synthesis process is based on lactonitrile production from reaction between acetaldehyde and hydrogen cyanide in liquid phase at high atmospheric pressures, as shown in Equation 2.1. The recovery lactonitrile is hydrolyzed by sulphuric acid or hydrochloric acid to produce lactic acid and ammonium salt. Then, esterification process is used to esterify lactic acid with methanol to generate methylactate. Finally, the methylactate is purified by distillation and hydrolyzed by water under acid catalyst to convert lactic acid and methanol. In this process, lactic acid production is a racemic mixture of L(+) and D(-)-lactic acid [36].

a. Addition of Hydrogen Cyanide

$$CH_3CHO + HCN \xrightarrow{\text{Catalyst}} CH_3CHOHCN$$
Lactonitrile

b. Hydrolysis by H_2SO_4

$$CH_3CHOHCN + H_2SO_4 \longrightarrow CH_3CHOHCOOH + 1/2\ (NH_4)_2SO_4$$
Lactic acid

c. Esterification

$$CH_3CHOHCOOH + CH_3OH \longrightarrow CH_3CHOHCOOCH_3 + H_2O$$
Methyl lactate

d. Hydrolysis

$$CH_3CHOHCOOCH_3 + H_2O \longrightarrow CH_3CHOHCOOH + CH_3OH$$
Lactic acid
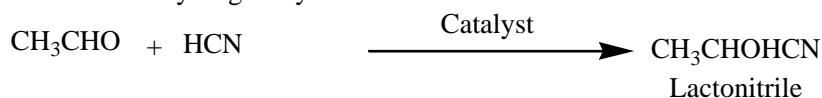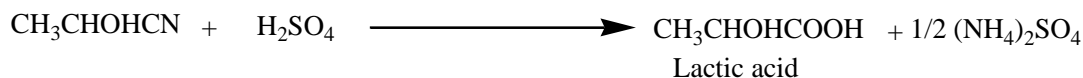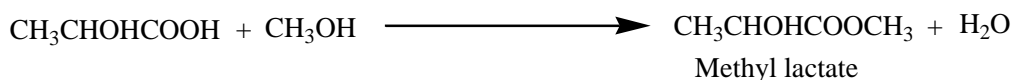
Equation 2.1: Chemical synthesis process of Lactic acid [36].

2.1.1.2 Microorganism Fermentation processes

Microbial fermentation of carbohydrates is used to produce a specific stereo type of lactic acid due to microbial strain selectivity. First, renewable resources were fermented by enzymatic saccharification, converting carbohydrates to sugars. Fermentable carbohydrates by microbial activity produced fermented broth. Then, separation and purification are applied to achieve lactic acid [20]. Currently, the commercial lactic production using lignocelluloses face many problems because of the complexity of raw materials. Lignocellulosic biomass firstly needs several steps to transfer carbohydrates' structure to simple sugars like glucose, xylose, arabinose, and manose. The lactic acid processing from lignocellulosic biomass has four main steps [37]

a) Pre-treatment is used to break down complex structure of the lignocelluloses.

b) Enzymatic hydrolysis converts the carbohydrates of lignocelluloses to small monomer sugars such as hexose and pentose.

c) Fermentation metabolizes the monomer sugars to lactic acid by activity of microorganisms.

d) Separation and purification of lactic acid is used to produce the standard quality of lactic acid for commercial applications.

10

2.1.1.2.1 Pre-treatment processes

Generally, lactic acid is produced by fermentation of carbon sources such as hexose or pentose sugars metabolisms. Due to increasing demand, several types of abundant renewable resources are of interested for use to synthesize this lactic acid. These resources, contains high content of cellulose and carbohydrate, are cheaper than the sugar raw materials. For instance, starch of rice, corn, wheat potato, or cassava is a renewable resource of agricultural products. On the other hand, the lignocellulosic wastes, such as wheat straw and bran, rice husk and straw, corncob, and corn stover is available as raw materials to produce lactic acid for commercial. Lignocellulosic biomass contains carbohydrates in a matrix with cellulose, hemicelluloses, and lignin [38]. In this case, the pretreatment process is important to remove lignin from the matrix and separates cellulose from hemicelluloses in order to increase the accessible surface area, partially depolymerize cellulose, and increases the porosity of materials to serve in the subsequent access of the hydrolytic enzymes. Pretreatment processes consist of physical treatments (milling and grinding), chemical treatments (alkaline, dilute acid, oxidizers, organic solvents), and physic-chemical treatments (steam condition, hydrothermolysis, wet oxidation), and biological treatment, as shown in Figure **2.3** [37].

In the pretreatment processes, lignocelluloses bioconversion is very important stage to transfer carbohydrates to cellulose, hemocellulose, and remove lignin. For instance, lignocelluloses resources like corn stover, wheat stover, rice stover, corncob, and mixcanthus were treated at 75ºC with sodium hydroxide condition. After pre-treatment, 56% cellulose and 40.6% hemicellulose were obtaioned from corn stover [39]. Acidic pre-treatment were also reported by many researchers. In this case, wheat straw was cleaned and pretreated with dilute sulfuric acid 2% w/v and treated at 121 ºC, and 59.96% cellulose, was obtained [40].

11
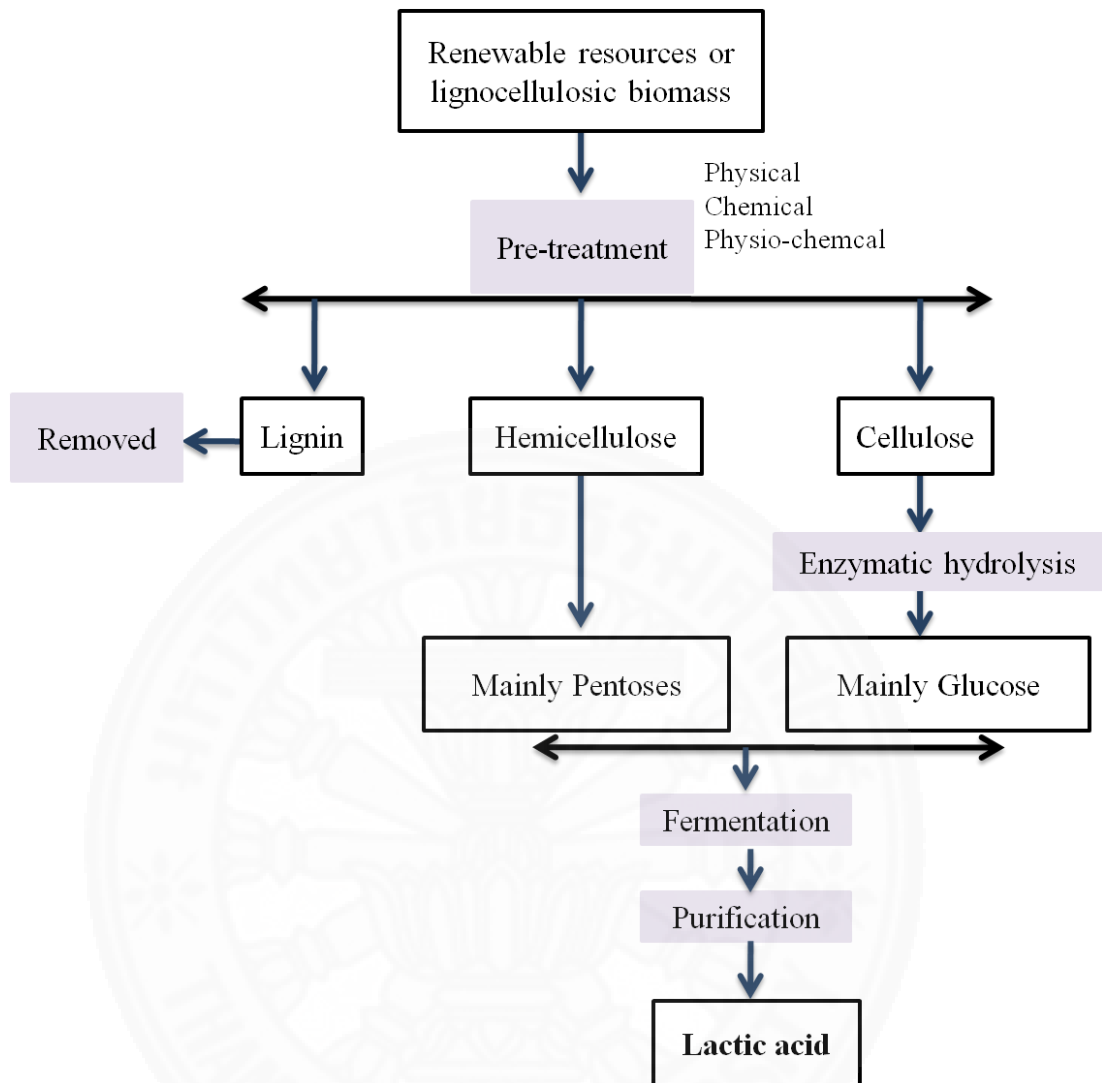
Figure 2.3: Schematic of lactic acid production from lignocellulosic biomass [37].

2.1.1.2.2 Enzymatic Hydrolysis

Enzymatic hydrolysis is the most important steps in fermentation processes to yield high sources of sugars to form lactic acid. This step is continued from pre-treatment process to remove lignin and separate cellulose from hemicelluloses. Solid state of cellulose products are polysaccharides chains insoluble in water. To obtain sugars soluble in water, cellulose and hemicelluloses need specific enzymes to cut down glycosidic linkages to form monosaccharide, as shown in Equation 2.2. The efficient of depolymerization of polysaccharide cellulose need alternative of cellulolytic enzymes, such as Endo-β-1, 4-glucanase (cleavage β-1, 4 bonds intramolecular of cellulose chains), Exo-β-1, 4-glucanase (cutting down glycosidic

12

linkages of cellulose at the end of chains to form glucose or cellobiose), and β-glucosidase (cleavage cellobiose into two glucose molecules) [37].
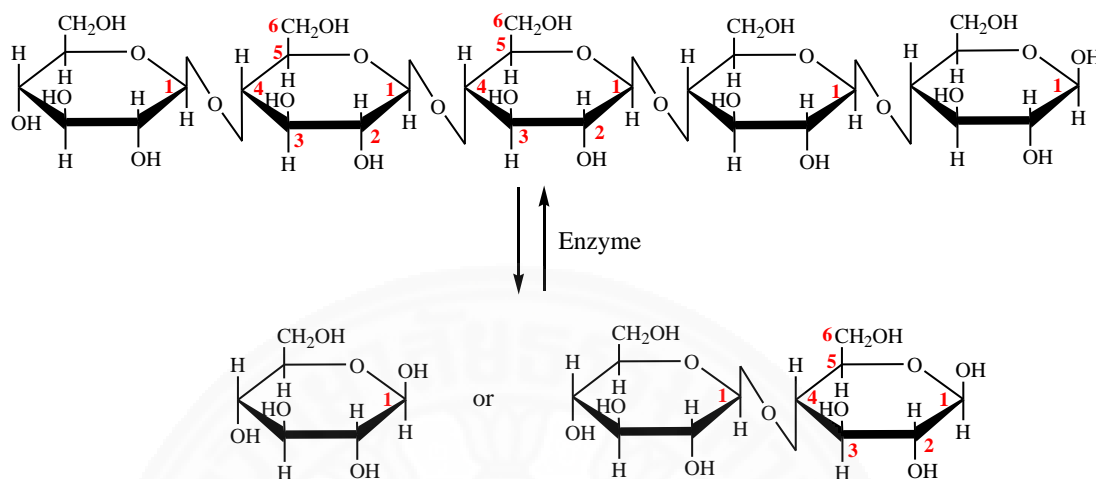
Equation 2.2: Cleavage of β (1, 4)-glycosidic bonds of cellulose.

Lignocellulose biomass contains very complicate structure of cellulose, xylan, and hemicelluloses after pre-treatment processes, though multi-enzyme are required to cleave glycosidic bonds. Enzymatic cellulase, β-glucosidase, and xylanase were used to cleave the polysaccharide chains [39]. The multi-enzyme hydrolytic on cellulose, xylan, and hemicelluloses depends on the enzyme properties and the ratio in the mixture.

2.1.1.2.3 Fermentation processes

Lignocellulosic biomass, after pre-treatment and enzymatic hydrolysis, contained sugars of hexoses and pentoses. Mostly, enzymatic hydrolysis of hemicelluloses formed pentose sugars (xylose and arabinose), while cellulose formed hexose sugars (glucose). These monomers of sugars then are applied to the fermentation process to produce lactic acid. Several researchers conducted their research to find the optimal condition of fermentation. In order to get maximum lactic acid yield, many kinds of microorganisms such as bacteria, fungus, or enzymes are employed. There are two important fermentation pathways of metabolites by bacteria activities, homolactic and heterolactic fermentation.

13

Homolactic process produces greater yield of lactic acid with lower metabolites. This fermentation process has two steps separately. Firstly, glycolysis pathway transferred glucose to pyruvic acid by using ATP, enzymes, NAD^+. Then, pyruvic acid transferred to lactic acid by reducing power in form of NADA, as shown in Figure **2.4**. The final productions of glycolysis glucose produced two molecules lactic acid and released two ATP. In this pathway, microorganisms were used only to consume carbohydrates (called Obligatory Homofermentative) including *lactobacillus acidophilus*, *lactobacillus amylophilus*, and *lactobacillus helveticus* [35].

Glucose Z 2 Lactic Acid + 2 ATP
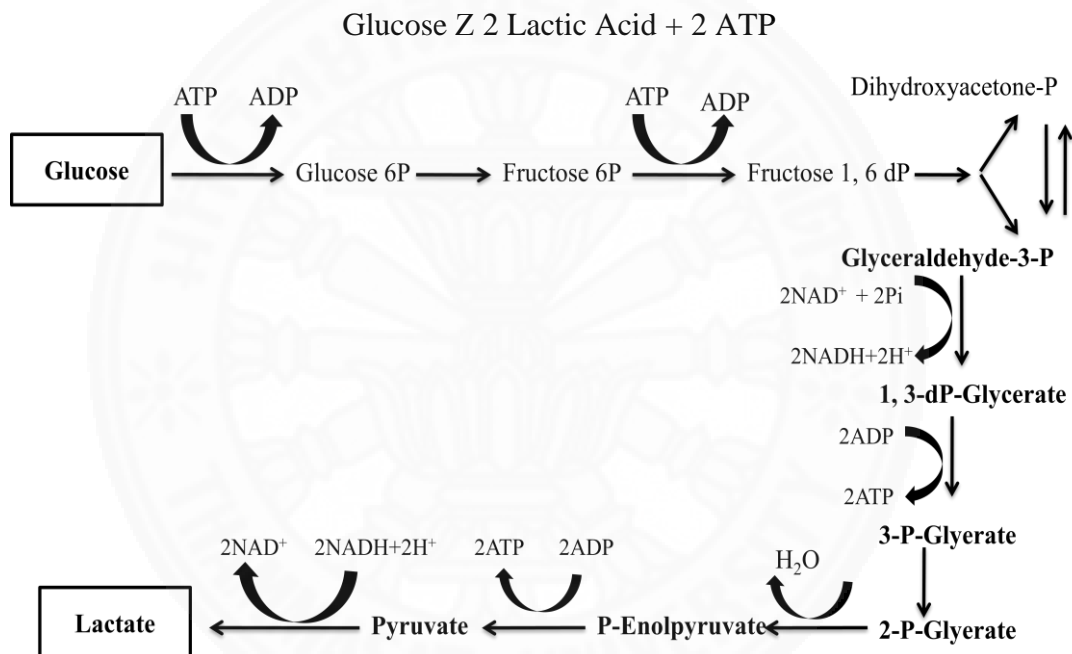
Figure 2.4: Homolactic fermentation pathway of lactic acid processing [35]

Heterolactic fermentation process produces co-products beside lactic acid, such as carbon dioxide, and ethanol and/ or acetic acid, as illustrated in Figure **2.5**. This process produces lactic acid with significant quantities of metabolites. First, hexose especially glucose transferred to pentose, in this condition ribolose-5-phosphate, through pentose phosphate pathway to generate glyceraldehydes-3-phosphate, acetyl-phosphate and carbon dioxide. Then, glyceraldehydes-3-phosphate shifted into glycolysis in step six to form lactic acid, otherwise acetyl-phosphate transferred to acetic acid or ethanol. In this process, microorganisms were used only to consume carbohydrates (called Obligatory Heterofermentative) including

14

Lactobacillus brevis, Lactobacillus fermentum, Lactobacillus parabuchneri, and *Lactobacillus reuter* [35].

Glucose Z Lactic acid + CO_2 + Ethanol + ATP

Glucose Z Lactic acid + CO_2 + Acetic acid + 2 ATP + 2 NADH
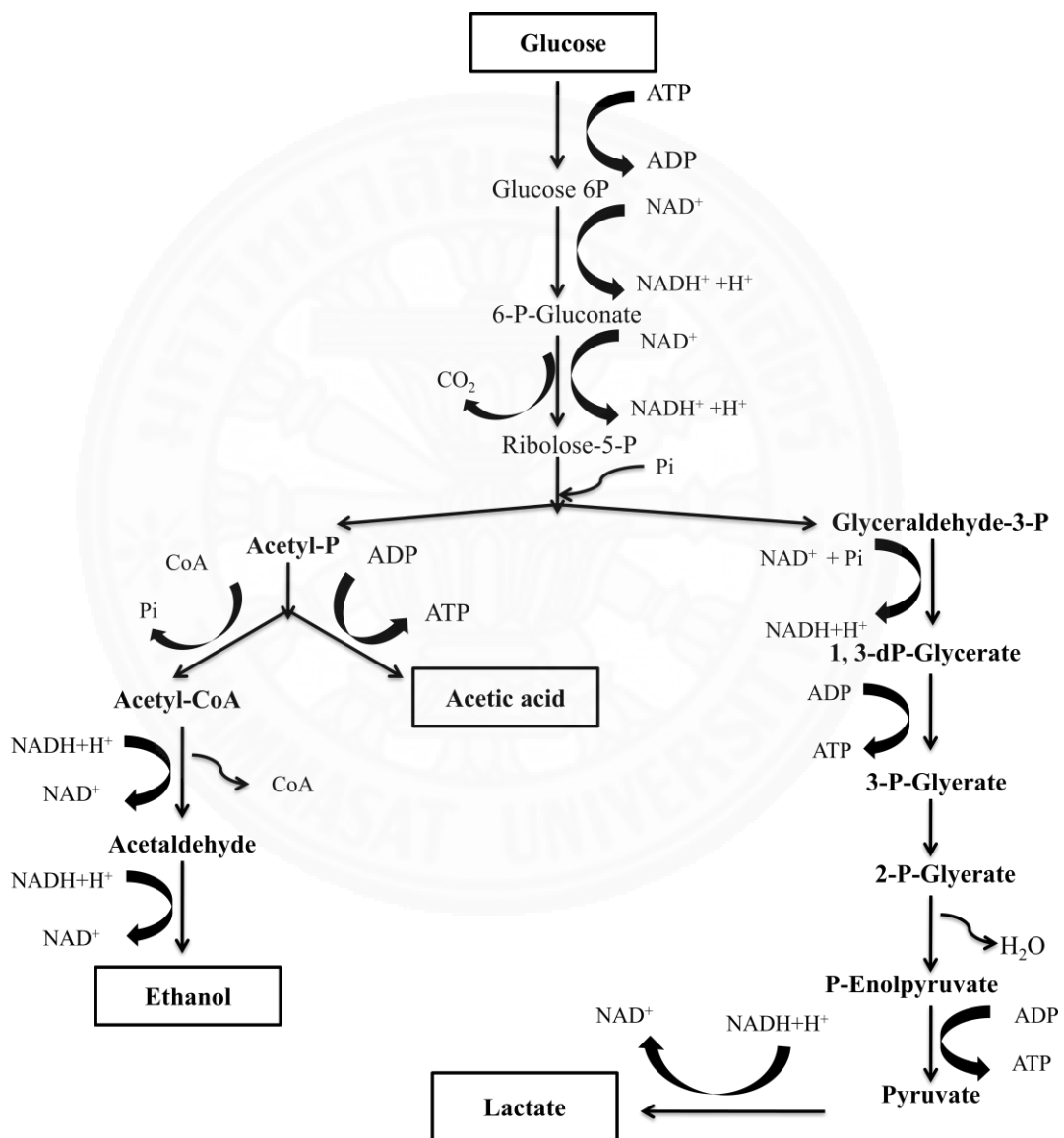
Figure 2.5: Heterolactic fermentation pathway of lactic acid processing [35].

2.1.1.2.4 Separation and Purification

15

Purification and recovery lactic acid product are very important steps in lactic acid processing after separation from fermentation broth. In fermentation broth container, impurities substances like residual sugars, color, nutrients, microorganisms' cells, organic acid, and other precipitation need to be removed in order to increase lactic acid purity , as shown in Figure **2.6**[17].
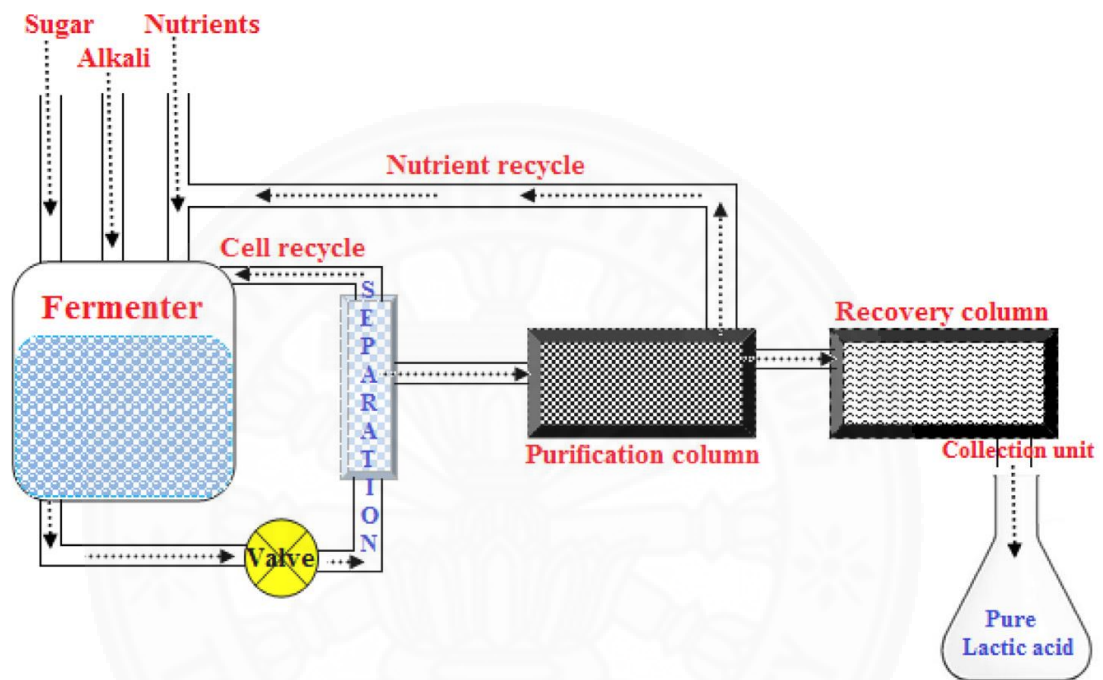
Figure 2.6: Purification processes of lactic acid from fermentation processes [17].

In addition, fermentation broth is neutralized by calcium carbonate or calcium hydroxide. The fermented broth of calcium lactate is filtered to remove cells, carbon treated, evaporated, and hydrolyzed with sulfuric acid to form lactic acid and calcium sulfate. The precipitation calcium sulfate is separated by filtration from lactic acid solution. Then, esterification and hydrolysis with water are used to regenerate lactic acid and methanol, as shown in Equation 2.3[36, 37].

a. Fermentation and neutralization

$$C_6H_{12}O_6 \quad + \quad Ca(OH)_2 \quad \xrightarrow{\text{Fermentation process}} \quad (2CH_3CHOHCOO^-)\,Ca^{2+} + H_2O$$

Carbohydrate   Calcium lactate

b. Hydrolysis by H_2SO_4

$$(2CH_3CHOHCOO^-)\,Ca^{2+} \quad + \quad H_2SO_4 \quad \longrightarrow \quad CH_3CHOHCOOH \quad + \quad CaSO_4$$

Lactic acid

c. Esterification

$$CH_3CHOHCOOH \quad + \quad CH_3OH \quad \longrightarrow \quad CH_3CHOHCOOCH_3 \quad + \quad H_2O$$

Methyl lactate

d. Hydrolysis

$$CH_3CHOHCOOCH_3 \quad + \quad H_2O \quad \longrightarrow \quad CH_3CHOHCOOH \quad + \quad CH_3OH$$
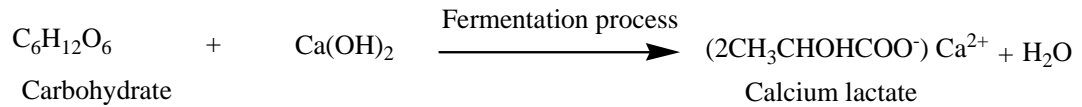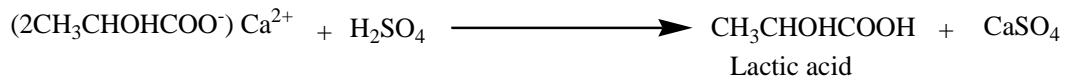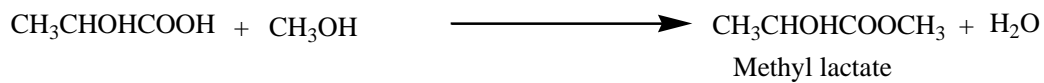
Lactic acid

Equation 2.3: Fermentation process of lactic acid production [36].

2.1.2 Polylactide polymerization

Polylactide polymerization requires high purity of lactic acid monomer, totally free of water and acid [41]. In addition, impurity contents such as hydroxyl, carboxylic, and water can interfere the main reaction and results in reduction of polymer quality. Hydroxyl impurities affect the reaction by increasing polymerization rate and decreasing of molecular weight of the polymer. They can make chain transfer and transesterfication by making the broadening molecular weight of the final polymer. In contrast, carboxylic perform as inhibitor and lowering the reaction rate by making complex with catalyst[42]. There are many reports focused on the conversion of lactic acid to form polymer. Several methods have been employed to manipulate high molecular weight polylactide, as shown in Equation 2.4.
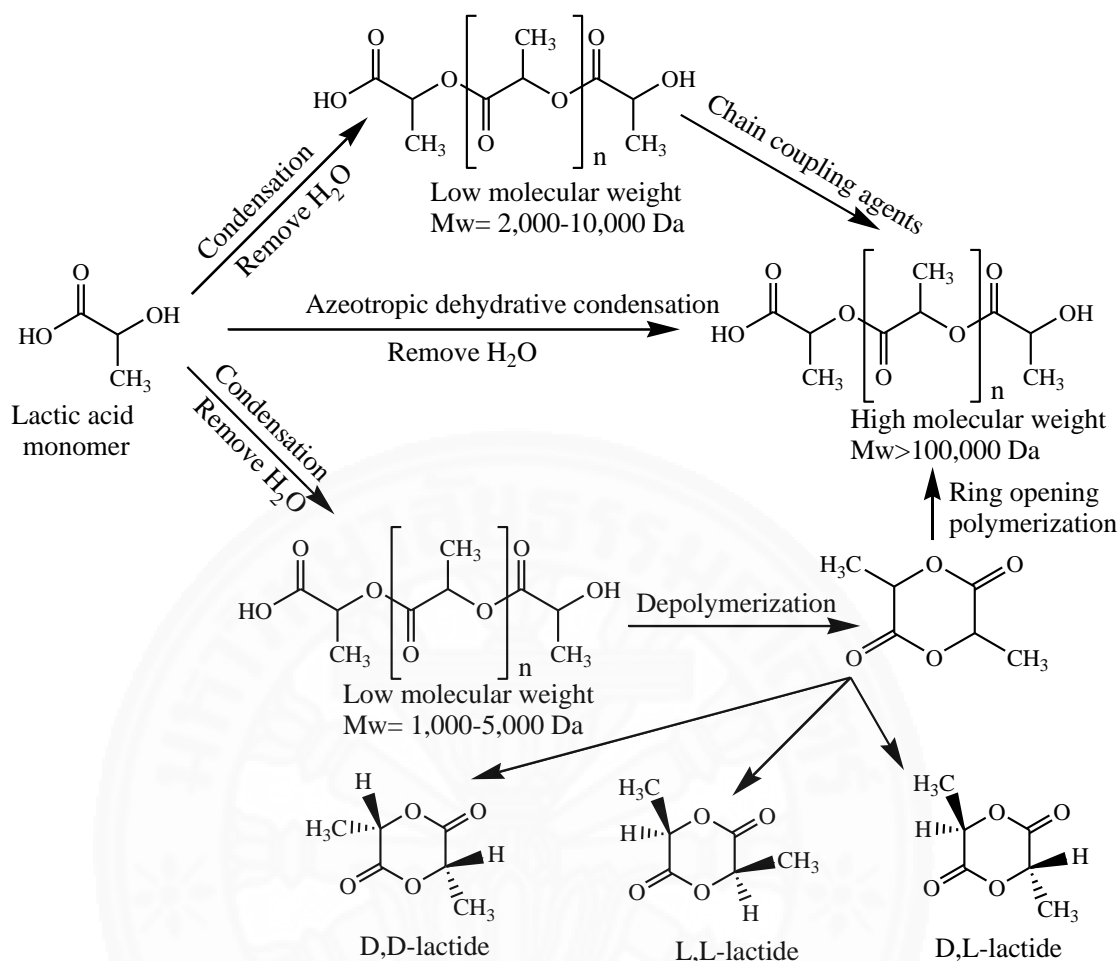
Equation 2.4: Overall steps for conversion lactic acid monomers to polylactide[43].

2.1.2.1 Direct polycondensation

Direct polycondensation (DP) of L-lactic acid is employed to synthesize oligo(L-lactide) or oligomer by the removal of water. Heat and vacuum are the critical factors for the condensation reaction. This reaction can be conducted with and without catalyst [44]. During this process, unzipping and ring closure reactions are also the main reaction, as shown in Equation 2.5. This is reasonable that low molecular weight can be obtained. Another reason is that highly viscous reaction mixture lead to difficulty in removing of water, resulting in low degree of polymerization. Oligomers with low molecular weight (500-2,000 Da) are obtained and can be separated and stored for the next processing. Obviously, DP method is applied only for low molecular weight PLA for some applications[41].

18
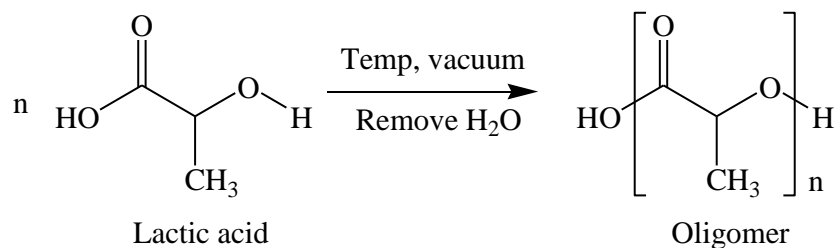
(A) Condensation reaction
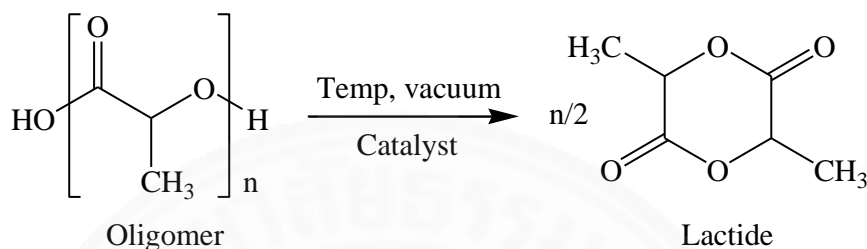
(B) Unzipping reaction

Equation 2.5: Synthesis of PLA oligomer and lactide dimer [41].

High molecular weight PLA is widely used in many applications, rather than low molecular weight polymer. This polymer is fabricated by using chain coupling agents. The low molecular weight oligomers chains are joined together to form high molecular weight polymer. In DP process, low molecular weight oligo(L-lactide) reach an equilibrium molar concentration of carboxyl and hydroxyl end-groups. Low molecular PLA can be modified by bi/multi-functional compounds to generate hydroxyl or carboxyl end groups. Several compounds have been investigated and used to produce hydroxyl end groups of PLA. These include 2-buthene 1,4-diol, dodecanol, glycerol, or 1,4-butanediol. Carboxyl ended PLA are also obtained by using several types of organic acid, such as succinic, maleic, or itaconic acids [42]. Equation 2.6 illustrates the mechanisms of hydroxyl (OH-PLA) and carboxyl (COOH-PLA) terminated PLA. OH-PLA is produced by the reaction between L-lactide and dodecanol under catalytic activation of zinc prolinate at 180°C. COOH-PLA is prepared by the reaction of OH-PLA with succinic anhydride, 4-dimethylaminopyridine (DMAP), and triethylamine (TEA) at room temperature[45]. Chain coupling agents react with the end-groups of polymer and result in increasing chain length of PLA. The plentiful coupling agents have been reported and employed for use in polymerization processing. Silane coupling agents are commonly use due to their several functional groups. These include vinyl, epoxy, methacryloxy, acryloxy,

19

amino, sulfide, and isocyanate groups. For instance, epoxy silane coupling agent composites with wood flour is used as polylactide modifier in order to extend polymer chains, as shown in Equation 2.7[46].
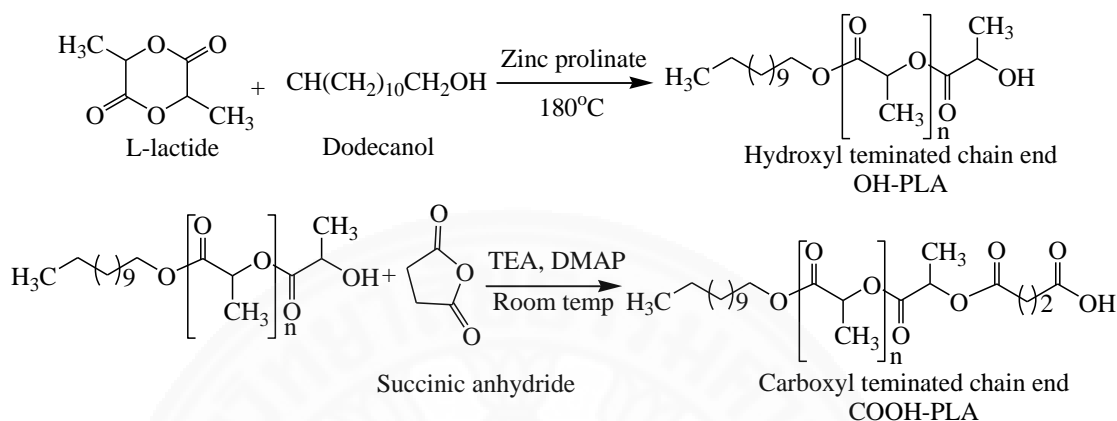
Equation 2.6: Hydroxyl and carboxyl terminated PLA [45].
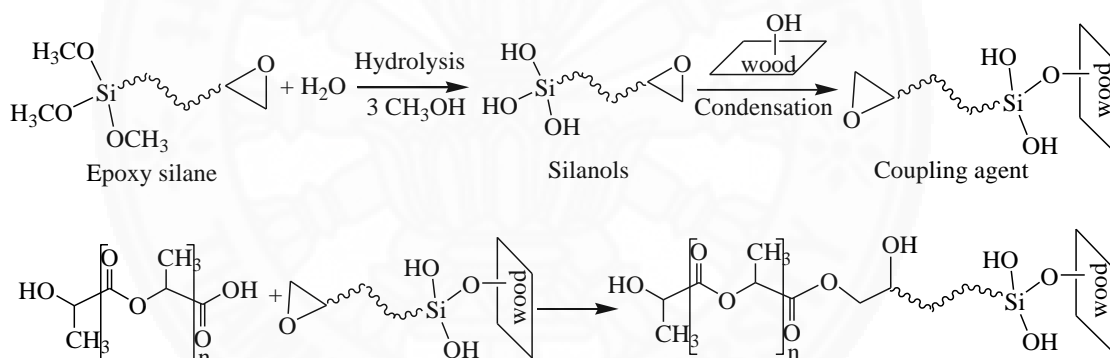
Equation 2.7: Epoxy silane coupling agent composite with wood flour for polylactide modifier [46].

2.1.2.2 Ring-opening polymerization

High molecular weight polymers are fabricated from its cyclic dimer by using ring-opening polymerization (ROP). This reaction is always carried out by using catalysts. For instance, stannous (II) chloride and stannous (II) 2-ethylhexanoate (tin octoate, $Sn(Oct)_2$) are used as catalyst to produce polymer for medical applications. Tin octoate is employed to avoid racemic product of polylactide. High molecular weight polymer with high stereo-regulation degree can be controlled during polymer

20

processing by using free hydroxyl groups compounds. e.g. water, hydroxy acids, esters, and alcohols have been investigated[41]. The ordinary ROP reaction, $Sn(Oct)_2$ catalyst react with alcohol to produce tin alkoxide bond, as shown in Equation 2.8[47, 48].

$$Sn(Oct)_2 + ROH \longrightarrow OctSnOR + OctH$$

$$OctSnOR + ROH \longrightarrow Sn(OR)_2 + OctH$$
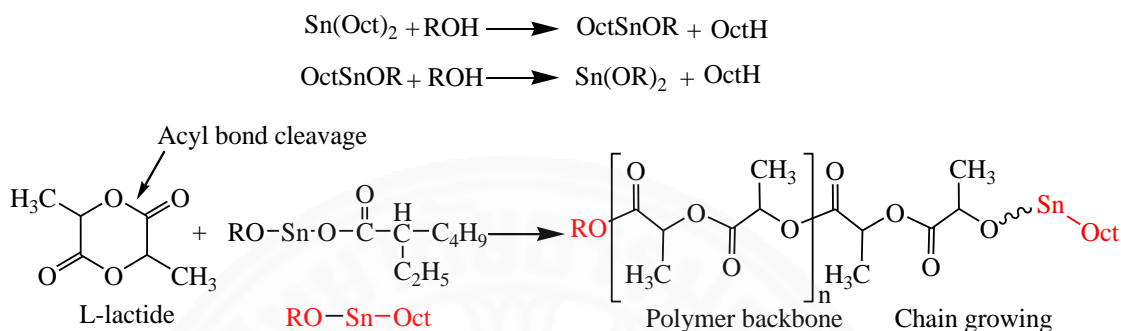
Equation 2.8: ROP mechanism of lactide by using tin octoate catalyst [41, 47].

2.2 Applications of TiO$_2$

Titanium dioxide is classified as a family of transition metal oxides, as also called titanium (IV) oxide. The material was discovered in 1821 and commercialized in early 20th century. In early of the 20th century, TiO$_2$ was used to replace toxic lead oxides as white pigment in paints. The consumption of TiO$_2$ is more than 4 million tons in the present such as white pigment paints (51%), plastic (19%), and paper (17%)[49]. After, a new period of heterogeneous photocatalysis have began since 1972, discovery of Fujishima and Honda on photocatalytic splitting of water on TiO$_2$ electrodes[50]. Many engineering researchers have begun to understand the fundamental process and started research on photocatalytic efficiency of TiO$_2$. Currently, environmental clean-up has become one of the most interesting areas in heterogeneous photocatalysis[51]. Due to photochemical property of TiO$_2$ as a heterogeneous photocatalysis, it is widely used in many fields like cosmetic products, water treatment (wastewater treatment and drinking water disinfection), photodegradation organic pollutants, environmental remediation, antimicrobial activity, sterilization,removal of volatile organic compounds (VOCs), air purification, cancer cells treatment, pharmaceutical and food industries, and health applications[49, 52-54].

21

2.2.1 Water treatment

Organic pollutants are one of the most concerned problems to the water contamination, especially dye pollutants that released into water resource from textile colorants, industrial wastes, and household waste water. Organic dyes causes high toxicity and visibility on the surface waters. In this case, decontamination and degradation of these pollutants have become a critical problem in wastewater treatment processes[55]. To remove dyes from wastewater, previously microorganisms are used. Otherwise, this method is very difficult because most of dye's structures are macromolecules and microorganisms cannot decomposes completely[7].

Table 2.2 summarizes the applications of TiO_2 in wastewater treatment pocesses. TiO_2/AC was synthesized by hydrolytic precipitation method and used to remove methyl orange (MO) under UV illumination. Almost 100% of MO was degraded in 140 minutes[56]. TiO_2/Ag was coated on polystyrene (PS) thin films by using sol-gel spin-coating method, and this material was used to investigate the photocatalytic activity of methylene blue (MB) photodegradation [57]. TiO_2/UV/O_3 was used to degraded 2-sec-butyl-4,6-dinitrophenol (DNBP) in water treatment application[58]. TiO_2/PES and TiO_2/PVDF were synthesized and used to degrade methylene blue (MB), drug diclofenac, and ibuprofen in hydrophilic condition. Results from photodegradation showed that TiO_2/PVDF degraded 100% MB and 70% MB for TiO_2/PES in 120 minutes. Also, TiO_2/PES degraded 68% of drug diclofenac and 55% for TiO_2/PVDF[59].

Table 2.2: Applications of TiO_2 materials for wastewater treatment processes.

TiO_2 catalyst	Method	Pollutants/Light source	Efficiency	Ref
TiO_2/AC (Activated carbon)	Hydrolytic precipitation	Methyl orange (MO) and UV lamp 40W	TiO_2/AC (0.5 g) with 47% TiO_2 content almost degrade 100% of MO in 140 min.	[56]
TiO_2 composite film	sol-gel technique and spin coating	Yellow X6G, Solophenyl red 3BL, and tertrodirect light blue R. UVA lamp 8W(λ = 365 nm)	Photodegradation irradiated in 300 min can remove Yellow X6G 95.7%, Solophenyl red 3BL 94.4%, and Tertrodirect blue R 94.7% respectively.	[60]

22

TiO$_2$/Ag polystyrene (PS) spheres thin films	Sol–gel spin-coating technique. PS diameter (50, 200, and 400 nm)	Methylene blue (MB) and UV-light 365 nm	Adding 1 mol% Ag of TiO$_2$/Ag-PS50, PS200, and PS400 degraded MB 84%, 100% and 95% respectively after 7 h.	[57]
TiO$_2$/UV/O$_3$	TiO$_2$ Degussa P25	2-sec-butyl-4,6-dinitrophenol (DNBP) and UV lamp (10 W, 254 nm)	TiO$_2$/UV/O$_3$ removed DNBP 99.1 % in 15 min at pH=9.5.	[58]
TiO$_2$/Polyethersulfone (PES) and TiO$_2$/polyvinylidene fluoride (PVDF) membrane	Hydrolysis method	Methylene blue (MB), diclofenac, and ibuprofen drugs. UVA lamp (7.6mWcm^{-2})	TiO$_2$/PVDF degraded 100% and TiO$_2$/PES degraded 70% MB in 120 min. TiO$_2$/PES degraded 68% and TiO$_2$/PVDF degraded 55% diclofenac in 120 min.	[59]

2.2.2 Air purification

Application of TiO$_2$ photocatalysis for indoor air purification is very attractive for new research today, especially photodegradation of volatile organic compounds (VOCs). Several species of VOCs have been considered as air pollution, such as nitrogen oxide (NO), formaldehyde, carbonyl compounds, aldehydes, and ketones. Most of these gases have affected human health. All of these gases usually are emitted from incomplete combustion of vehicles, fuel, and household materials. Formaldehyde is one of carcinogenic VOCs found in indoor environment, and used widely in household and building materials. Principally, urea-formaldehyde (UF) is used in wood materials as compressing. Several sources of formadelyde have been detected in smoking of cigarette and fuel[61, 62].

Table 2.3 describes the applicaitions of various TiO$_2$ materials in air purification pocesses. TiO$_2$/glass fiber filter (Whatman) was synthesized, and used to degrade BTEX (benzene, toluene, ethylbenzene, and o-xylene) and nitrogene oxide (NO). The removal of benzene, toluene, ethylbenzene, o-xylene and NO were 24, 67, 84, 86, and 90% respectively [63]. TiO$_2$ immobilized on activated carbon (TiO$_2$/AC) was prepared and used to degrade NO and toluene pollutants under UV-light [64]. Nitrogen (N)-doped TiO$_2$ was prepared to remove VOCs (benzene, toluene, ethyl benzene, and *o,m,p*-xylenes) under visible-light illumination at different relative humidity (RH) condition [65]. Polyvinylpyrrolidone/TiO$_2$ (PVP/TiO$_2$) was synthesised via electrospinning technique and observed the ability of

23

trichloroethylene (TCE) photodegradation. The best efficiency of photodegradation occurred at a 1:1.3 of PVP:TiO_2 ratio that degraded 94% of TCE [66]. Additionally, TiO_2 was also reported on acetylene degradation in various conditions [67-70].

Table 2.3: Applications of TiO_2 materials for air purification processes.

TiO_2 catalyst	Method	Pollutant/Light source	Efficiency	Ref
TiO_2/glass fiber filter	Degussa P25 coated on glass fiber filter	Benzene, toluene, ethyl benzene and o-xylene (BTEX) and NO. UV lamp 6W, 365 nm and $600\mu W/cm^2$	Removal of benzene, toluene, ethylbenzene and o-xylene were 24, 67, 84 and 86% respectively. Removal of NO was 90%.	[63]
TiO_2/AC	Degussa P25 was loaded on activated carbon filter	Nitrogen oxide (NO) 200 ppb and toluene. UVC-lamp 6W, 254 nm, and $2.76mW/cm^2$	TiO_2/AC filter degraded NO 97% and generated NO_2 1.6%.	[64]
TiO_2	TiO_2 P25 and PC500-Millennium (anatase)	Acetylene C_2H_2. UV lamp 125W	TiO_2 P25 has higher degradability of C_2H_2 than PC500.	[70]
N-TiO_2, NC-TiO_2, BA-PW25, and TiO_2 P25	NH_3 treatment of anatase and calcination of Ti^{4+}-bipyridine complex	Acetylene C_2H_2. Philips HPK-125 W lamp.	BA-PW25 has the highest ability to degrade C_2H_2 compared to N-TiO_2, NC-TiO_2, and TiO_2 P25.	[67]
N-doped TiO_2	Degussa P25	VOCs (benzene, toluene, ethyl benzene, and o,m,p-xylenes).	N-doped TiO_2 removed more than 90% for ethyl benzene, o,m,p-xylenes. Benzene and toluene removal were obtained in range 17 to 36% and and 44 to 74% respectively.	[65]
TiO_2/SiO_2 Polyester Fiber	Spray coating method	Formaldehyde (HCHO). UV lamp (λ=368 nm) E=3692 $\mu W/cm^2$	The removal efficiency of HCHO before stability was (92.86% $\pm$ 2.58%) and after stability (91.96% $\pm$ 2.42%) in 105min.	[62]
PVP/TiO_2 (PT)	Electrospinning method	Trichloroethylene (TCE). UV lamp 8W.	PT has radio 1:1.3, 1:0.7, 1:0.35 and 1:0.1 can degrade TCE with 94%, 91%, 88%, and 84% respectively over 3h.	[66]
TiO_2 P25 and commercial Au/TiO_2		Acetylene C_2H_2. UV light $4mW/cm^2$.	Almost 100% of C_2H_2 was degraded by TiO_2 P25 higher than commercial Au/TiO_2.	[68]
TiO_2 P25 deposited on glass fibers		Acetylene C_2H_2 100 ppm and flow rate 500 mL/min. UV lamps (365 nm, 8 to 10 mW/cm^2	The acetylene conversion rate yield 70% after 0.5h and tend to decrease to 40% after 12h.	[69]

24

2.2.3 **Antimicrobial activities**

Antibacterial activity of TiO_2 makes it become an excellence choice for applications in eliminating microorganisms. It has been used to replace chemical cleaning agents and biocides in pharmaceutical and food industries. The American Food And Drug Administration has approved the use of TiO_2 in humankind products, such as foods, drugs, cosmetics, and food packing materials [71]. For instance, TiO_2 can inactivate Escherichia coli *(E.coli)* *in vitro* by using powder-coated packaging film process. *Chawengkijwanich. C* et. al. performed a test on a cut lettuce that stored in a TiO_2-coated film bag under UV-light. The material showed the efficiency for reduction of *E.coli* colonies. This result reflected that TiO_2 coated film could remove microbial contamination on solid food surface and decrease microbial growth in packaging[71].

Surface disinfection on food processing industries is also a main concern, especially in the cleaning of pathogenic germs on the surface of the production equipments. The study on *E.coli* by synthesized curli showed that substrate that allows bacteria to attach on its surface and form biofilms can inactivate these bacteria due to UV-light activated TiO_2. The result showed that no bacterial cultivability was found after 48 hours in dark condition [72]. Other applications of TiO_2 materials are illustrated in Table 2.4. Au-capped TiO_2 and vanadium-doped TiO_2 were successful synthesized by sol-gel and chemical reduction. These nanocomposites were used as photocatalysts to degrade *Escherichia coli* (DH 5R) and *Bacillus megaterium* (QMB1551) under room light (low power UV LED) [73]. Ag/TiO_2 nanocomposites were fabricated by one-pot sol-gel technique and used to kill *Escherichia coli* under ambient light condition [74]. Nano-TiO_2 (NT) doped with Fe^{3+} and Ag (Fe-Ag/NT) modified by 3-methacryloxypropyltrimethoxysilane (MPS) were synthesized and applied on fluorocarbon coatings (FCC). The efficiency was observed due to photodegradation *Staphylococus* and *Escherichia coli* under UV irradiation [75]. TiO_2-chitosan-poly(vinyl alcohol) (TiO_2/CS/PVA) and CS/PVA/$AgNO_3$ added with $AgNO_3$ were fabricated by using electrospinning method. The photocatalytic activity of the catalysts were examined with gram-negative *Escherichia coli* and gram-positive *Staphylococus aureus* degradation under UV-light. The highest

photodegradation efficiency occurred while HCS/PVA with 0.03wt% TiO_2 and 0.04wt% $AgNO_3$ content [76].

Table 2.4: Application of TiO_2 materials for antibacterial applications processes.

TiO_2 catalyst	Method	Pollutant/ Light source	Efficiency	Ref
Au-capped TiO_2, and vanadium-doped TiO_2	Sol-gel , and chemical reduction method	E. coli and Bacillus megaterium. Room light (low power UV LED)	Au-TiO_2 had strong ability to degrade bacteria (60-100% killing efficiency)	[73]
Ag/TiO_2	one-pot sol-gel technique	E. coli. Ambient light	Ag/TiO_2 (7.4wt% Ag content) killed bacteria 98.8% at Ag concentration 1.2μg/mL and completely degraded at 2.4μg/mL. Ag/TiO_2 (3.9 wt% Ag) killed bacteria 99.9% at 1.6μg/mL Ag	[74]
TiO_2/$Fe^{3+}$and Ag (Fe-Ag/NT)	Sol-gel and emulsion coating method modified by fluorocarbon coatings (FCC)	Staphylococcus and E. coli. UV lamp 253.7nm.	FCC/Fe-Ag/NT (TiO_2 2wt %) degraded Staphylococcus 66% and E.coli 68%. FCC/MPS-Fe-Ag/NT with TiO_2 2wt% degraded Staphylococcus 93% and E.coli 92%.	[75]
TiO_2/CS/ PVA and CS/ PVA/$AgNO_3$	Electrospinning method and using low and high-vicosity chitosan (LCS and HCS)	Gram-negative E. coli and gram-positive S. aureus. UV-light.	TiO_2/HCS/PVA with 0.03wt% TiO_2 degraded S. aureus (90%) and E.coli (85%). $AgNO_3$/HCS/PVA degraded 99% of S. aureus and 98% of E. coli	[76]
TiO_2/ Poly(vinyl alcohol) (PVA)	Electrospinning method	S. aureus and Klebsiella pneumonia. Formaldehyde (HCHO) and ammonia. UV-irradiation.	TiO_2/PVA with TiO_2 (2 wt %) reduced 99.3% of S. Aureus. TiO_2/PVA with TiO_2 (3 wt %) reduced 85.4% of K. pneumonia. TiO_2/PVA with TiO_2 (3 wt %) decomposed (HCHO) 40% (2h), 60% (4 h), and 80% (15 h). And TiO_2/PVA with TiO_2 (3 wt %) degraded ammonia 32.2% (2h)	[77]

2.2.4 Anti-cancer activities

Chemotherapy by TiO_2 is also a promising component to degrade cancer cells in medical applications. Many researchers have developed several techniques for drug delivery to destroy cancer cells, but due to chemotherapeutic agents habitually used, there still not be able to specify target of cancer cells[78]. In addition, chemotherapy for cancer treatment is still an attractive challenge to accumulate specific drug at tumor sites [79, 80]. For targeting of tumor, nanocarriers have been improved in

chemotherapy to control the delivery of anticancer drugs. An acceptable strategy to generate a target of tumor nanocarriers is to adapt the carrier to target ligands, such as antibodies [81], folate conjugates (receptor) [82, 83]. They can recognize and bind to the receptors' surface to express on cancer cells, to make specific uptake. Furthermore, the loaded drug sealed is very important to avoid the toxicity and side effects during flowing in bloodstream to reach tumor cells[84]. In addition, porous TiO_2 is one of the most efficiency photocatalyst, which has been reported to combine with anti-cancer drug [78].

Several reseachers have focused on cancer cells treatment by using various techniques. Table **2.5** lists some applications of TiO_2 for cancer cells treatment. Antibody–TiO_2 conjugation and electroporation was synthesized and used to kill LoVo cancer cells and TE353.sk normal cells under UV irradiation [85]. Pt/TiO_2 and Au/TiO_2 were fabricated via hydrolysis and photoinduced deposition method (metal-doped TiO_2). These particles were investigated to treat HeLa cells under UV-light condition [86]. The behavior of paclitaxel (PAC) drug delivery onto anti-cancer cell was investigated by using folate targeted PEGylated and TiO_2 nanoparticles (TiO_2-PEG-FA-PAC). The material was injected onto heptocellular carcinoma cells HepG2 cell and used MTT assay to measure cell viability. The result showed that HepG2 cells viability decrease while increase the concentration of TiO_2-PEG-FA-PAC[82].

Table 2.5: Applications of TiO_2 materials for cancer cells treatment processes.

TiO_2 catalyst	Method	Cells/Light source	Efficiency	Ref
Antibody–TiO_2	Electroporation treatment	LoVo cancer cells. UV light (253.7 nm). and (365 nm)	Almost 100% of LoVo was killed by using UV (253.7 nm) in 30 min and UV-(365 nm) in 90 min.	[85]
Pt/TiO_2 and Au/TiO_2	Hydrolysis of titanium iso-propoxide (TiO_2) and photoinduced deposition method (metal-doped TiO_2)	HeLa cells. UVA lamp 365 nm.	Pt/TiO_2 showed the surviving fractions of the cancer cells 70%, 36%, 20% and 15% at concentration of 25, 50, 100 and 200µg/mL, respectively. The Pt/TiO_2 has the higher efficiency than Au/TiO_2.	[86]
TiO_2-PEG-FA-PAC		Heptocellular carcinoma cells HepG2 cell	TiO_2-PEG-FA-PAC was more efficiency to inactivate cancer cells than TiO_2-PEG-FA- particles. The cell viability decreased while increased the catalyst dose	[82]

27

			1.953 to 1000 µg.mL^{-1}.	
TiO$_2$–PEG–FA–Dox (Doxorubicin)	Hydrothermal follow by sol–gel technique	Human fetal foreskin fibroblasts (HFFF2) and human breast cancer cells (SKBR3). UV-light (4×6 W)	Catalyst dose 1.25 g/L (FA/TiO$_2$=0.5) reduced cancer cells viability down to 5% and 30% of HFFF2 and SKBR3 respectively.	[87]

2.3 Applications of TiO$_2$/polymeric nanofibers

Most plastics have slow degradability or non-degradability and become major concerned problems for the environment. Applications of biopolymers are considered as one of effective ways to replace plastics, especially petroleum-based plastics, and also reduced plastics waste to the environment. Biopolymers have many positive points, such as biodegradability, non-toxic, reduced environmental waste, and easy to recycle [88]. Many applications of these biodegradable polymers are investigated and applied to several fields, such as food packaging, biomedical (drug release control, drug targeting), wound dressing, and agricultural product packaging.

Recently, TiO$_2$ composites polymers are of great interest, due to its unique dielectric and optical properties. For instance, nanofibers of TiO$_2$ deposited on polyamide were synthesized by using electrospun technique and follow by RF magnetron sputter coating[89]. Some applications of TiO$_2$-polymer nanofibers prepared via electrospinning technique are listed in Table 2.6. Poly(ethylene oxide) (PEO)/TiO$_2$[90], poly(acrylonitrile) (PAN)-multiwalled carbon nanotubes (MWCNT)-TiO$_2$[91], and TiO$_2$-poly(p-phenylene vinylene) (PPV) [92] were fabricated and investigated. Moreover, polyacrylonitrile (PAN)/TiO$_2$[93] and poly(acrylonitrile) (PAN)-multiwalled carbon nanotubes (MWCNT)-TiO$_2$ [94] were designed to degrade dye *rhodamine B* and *rhodamine 6G*, respectively under UV-light illumination. Nanofibers of polysolfone with TiO$_2$ (PSF/TiO$_2$) was synthesized and its efficiency as a filtrater to remove humic acid was examined[95]. To apply TiO$_2$ as a photocatalyst, fabrication of TiO$_2$-reduced graphene oxide (RGO)/nylon-6 [96] and TiO$_2$-tourmaline (TM)/nylon-6 [97] were used to degrade methylene blue, a model of an organic pollutant. Polystyrene and TiO$_2$ (PS/TiO$_2$) was synthesized by filling with poly (butylene succinate-co-adipate) (PBSA) matrices [98].

Table 2.6: Preparation of TiO$_2$/polymer nanofibers by electrospinning method and applications

TiO$_2$/ polymer	Method	Pollutants/Light source	Efficiency	Ref
poly(ethylene oxide) PEO/TiO$_2$	Electrospinning		Investigation fiber morphology (75–80 wt.% TiO$_2$)	[90]
Poly(acrylonitrile) PAN/MWCNT/TiO$_2$	Electrospinning multiwalled carbon nanotubes (MWCNT)			[91]
PAN/TiO$_2$ (polyacrylonitrile)	Electrospinning	Dye Rhodamine B. UV-365 nm, 15W	PAN/TiO$_2$ degraded 80% of dye in 38 h	[93]
PAN/MWCNT/TiO$_2$	Electrospinning	Dye rhodamine 6G, acetone, and fibers themselves. UV light (365 nm).	PAN/MWCNT/TiO$_2$ degraded R6G faster than PAN-TiO$_2$. Acetone was degraded by the presence of CNTs is more efficiency.	[94]
Polysolfone/TiO$_2$ (PSF/TiO$_2$)	Spinning method	Filtration experiment remove humic acid	Removal of humic acid is up to 91%.	[95]
TiO$_2$-PPV Poly(p-phenylene vinylene)	Electrospinning			[92]
TiO$_2$-RGO/nylon-6 (reduced graphene oxide RGO)	Electrospinning and hydrothermal treatment	Methylene blue. UV-365 nm.	P25-RGO/ nylon-6 were more efficiency than TiO$_2$/nylon-6 to degrade MB.	[96]
TiO$_2$-tourmaline (TM)/ nylon-6	Electrospinning process	Methylene blue 663 nm (MB). UV light (320–500 nm, Omnicure)	TiO$_2$-TM/nylon-6 has high efficiency to remove methylene blue compare to TM/nylon-6 and neat nylon-6 in 180 min.	[97]
poly(butylene succinate-co-adipate)- polystyrene /TiO$_2$ (PBSA–PS/TiO$_2$)	Electrospun	Degradability in soil (100 wt% moisture)	Pure PS fibers and PS/5%-TiO$_2$ had slower degradation rate. The higher TiO$_2$ content (15 and 25%) on fibers showed similar degradation as pure PBSA.	[98]
TiO$_2$/polyamide-6 (PA-6)	Electrospinning technique	Methylene blue 663 nm (MB). Ultra-Vitalux lamp 300W (5 mW/cm^2)	Degradation activity end-up with 84% after 2 h and tend to 99% after 6 h for post-functionalised sample.	[99]

2.3.1 **TiO$_2$-polylactide composites**

29

Polylactide (PLA) has become one of the most attractive commercial polymeric products. It has been applied for packaging, agriculture, electronic devices, automobile, textile, tissue engineering, wound dressing, drug delivery, and anti-microbial materials. Furthermore, PLA is biodegradable plastics with good properties, such as high mechanical properties, thermal plasticity, fabric ability, resistance to water, good transparency[13], biocompatibility (degrade to non-toxic components) [14], degradation in biological environment [15, 16]. Zhuang, W., et al suggested that improvement of PLA polymeric physicochemical properties by dispersion of nanoscale particles to form nanocomposites is promising and exhibites higher Young's molulus, higher thermal stability, and higher efficiecy for gas barrier properties than pure polymers. In addition, polymeric nanocomposites have more functions, such as antibacteria, biodegradability, and biocompatibility [100]. The composition of PLA and photosensitve TiO_2 particle, produce strong oxidizing oxygen species agent, performs as self degradation by attacking and cleavage the interfacial polymer chains under UV light activator. PLA-TiO_2 nanocomposites are higher photodegradable and biodegradable than neat PLA, due to some conditions. These materials are promising as packaging films to regulate oxygen-sensitive and barrier properties to extend shell-life of food products[11]. Importantly, these materials not only have ability to degrade bacteria, but also degrade toxic gases, aroma barrier, gases barrier and scavenger, and permeability properties. In this section, the application of PLA/TiO_2 nanocomposite films and fibers were specified on agricultural and epoxidation applications.

2.3.2 Applications of composites

Polylactide, a thermoplastic and aliphatic bio-polyester, is a biodegradable plastic with rigidity and transparency properties that is suitable for applications as packaging for food and agricultural products. In agricultural applications, biopolymer can be applied as mulching, hydromulching, seed coating, weed control, radiation control, and soil humidity control. PLA can increase soil temperature and extend the growing season in early spring time during late rainfall, and improve water consumption efficiency [101]. Notably, PLA has promising applications in

30

agricultural packaging products, especially harvesting fruits, vegetables, herbs, spices, crops, oils, fibers, and meats products. PLA has good barrier properties, such as aroma, flavor, oils, and greases. Furthermore, the barrier of PLA against small molecules, such as O_2 (oxidizing agent), CO_2, and H_2O are also a critical matter [102, 103].

According to the properties of PLA and TiO_2, synthesis of TiO_2 composite with polylactide nanofibers and films become more interesting, due to their improved optical, thermal, mechanical properties, antibacterial[100], high biocompatibility, large surface area [104], photocatalytic activity[105], and barrier properties[11]. There are several articles focused on synthesis of TiO_2/PLA by using various methods, as listed in Table 2.7. Poly(L-lactic acid)/TiO_2 nanocomposites was synthesized by using incorporating surface modified method with 1, 5 and 10 wt% TiO_2 contents. The photodegradation of pure PLA and PLA-TiO_2 films were investigated under UV-light and recorded the weight loss[13]. TiO_2/polylactide (PLA) nanocomposites with different contents of TiO_2 and PLA were fabricated via in situ polymerization method[100], solution casting method[14], hydrothermal in situ, electrospinnig technique[10], and twin-screw microcompounder [106]. Poly (lactic acid)/Anatase-TiO_2 (PLA/A-TiO_2) and PLA/Rutile-TiO_2 (PLA/R-TiO_2) were investigated their performance under UV illumination and mechanical properties testing [107]. Photodegradability of poly (L-lactic acid)/polyethylene/TiO_2 (PLA/PE/TiO_2) with TiO_2 nanospheres and nanotubes were examined [108].

Table 2.7: TiO_2/PLA nanocomposites synthesis technique and their applications.

TiO_2/ PLA	Method/ application	Pollutants	Efficiency	Ref
PLGA/TiO_2 foams	Thermally induced solid–liquid phase separation (TIPS). Tissue engineering scaffolds.	Immersion in simulated body fluid (SBF) for 28 day.	SBF resulted that the PLGA + 5wt% TiO_2 exhibited the formation of hydroxyapatite on surfaces.	[109]
PLA/ TiO_2	Incorporating surface modified method	Investigate of PLA degradation in air condition under UVA lamp: 340 nm.	PLA-TiO_2-5 had weight loss (13.3%) under UV light higher than PLA-TiO_2-1 (10.6%), PLA-TiO_2-10 (9.7%) in 4 days, and pure PLA in 11 days.	[13]
TiO_2/PLA	In situ	PLA and TiO_2/PLA	The degradation under UV-	[100]

31

films	polymerization method. Antibacterial activity	films were degraded under UV (315 nm) and soil-extraction solution. Antibacterial of S.aureus.	light and in soil-extraction solution of PLA was fast with TiO$_2$/PLA (10% TiO$_2$). TiO$_2$/PLA (3wt% TiO$_2$) showed the greatest antibacterial.	
PLLA/ TiO$_2$ /PVP/ ZnCl$_2$	Electrospinning method. Semi-occlusive wound dressings	S. aureus, E. coli, and diethylamine	TiO$_2$: PVP-I: PLLA ratio 2.3:1:5 and 2.3:2:5 reduced S.aureus 99.9%，E. coli 99.9% and made diethylamine fall from 2% down to 1.2%.	[105]
PLA/A-TiO$_2$ and PLA/R-TiO$_2$ films	Spin coating method and extrusion-injection. Anti-UV performance	Investigate performance under UV light (two lamps with 25W, 254nm, 200 mW/cm^2) and mechanical performance testing.	PLA/R-TiO$_2$ (thin films) good light shielding effects but PLA/A-TiO$_2$ (thin films) instability and quickly degraded. PLA/R-TiO2 (thick films) could not degrade and play the same rule as PLA/R-TiO$_2$ for anti-UV.	[107]
PLA/TiO$_2$ films	Solution casting method with TiO$_2$ (0.5, 1, 2, 5, and 10 wt %).	PLA degradation under UV (365 nm), hydrolytic, and enzymatic conditions.	PLA-10 was degraded with high yield under UV (190 h). PLA-10 showed high degradation in hydrolytic condition in 720 min. But, PLA-0.5 showed high enzymatic degradation in 126 h.	[14]
PLA/TiO$_2$ films		Degradation films using PBS buffer at pH 7.4	Increasing the TiO$_2$ contents have increased the degradation rate of PLA. The degradation decreased by increasing the crystalnity of PLA.	[110]
PLLA/TiO$_2$ thin films	In situ synthesized. Stability under UV light		TiO$_{2(anatase)}$ degraded PLLA chain to generate new carbonyl groups and other products. TiO$_{2(rutile)}$ acted as screening effect.	[111]
PLA/TiO$_2$ fibers	Hydrothermal in situ and Electrospinning. Antimicrobial activity and UV protection	S. aureus and E. coli under UV light irradiated 4 h.	PLA-Ti-90 (90 min hydrothermal treated) can reduce 70% bacterial growth.	[10]
PLA-TiO$_2$ films	Twin-screw microcom-pounder. Antimicrobial activity	Klebsiella pneumoniae and S. aureus	PLA-TiO$_2$ (5wt% PLA) exhibited no bacteria were detected.	[106]
PLA/PE/Ti O$_2$ nanospheres and		Photostability of the exposed films (xenon lamp with 300W, 100 mWcm-	TiO$_2$ nanospheres degraded nanocomposites film faster than TiO$_2$ nanotubes without negative effects.	[108]

32

PLA/PE/TiO$_2$ nanotubes		^{2}) and measure mechanical properties	PLA/PE/TiO$_2$ nanotubes vibrated PLA less than PLA/PE/TiO$_2$ nanospheres	
PLA/TiO$_2$ films	Casting method. Gas Barrier		Barrier properties of O$_2$ transmission rate were decreased when increased the TiO$_2$ contents.	[11]
TiO$_2$-PLA porous	Thermally induced phase-separation (TIPS). Bioactivity to the scaffolds		Scaffold mineralization by supersaturated Ca/P solution for 6h of PLA (1%) and PLA/TiO$_2$-10 (4%).	[112]

2.3.3 Catalysts for Epoxidation Application

Vegetable oils such as palm oil, sunflower oil, soybean oil, olive oils, or canola oil are fat or lipid compounds containing different amounts of unsaturated and saturated fats. Unsaturated fats components contain glycerol and triesters, fatty acid with the presence of one or more double bonds (olefinic bonds), in common form of triglycerides. These triglycerides undergo several reactions like epoxidation, hydroxylation, hydrogenation, halogenation, oxidation, carboxylation, isomerization, and acrylation by using catalysts, strong reactants, and vary conditions. Olefinic bonds present in vegetable oils (VO) are promising for epoxidation reaction, formation of epoxy group (oxirane), to valuable commercial products. The wide variety applications of epoxidation of VO have been reported such as diluents, lubricants, coatings, stabilizers and plasticizers for plastic, such as in PVC. Moreover, they are non-volatile compounds that can be used to replace phthalates, which shows adverse effect on human health, as plasticizers [113].

Epoxidation of VO by catalyst and peroxyacid is a promising method to increase the yield of olefinic conversion and selectivity. Several catalysts have been designed and investigated, in terms of activities and stabilities in epoxidation reactions, as listed in Table 2.8. For instances, Ti(IV)-grafted silica , Ti/SiO$_2$, Nb$_2$O$_5$–SiO$_2$, sulfated Ti-SBA-15, sulfated-SnO$_2$, and Ti-MCM-41 catalysts exhibited good activities and stabilities for epoxidation different olefins in organic carboxylic acids and hydrogen peroxides at various temperatures and times. The catalytic activities of Ti-grafted silica and Ti/SiO$_2$ showed with high yield conversion of FAME mixture [114], palm oil [113], and cotton seed oil [115]. The investigation of mechanism of

33

epoxidation was carried out by the reaction between peroxyacids (RCOO-OH), derived from reaction between carboxylic acid and hydrogen peroxide and play the role as oxygen carrier, and double bonds of unsaturated fatty acid. Equation 2.9 (A) shows the mechanism of performic acid formation by the reaction between formic acid and hydrogen peroxide [116]. Equation 2.9 (B) shows the palm oil structure, saturated fatty acid (palmitic acid) and unsaturated fatty acid (oleic and linoleic acids), and epoxidation reaction by Ti-grafted silica catalyst in mixture of performic acid reactants [113]. Because of the high activity of Ti compound in the catalyst, TiO_2/PLA fibers and films are hopeful for high degree of epoxidation of vegetable oils.

Table 2.8: Catalystic systems for epoxidation reactions.

Solid Catalyst	Liquid catalyst	Oils/ condition	Efficiency yield	Ref
Ti(IV)-grafted silica	Ethyl acetate and *tert*-butylhydroperoxide	FAME mixtures. At 363K and vary time 1, 3, 6 and 24 h	Ti–MCM-41 showed high conversion (C) and selectivity (S) of epoxidation of castor oil (C=97%, S>98%) or soya-bean oil (C=90%, S=56%) FAME mixtures.	[114]
Ti/SiO$_2$	(i) H$_2$O$_2$ and HCOOH (ii) H$_2$O$_2$, acetonitrile, and butyronitrile	Cotton seed oil. At 35 °C/3 h (i) and 35 °C/6 h under UV radiation (125 W) (ii).	Ti/SiO$_2$ in conditions (i) and (ii) showed with a high epoxide yield (100%).	[115]
Nb$_2$O$_5$–SiO$_2$	H$_2$O$_2$	Soybean oil. At 50 ºC/14 min and then increased to 180 ºC (20ºC/min)		[117]
Sulfated Ti-SBA-15	Acetic anhydride	Epoxy canola oil. 130 ºC/5 h.	SulfatedTi-SBA-15 (Si/Ti=10) exhibited 100% conversion of epoxy canola oil to esterified product.	[118]
Titanium-Grafted Silica	H$_2$O$_2$ and HCOOH	Palm oil. At 60 °C/5h	Ti-Si 0.5 epoxidized palm oil with 84% yield.	[113]
Sulfated-SnO$_2$	H$_2$O$_2$ and acetic acid	Canola oil. At vary temperatures 50, 60, 70, and 80 °C	Sulfated-SnO2 showed high conversion (100%) of canola oil in 6 h.	[119]
Nb$_2$O$_5$ /SiO$_2$	H$_2$O$_2$	Methyl oleate. At 80ºC/5 h	Commercial Nb$_2$O$_5$ and Nb*imp* (20wt% of Nb$_2$O$_5$) exhibited a good	[120]

34

			conversion about 70%	
Ti-MCM-41	Tert-butyl hydroperoxide (TBHP)	Cyclohexene. At 333 K/5 h	Ti-MCM-41 (8.95wt% of C) exhibited of olefin conversion 75% and selectivity close to 98%.	[121]
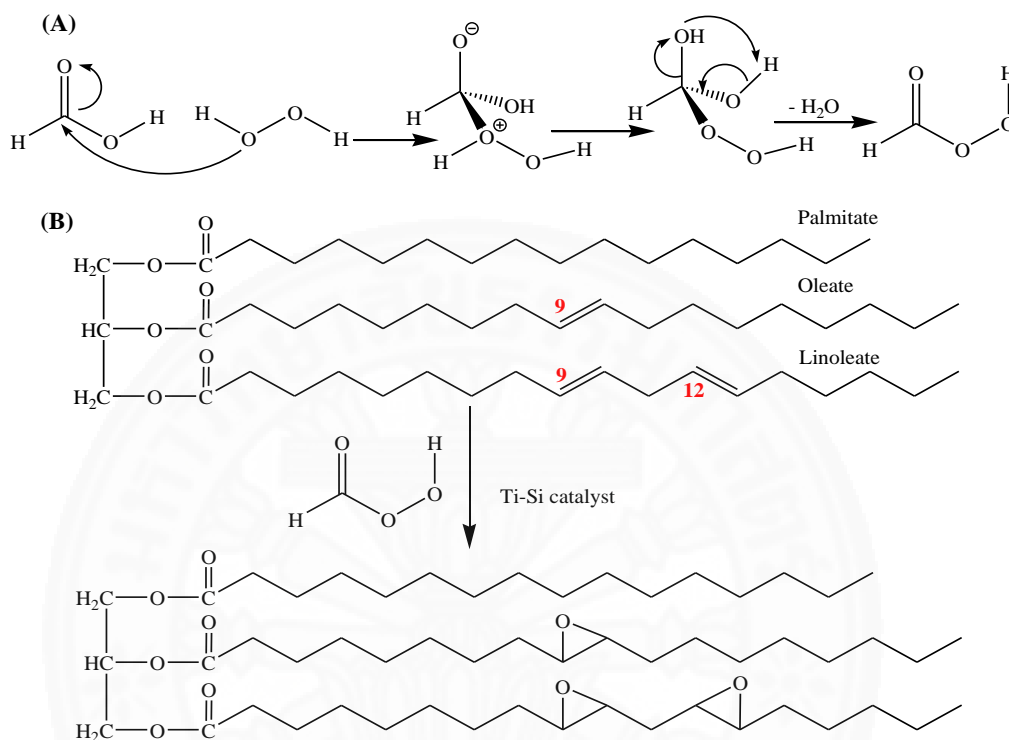
Equation 2.9: (A) The mechanism of performic acid formation [116]. (B) Epoxidation reaction of palm oil by Ti-grafted silica catalyst [113].

2.4 Electrospinning technique

Several researce on TiO_2/PLA preparation reported that many techniques have been used to fabricate nanocomposite films and fibers. For instance, electrospinning, solution casting, incorporating surface modified method, in situ polymerization, nanoprecipitation, sol-gel, spin coating, and hydrothermal in situ method, as shown in Table 2.7. Among these methods, electrospinning is the most promising method for polymeric nanofibers preparation. Modern nanotechnology of nanofibers has become attractive in applications, especially polymer nanofibers, such as high efficiency filters[95], biomaterials, wound bandage, drug delivery, sensors, photodegradation catalysts[96, 97, 99], and tissue engineering. In addition,

35

electrospinning technique has been considered as an interesting method because of its productivity is possible to control on structures, porosity, orientations and dimensions , such as one-dimensional (1D), two-dimensional (2D), and three-dimensional (3D)[122, 123].

Electrospinning is an advanced technique using electrostatic forces to generate fine fibers from polymer solutions. This technique is used to form fibers with thin diameter, nanometer or micrometer, with large surface area [124]. There are two types of electrospinning method, melt spinning and wet spinning. The melt spinning is done by heating the materials to melt for spinning, but the component of wet spinning is dissolved in a solvent system to make a solution that can be spun by applying high electrostatic voltage[125]. Figure 2.7 shows apparatuses and conditions that are applied in electrospinning process. In this process, the polymeric solution is pumped into a syringe with a small diameter spinneret (needle). Then, high voltage source is applied on solution droplet, makes the pendent liquid drop becomes charged, while solution is being sprayed on a collector. The drop has electrostatic repulsion force with surface tension charge and distort into conical object (Taylor cone). Continuously, liquid jet is stretched and the solvent evaporated that reduced the diameter of the jets to become very small in nano or micro scale fibers[126].
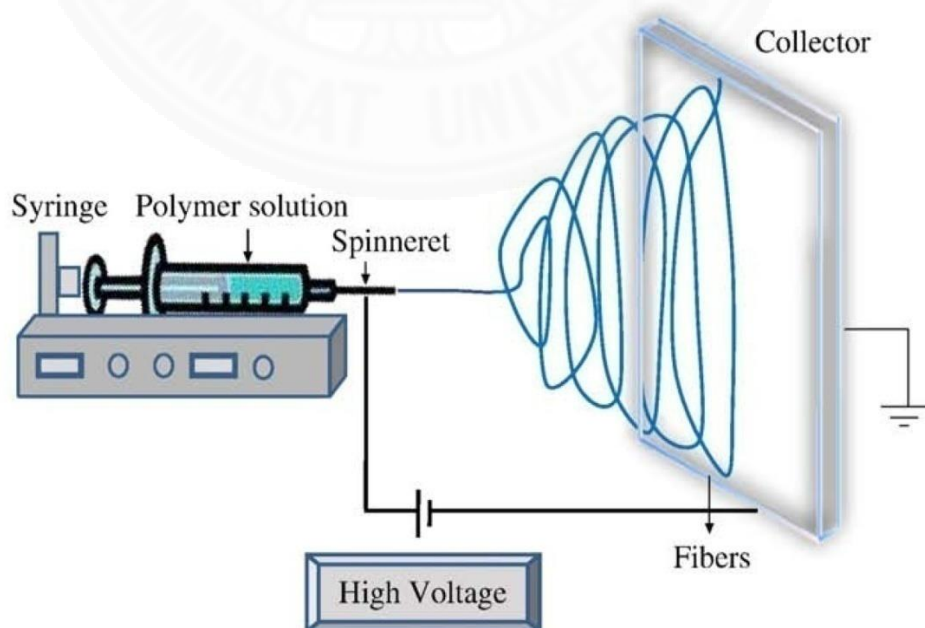
Figure 2.7: Electrospinning apparatus for the preparation polymeric nanofibers [124].

36

Chapter 3

Methodology

3.1 Part I: Preparation of PLLA-PVP-TTIP composite fibers

3.1.1 Materials

Poly(L-lactide) 4043D was supplied by NatureWork®. Poly(vinlylpyrrolidone) K29-32 (Mw=58,000 g/mol) and Titanium (IV) Isopropoxide, $Ti(OiPr)_4$ (TTIP), precursor (98$^+$ %) were purchased from Acros company. Chloroform RPE (>99%), N,N-Dimethyformamide (DMF) (99.8%), and Isopropyl alcohol (99%) (IPPA) solvents were purchased from Carlo Erba. Sodium dihydrogen phosphate monohydrate ($NaH_2PO_4.H_2O$) and disodium hydrogen phosphate heptahydrate ($Na_2HPO_4.7H_2O$) were supplied by Carlo Erba and PANREAC, respectively.

3.1.2 Preparation of polymer blends and composites

PLA/PVP blends were prepared by mixing PLA (0.84 g) and PVP at a ratio of 5:1 wt./wt., in chloroform (9 g), with stirring until completely dissolved. A TiO_2 precursor mixture was prepared from TTIP (200 μL), mixed with DMF (3 g) and IPPA (1.5 g), followed by adding of DI water (100 μL) drop wise. The mixture was stirred at room temperature for 1 h. IPPA was used to slow down the precipitation rate of TiO_2 particles. The polymer mixture was then mixed with the precursor mixture and stirred at room temperature for 1 h to generate suitable solutions for electrospinning. A summary of the samples compositions and sample names is listed in Table 3.1 and Figure 3.1.

Table 3.1: Summery of sample compositions and sample names.

Samples	PLA (g)	PVP (g)	TTIP (μL)	IPPA (g)
Neat PLLA	0.84	0	0	0
P-P-T	0.84	0.168	200	0
P-P-I-T	0.84	0.168	200	1.5

37
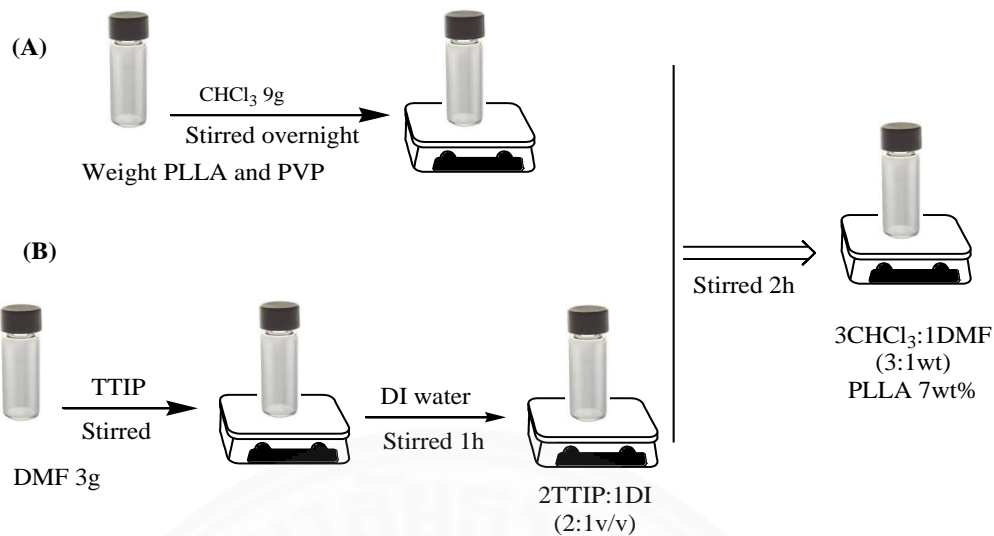
Figure 3.1: Overall preparation process of blended polymer mixture.

3.1.3 **Electrospinning set up**

The fiber mats were fabricated by an electrospinning technique. The composited mixture was placed in a syringe (capacity 3 mL) connected to a syringe-stainless needle. The syringe was placed on a flow controller (KD Scientific KD 100 Syringe Pump), with a flow rate of 1 mL/h. The distance between the collector and the needle tip was 15 cm. A voltage of 10 kV was applied by using a Gamma high voltage (0-40 kV) power supply. The electrospun fibers were gathered on an aluminum foil collector. The electrospinning apparatuses are listed in Table 3.2.

Table 3.2: Electrospinning apparatus.

Apparatus	Grade
High voltage power supply	Gamma high voltage (0-40 kV)
Flow controller	KD Scientific KD 100 Syringe Pump
Collector	Stainless steel
Syringe	3 mL
stainless steel needle	22×1½ mm

3.1.4 **Characterization**

Fourier Transform Infrared (FTIR) spectroscopy, equipped with an attenuated total reflectance (ATR) accessory (Nicolet iS5 Spectrometer), was employed to determine functional groups and interactions of the electrospun fiber mats. Scanning electron microscopy (SEM-SU8030) was used to investigate size and surface morphology of the samples. Energy-dispersive X-ray (EDX-SU8030) was employed to observe surface compositions of each component. A UV-Vis spectrophotometer (Genesys 10S) was uesed to examine the absorption behaviors of the fiber mats.

3.1.5 Degradation experiments

Degradation behaviors of the fiber mats were examined in phosphate buffer solutions (PBS) at pH 7.4 at ambient temperature. Neat PLA, P-P-T, and P-P-I-T fiber mats were cut into 2×2 cm^2. Each specimen was immersed into 50 mL PBS and placed at a 22 cm distance under UVA light (UVA 15WT8 lamp). The experiments were conducted for 6 days, and after that the specimens were removed from the solution and washed with DI water and dried at 40°C in a vacuum oven for overnight. FTIR and UV-Vis spectroscopy were used to examine the structures of the samples as a function of degradation time.

3.2 Part II: Preparation of PLLA-PVP-TiO$_2$ nanofibers

3.2.1 Chemical reagents

Poly(L-lactide) 4043D was purchased from NatureWork$^{®}$. Poly(vinlylpyrrolidone) K29-32 (Mw=58,000 g/mol) was supplied from Acros company. TiO$_2$ (>99.5%), particle size of 21 nm, was supplied by Sigma Aldrich. Chloroform RPE (>99%) and N,N-Dimethyformamide (DMF) (99.8%) solvents were purchased from Carlo Erba. Sodium dihydrogen phosphate monohydrate (NaH$_2$PO$_4$.H$_2$O) and disodium hydrogen phosphate heptahydrate (Na$_2$HPO$_4$.7H$_2$O) were obtained from Carlo Erba and PANREAC, respectively. Sunflower oil (SFO) (Big C sunflower oil) was used in epoxidation experiments. Formic acid (90%) and sodium carbonate anhydrous (99.8%) were supplied by AJAX. Hydrogen peroxide (35%) was purchased from Chem Supply.

3.2.2 **Preparation of PLLA/PVP blends**

Mixtures of PLLA (0.7g) and varied amounts of PVP, (PLLA/PVP ratios of 5:0 and 5:1), were prepared. TiO_2 particles, with average size of 21nm, were then added to each mixture at a constant weight composition of 5wt% of PLLA. The polymer mixtures were dissolved in chloroform (9 g) and stirred overnight at room temperature. After the mixture was completely dissolved, DMF (3 g) was added and further stirred at room temperature for 4 hours to generate suitable solution for electrospinning. Solution cast films of the mixtures were also prepared by casting the solutions on a glass surface, in which the solvents were evaporated at room temperature for 2 days, followed by vacuum drying for a week. Details on sample preparation are summarized in Table 3.3 and Figure 3.2.

Table 3.3: Summary on the samples preparation conditions.

Samples	PLLA (g)	PVP (g)	TiO_2 (g)	$CHCl_3$ (g)	DMF (g)
PLLA	0.7	0	0	9	3
PLLA/TiO_2 (5%)	0.7	0	0.0368	9	3
PLLA/PVP (5:1)/TiO_2 (5%)	0.7	0.14	0.0368	9	3
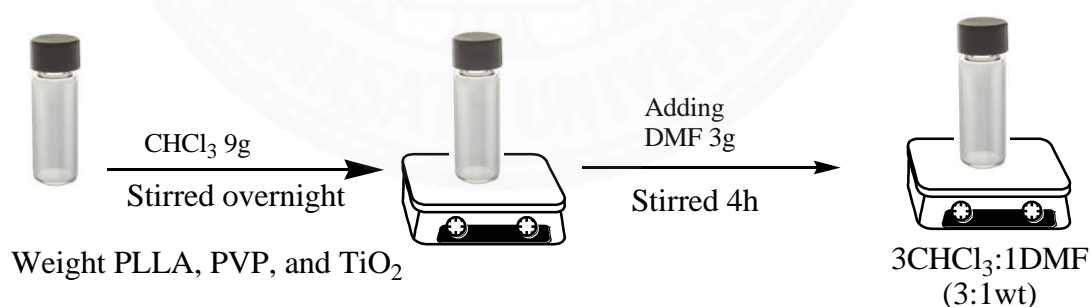
Figure 3.2: Preparation of PLLA/PVP/TiO_2 composites.

3.2.3 **Fabrication of electrospun fibers**

A horizontal electrospinning setup was employed to prepare nonwoven fibers. The electrospinning apparatus consists of a high voltage power supply (Gamma high voltage research 0-40 kV), a flow controller (KD Scientific KD100 Syringe Pump), an aluminum collector, a syringe (5mL), a stainless steel needle (22×1½ mm), and

40

aluminum foil. Essentially, the polymer mixture was pumped into a syringe connected with a stainless needle, at a flow rate of 1 mL/h. The distance between the needle tip and the collector was fixed at 15 cm, while the voltage was varied from 10-15 kV. The nonwoven fiber mats were collected on an aluminum foil connected to a ground electrode, as shown in Figure 2.7.

3.2.4 Characterizations

The electrospun fibers of PLLA/TiO_2 and PLLA/PVP/TiO_2 composites were characterized by Fourier Transform Infrared (FTIR) spectroscopy in an Attenuated Total Reflectance (ATR) mode on a Nicolet iS5 spectrometer. Each sample was recorded at 64 scans, with a resolution of 2 cm^{-1}. X-ray diffraction (XRD) spectroscopy was used to measure the crystalline characteristics of all fiber mats and solution cast film samples. The measurements were conducted on an X'Pert PRO spectrometer using the following conditions, Cu/K-alpha radiation (λ=1.54056 Å) at 40 kV, 30 mA, and a scanning rate of 2°/min from 2θ= 4° to 45°. Scanning electron microscopy (SEM-SU8030) and energy-dispersive X-ray (EDX-SU8030) were employed to measure surface morphology and surface composition of each component. A Genesys 10S UV-Vis spectrophotometer was used to observe the absorption characteristics of the fiber mats and phosphate buffer solution (PBS) obtained from degradation experiments of electrospun fiber samples.

3.2.5 Degradation experiments

The nonwoven fiber mats were cut into 2×2 cm^2 specimens for degradation experiments. Each specimen was pre-weighed (W_0) and placed in a beaker filled with 50 mL of PBS (pH 7.4) at room temperature. The buffer solution was prepared by mixing of $NaH_2PO_4.H_2O$ and $Na_2HPO_4.7H_2O$ using distilled water. The fiber specimens were immersed in PBS and irradiated with UVA light (UVA 15WT8 lamp, with wavelength 315-400 nm). The samples were placed at a 22 cm distance from the lamp. Each specimen was removed from the PBS solution at an interval of 1 day and washed with a large amount of distilled water to remove residue buffer solution. The

41

specimens were wiped with Whatman filter papers to remove surface water and then dried at 37°C until a constant weight (W_d) was reached. The experiment was conducted for duration of 7 days. The experiment set up is shown in Figure 3.3.
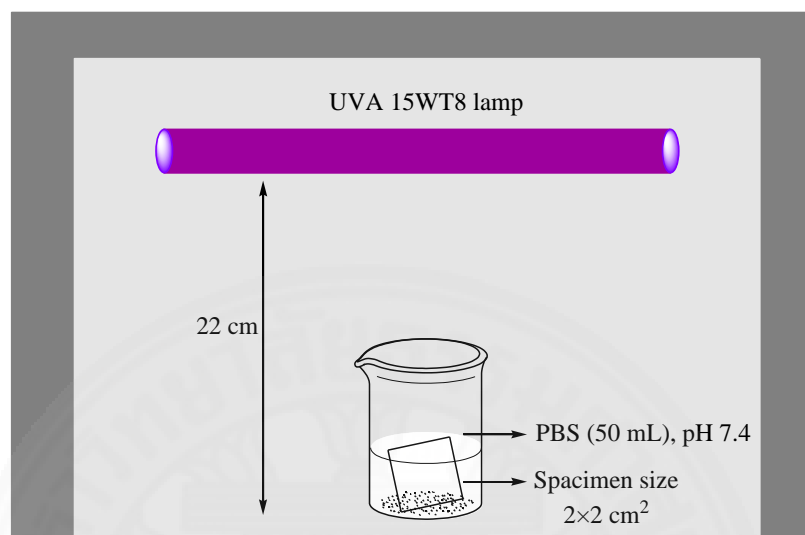
Figure 3.3: Self-degradation experiment in PBS solution at pH 7.4.

3.2.6 Epoxidation experiments

The nanofiber composites were applied as surface-enhanced catalyst in the epoxidation of sunflower oil (SFO) in the presence of formic acid and hydrogen peroxide. The reactions at room temperature (29-31°C) and 65°C are investigated. The fibers catalyst was added to the reaction flask containing the oil and formic acid. Hydrogen peroxide was, then, added drop wise with continuous stirring. The mixture was irradiated with UV light (254 nm), using a UV lamp Spectroline® (ENF-260C/FE) at 10 cm distance, and continued stirring for 3 h. The fiber catalyst was removed from the mixture, where the organic layer of the epoxidized oil was transfered to a separatory funnel. The epoxidized oil was washed with Na_2CO_2 (0.1M) solution for 3 times, followed by distilled water for 5 times, to remove residue aqueous phase. The organic layer was finally dried overnight at 65°C.

Effect of the contents of oxidizing agents and the use of nanofiber composites catalyst on efficiency of the expoxidation reaction was examined by varying the $HCOOH/H_2O_2$ ratios from 0.5/1, 0.75/1.5, and 1/2 mL. This was obtained by fixing the amount of SFO at 5 g and the amount of electrospun fibers at 10.8 g. The samples are denoted as follows: epoxidized sunflower oil is defined as ESFO, PLLA/TiO₂ 5%

42

(15kV) is defined as P-T, and PLLA/PVP (5:1)/TiO$_2$ 5% (15kV) is defined as P-P-T. The overall procedure is summarized in Table 3.4 and Figure 3.4.

Table 3.4: Summary on epoxidation conditions of sunflower oil (SFO).

Defined	Oil samples	Reagents		Fibers		Temp and Time
		HCOOH (mL)	H$_2$O$_2$ (mL)	P-T (mg)	P-P-T (mg)	UV (254 nm)
ESFO-0.5	SFO (5 g)	0.5	1	-	-	Condition 1: Room temp, 3 h
P-T-ESFO-0.5				10.8	-	
P-P-T-ESFO-0.5				-	10.8	
ESFO-0.75		0.75	1.5	-	-	
P-T-ESFO-0.75				10.8	-	
P-P-T-ESFO-0.75				-	10.8	
ESFO-1		1	2	-	-	Condition 2: 65°C, 3 h
P-T-ESFO-1				10.8	-	
P-P-T-ESFO-1				-	10.8	

Where:

Epoxidized sunflower oil is defined as ESFO.

PLLA/TiO$_2$ 5% (15kV) is defined as P-T.

PLLA/PVP (5:1)/TiO$_2$ 5% (15kV) is defined as P-P-T.

43

H$_2$O$_2$ (35%)

Na$_2$CO$_3$ 0.1M (10 mL 3 times) and
DI water (10 mL 5 times)

(a)

(b)

(c)

H$_2$O$_2$ drop wise

UV lamp
254 nm

10 cm

Oils sample (5 g)
Fiber (10.8 mg)
Formic acid (90%)

Stirred at 65°C

Stirred at 65°C, 3 h

Washing and separation
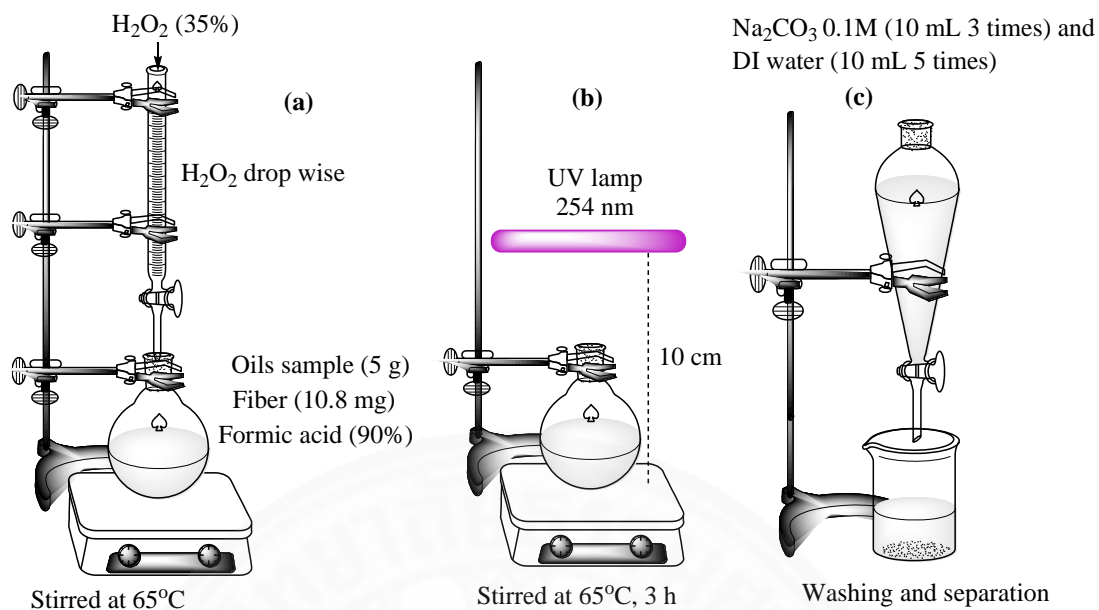
Figure 3.4: Epoxidation reaction of sunflower oil (SFO).

44

Chapter 4

Results and Discussion

4.1 Part I: Preparation of composite fibers

4.1.1 ATR-FTIR Spectroscopy

ATR-FTIR spectra of spun fiber samples of neat PLA, P-P-T, and P-P-I-T are shown in Figure 4.1. Band characteristics of PLA and PVP are observed, indicating the presence of the 2 components on a filament's surface. A strong band at 1753 cm^{-1} is assigned to the vibration of C=O of PLA chains, whereas that at 1659 cm^{-1} corresponds to the amide (N-C=O) vibration. Both P-P-T and P-P-I-T show similar FTIR spectra pattern. This reflects that the technique may not be able to differentiate the nature of the two samples. Nonetheless, a broad band centered at 3400 cm^{-1} (O-H stretching), observed in these 2 samples but not in neat PLA, indicates the presence of remaining isopropyl alcohol after the TiO$_2$ particle formation, and also bound water molecules due to the hygroscopic nature of PVP.

Band (cm^{-1})	Assignment
3400	ν O–H
2994	$\nu_{as}CH_3$
2944	ν_sCH_3
1753	νC=O
1659	νN–C=O
1453	$\delta_{as}CH_3$
1381	δC–H
1362	δ_sCH_3
1182-1087	ν C–O
870	ν C–C

Figure 4.1: ATR-FTIR spectra of fiber mats: (a) Neat PLLA, (b) P-P-T, and (c) P-P-I-T.

45

4.1.2 **Scanning Electron Microscopy**

Figure 4.2 shows surface morphology of P-P-T and P-P-I-T mats examined by SEM. Significant differences between the 2 samples are observed. Both sample mats show rough and irregular surface morphology, which is different from that of neat PLA, as reported earlier [127]. This is likely due to the interplay between the 2 polymeric components during electrospinning. Nonetheless, it is clearly observed that the surface of P-P-I-T fibers is smoother than that of P-P-T. The fiber mats of P-P-I-T show that embedded TiO_2 beads are more uniform than those in P-P-T, as the addition of IPPA slows down the TiO_2 precipitation rate. The regions of irregular fiber (beads) shape are caused by agglomeration of TiO_2 particles present as beads embedded in the filaments. This is confirmed by EDX results, as illustrated in Figure 4.3. The Ti content in the beads is very high, compared to that in the regular fiber region. The size distribution of the filaments is compared in Figure 4.4. The P-P-T fibers have an average diameter of 800 nm, slightly smaller than that of P-P-I-T (827 nm).
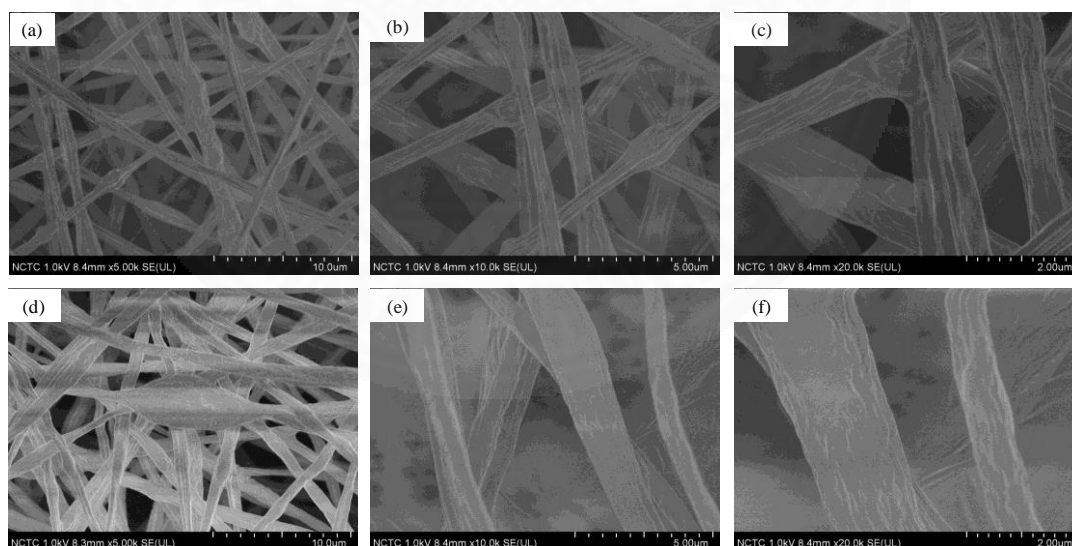
Figure 4.2: SEM images of electrospun fibers (a)-(c) P-PT and (d)-(f) P-P-I-T with 5,000×, 10,000×, and 20,000× magnifications.
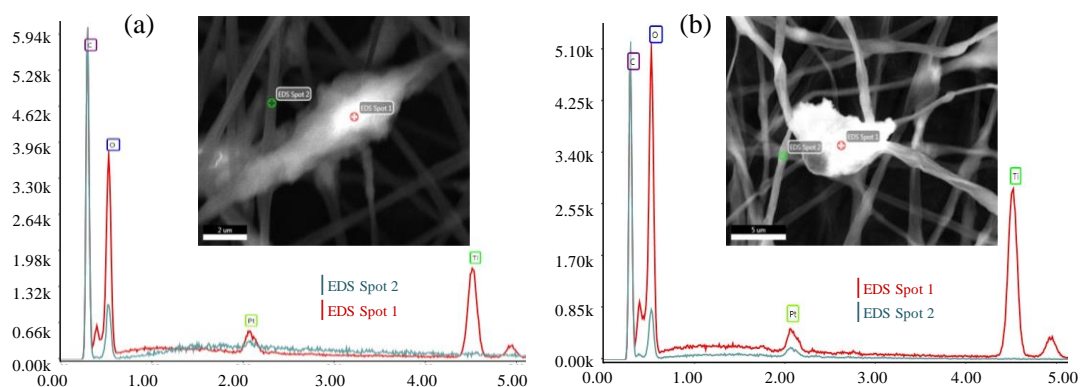
Figure 4.3: EDX spectra of bead defects with different sizes present in (a) P-P-T and (b) P-P-I-T fibers.
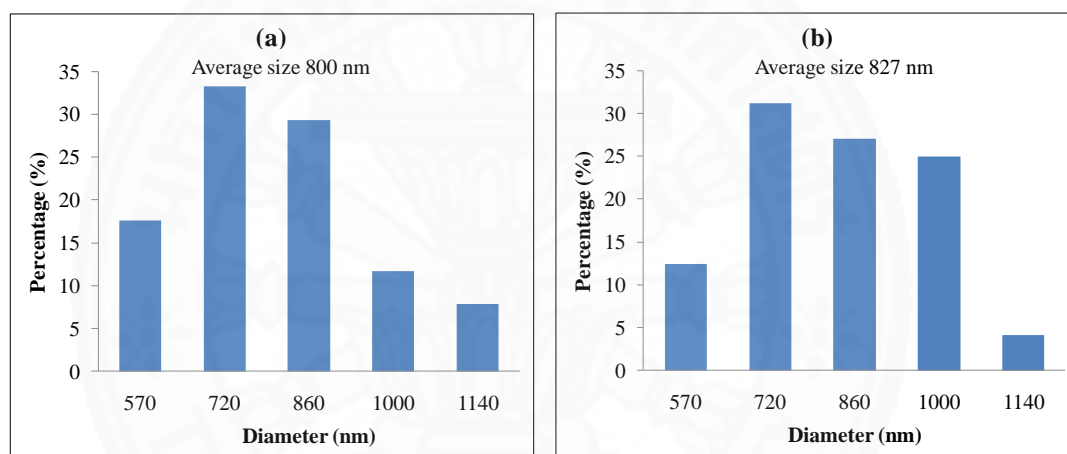
Figure 4.4: The size distribution of (a) P-P-T and (b) P-P-I-T fiber mats.

4.1.3 UV-Vis Spectroscopy

UV-Vis spectroscopy is used to examine absorption behaviors of the materials, as shown in Figure 4.5. P-P-T and P-P-I-T fibers show major absorption bands at λ_{max} 214 nm. This is due to the n→π* transition of the carbonyl groups in PLA, which is similar to that observed in spun fibers of neat PLA. All samples also show a broad absorption covering the full visible region, likely due to the opaque nature of the fiber mats. A distinct absorption band is observed at 300 nm for P-P-T and P-P-I-T fiber mats, indicating the presence of TiO_2 particles. This enables the materials to possess photo-catalytic activity for use in many applications, such as epoxidation of unsaturated oils or degradation of organic molecules in contaminated water.
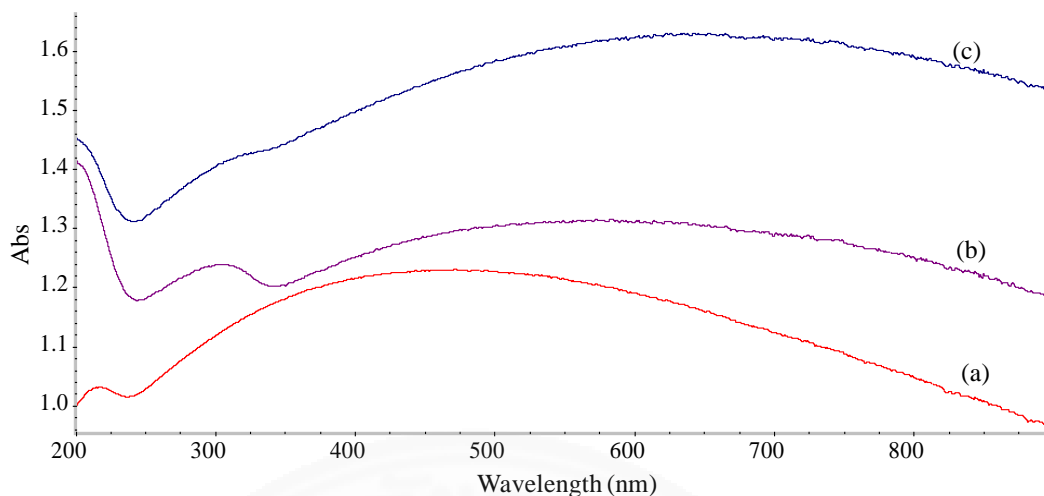
Figure 4.5: UV-Vis spectra of (a) neat PLLA, (b) P-P-T, and (c) P-P-I-T fibers.

4.1.4 Degradation mechanisms

Degradation behaviors of the spun fiber mats are examined in PBS solutions by activation with UVA light. The fiber samples were soaked in PBS at 1, 4, and 6 days, and their FTIR and UV-Vis spectra were recorded (Figure 4.6). ATR-FTIR and UV-Vis spectra show evidences of PLA degradation as a function of time, similar to those reported in our previous work [128]. Both P-P-T and P-P-I-T mats show similar FTIR changes, and the latter is chosen to show the changes. A decrease in intensity of the 1659 cm^{-1} band of the amide group of PVP reflects that during the degradation, PVP present on the surface of the filaments is released and dissolves in PBS solutions. However, a weak band in the same region is observed at 1650 cm^{-1}, associated with carboxylate of degraded PLA.

48
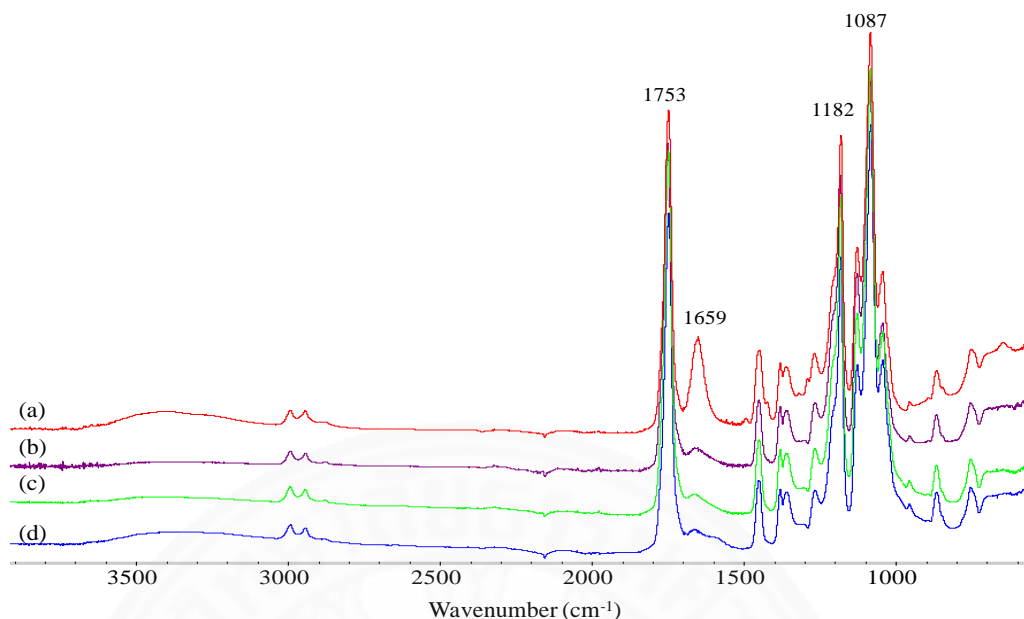
Figure 4.6: ATR-FTIR spectra of electrospun P-P-I-T (10 kV) fiber soaking in PBS solution at: (a) 0, (b) 1, (c) 4, and (d) 6 days.

Results from UV-Vis spectra of the PBS solutions after P-P-I-T fiber mats are soaked for 1, 4, and 6 days, as shown in Figure 4.7, illustrates an absorption band of lactate oligomers, products from the degradation of PLA, at 202 nm. The intensity of the band increases with the degradation time, indicating that degradation of the PLA component takes place very early. This is likely because of the presence of TiO_2 catalytic particles and the dissolubility of PVP from the filaments, which in turn, exposes the PLA component to a higher degree of hydrolysis.
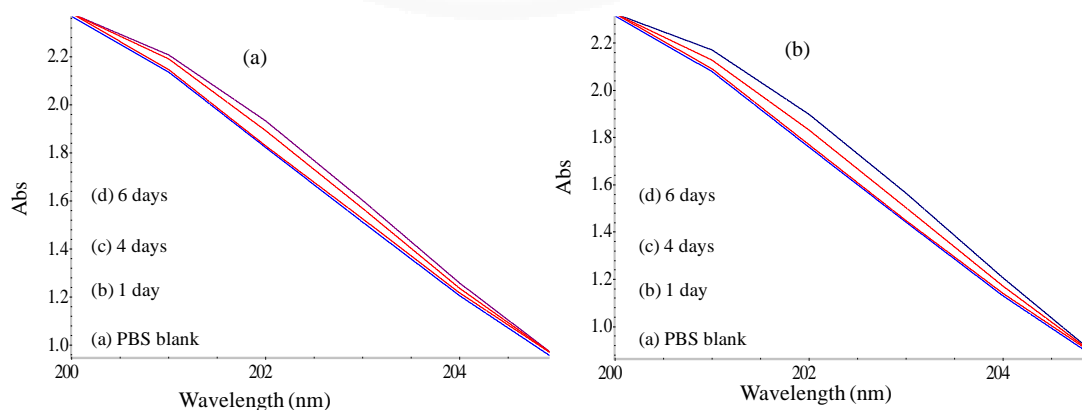
Figure 4.7: UV-Vis spectra of (a) P-P-T and (b) P-P-I-T fiber mats, as a function of degradation time from 1, 4, and 6 days.

49

4.2 Part II: Degradability and Activity of composite fibers

4.2.1 **ATR-FTIR spectroscopy**

Solution-cast films and electrospun fiber samples of PLLA/TiO$_2$ and PLLA/PVP (5:1)/TiO$_2$ are characterized by ATR-FTIR, as shown in Figure 4.8. The characteristic band at 3400 cm^{-1} corresponds to the stretching mode of -OH group. The bands at 2994, 2944, 1455, and 1359 cm^{-1} belong to vibration of –CH$_3$ asymmetric, –CH$_3$ symmetric, bending of –CH$_3$ asymmetric, and –CH$_3$ symmetric modes. The bands at 1753, 1652, 1381, 1182-1086, and 871 cm^{-1} are assigned to the vibration of υ(C=O), υ(N-C=O), C-H bending, υ(C-O), and υ(C-C), respectively [129]. The characteristic mode located at 920 cm^{-1} indicates the appearance of crystalline domains of PLA [130]. This band has high intensity in film samples, but disappears as a result from fibers formation, which reflects a complete amorphous nature. The vibrational mode of Ti-O-Ti is observed at 802 cm^{-1}, indicating the presence of TiO$_2$ particles on the fibers. The carbonyl stretching mode, υ(C=O), of film samples, shows two clearly separate bands at 1747 and 1755 cm^{-1}. This reflects semi-crystalline nature of the samples, in which the higher frequency band is associated with crystalline domain and the lower one is derived from amorphous region. In contrast, the corresponding mode of PLLA/TiO$_2$ and PLLA/PVP/TiO$_2$ fibers shows only 1 peak at 1753 cm^{-1}, as examined by 2nd derivative FTIR spectra, as shown in Figure 4.9. This indicates a complete amorphous nature of the samples.
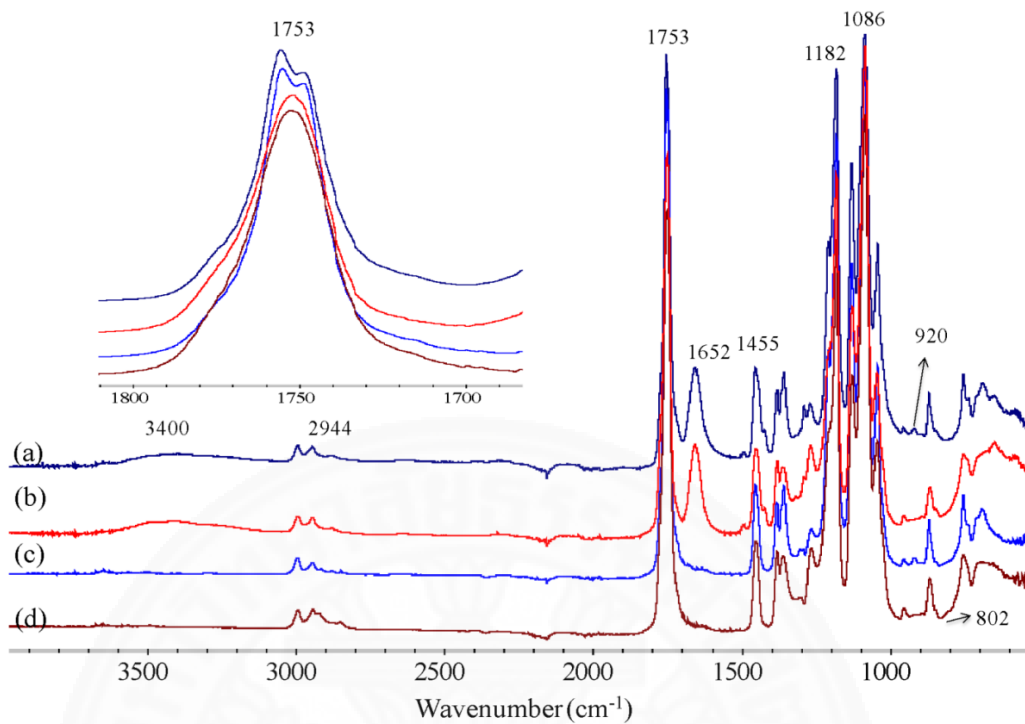
Figure 4.8: ATR-FTIR spectra of PLLA/PVP (5:1)/TiO$_2$: (a) film and (b) 15 kV fiber, and PLLA/TiO$_2$: (c) film and (d) 15 kV fiber.
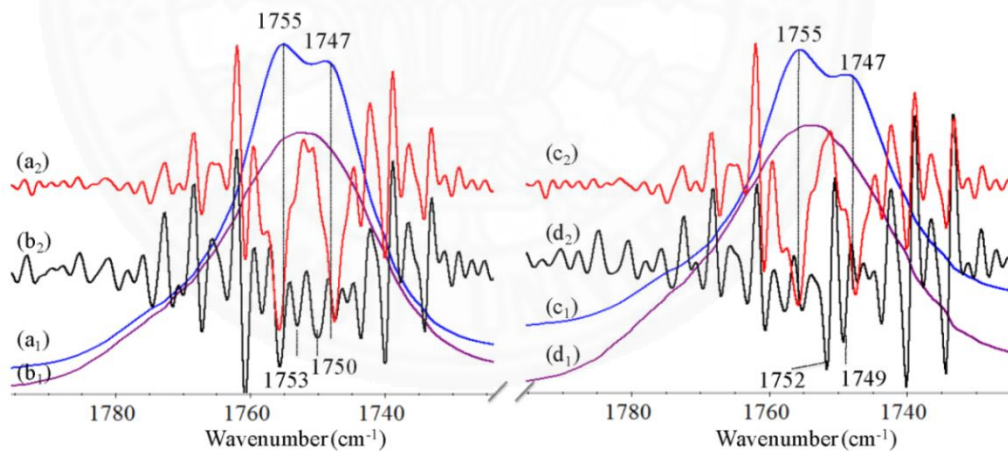
Figure 4.9: 2nd derivative ATR-FTIR spectra of PLLA/TiO$_2$: (a$_1$) & (a$_2$) film and (b$_1$) & (b$_2$) 15 kV fiber, and (c$_1$) & (c$_2$) PLLA/PVP (5-1)/TiO$_2$: (c$_1$) & (c$_2$) film and (d$_1$) & (d$_2$) 15 kV fiber.

4.2.2 **X-Ray Diffraction (XRD)**

XRD spectra of solution-cast films and fiber samples are shown in Figure 4.10. Signals at 2θ= 14.9º, 16.8º, 19.1º are observed in the spectra of film samples,

51

corresponding to crystalline planes (010), (110/200), and (203) of PLA, respectively. The sharpest peak at 2θ=16.8° and the peak at 2θ=19.1° reflect orthorhombic lattice of the α-form [11, 112]. The electrospun fiber samples, however, show only a broad signal covering a 9-22° region, reflecting complete amorphous domains of PLLA. Both samples either containing PVP or without PVP show similar characteristic spectra. The solution cast samples show only characteristic signals of PLA, reflecting that the PVP minor phase cannot form its separate crystalline domains. A slight shift in 2θ value is observed in the signal of (200)/(100) planes at 16.8°, indicating an interruption of PLA's crystalline structure by the presence of PVP.

During the electrospinning process, the voltages are varied from 10 to 15 kV and the resulting fiber's XRD spectra. These conditions affect on the crystalline formation. Higher potentials break down surface tension of the blended polymer solution, especially hydrogen bonding and molecular charge interaction more effectively, leading to refolding fibers mats come through the needle tip. In addition, the rearrangement of polymer chains during electrospinning, fiber formation, is quite difficult to get well folding. The small peak located at 2θ=25.4° is associated with crystalline characteristic of TiO_2 nanoparticles [112]. This peak appears with high intensity for film samples, but with lower intensity for electrospun fibers.
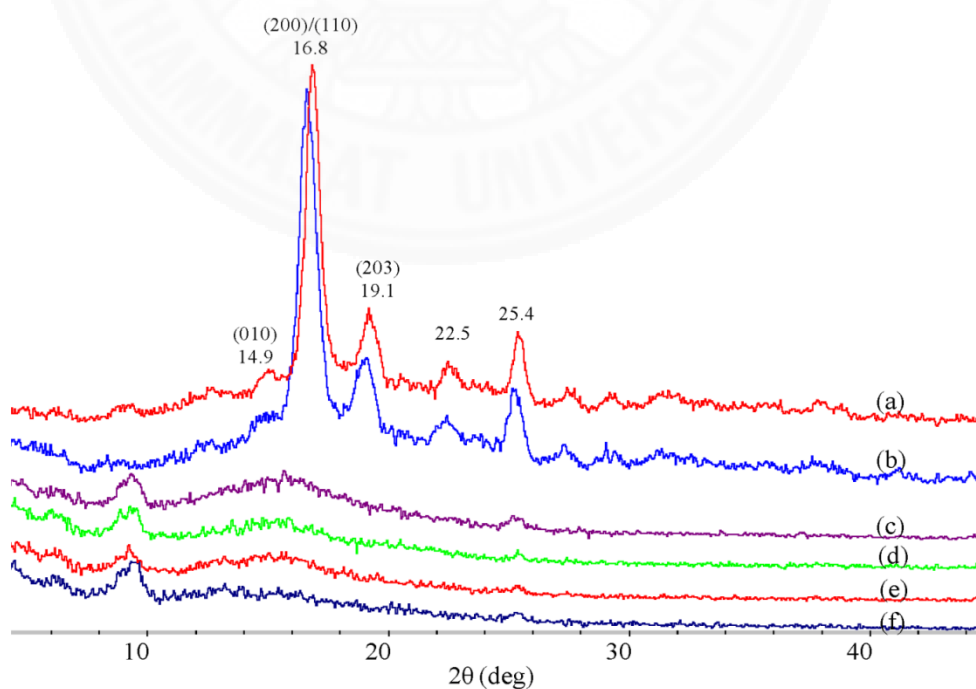
Figure 4.10: XRD spectra of (a) PLLA/PVP (5:1)/TiO$_2$ films, PLLA/TiO$_2$: (b) film, (c) 15 kV, (d) 13 kV, and (e) 10 kV, and (f) PLLA/ PVP (5:1)/TiO$_2$ (15 kV) electrospun fibers.

4.2.3 SEM and EDX surface composition

Surface morphology of electrospun composited fibers is examined by SEM, as shown in Figure 4.11. Smooth fibers containing several beads are obtained. The electrospinning operation at 10 kV produces fibers with more beads than those at 15 kV. The surface of fibers of PLLA/TiO$_2$ blends either with or without PVP electrospun at 15 kV is more uniform than those at 10 kV. TiO$_2$ nanoparticles present as beads on the filaments, especially in the region of irregular fiber shape, as clearly seen in Figure 4.12. It is noted that most of bead defects with bigger size is not caused by the agglomeration of TiO$_2$ particles. This is confirmed by EDX results, as shown in Figure 4.13, in which the different percentage Ti contents in the fine fiber region is higher than that of the beads defects. Figure 4.14 shows the average diameter and size distribution of the electrospun nanofibers of PLLA/TiO$_2$ (10 kV), PLLA/TiO$_2$ (15 kV), PLLA/PVP (5:1)/TiO$_2$ (10 kV), and PLLA/PVP (5:1)//TiO$_2$ (15 kV). The average sizes of corresponding fibers are 754 nm, 686 nm, 759 nm, 980 nm, reflecting that an increase amounts of PVP leads to an increase in the size of the electrospun fibers.
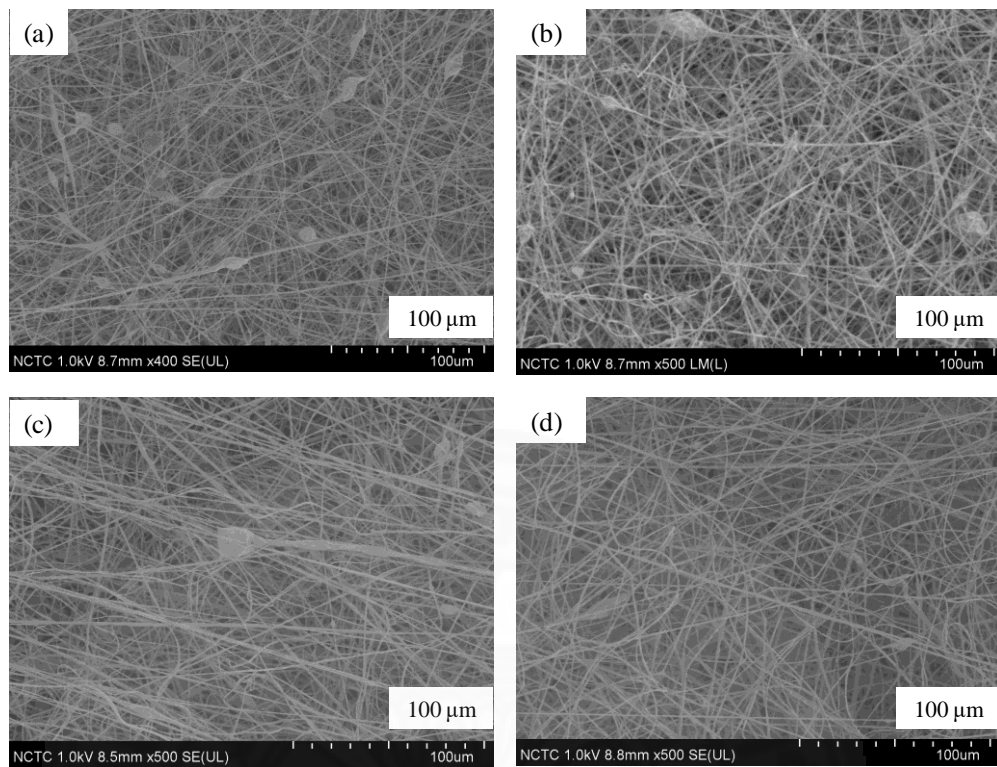
Figure 4.11: SEM images of electrospun fibers of (a) PLLA/TiO$_2$ (10 kV), (b) PLLA/TiO$_2$ (15 kV), (c) PLLA/PVP (5:1)/TiO$_2$ (10 kV), and (d) PLLA/PVP (5:1)/TiO$_2$ (15 kV), at 500× magnification.

54
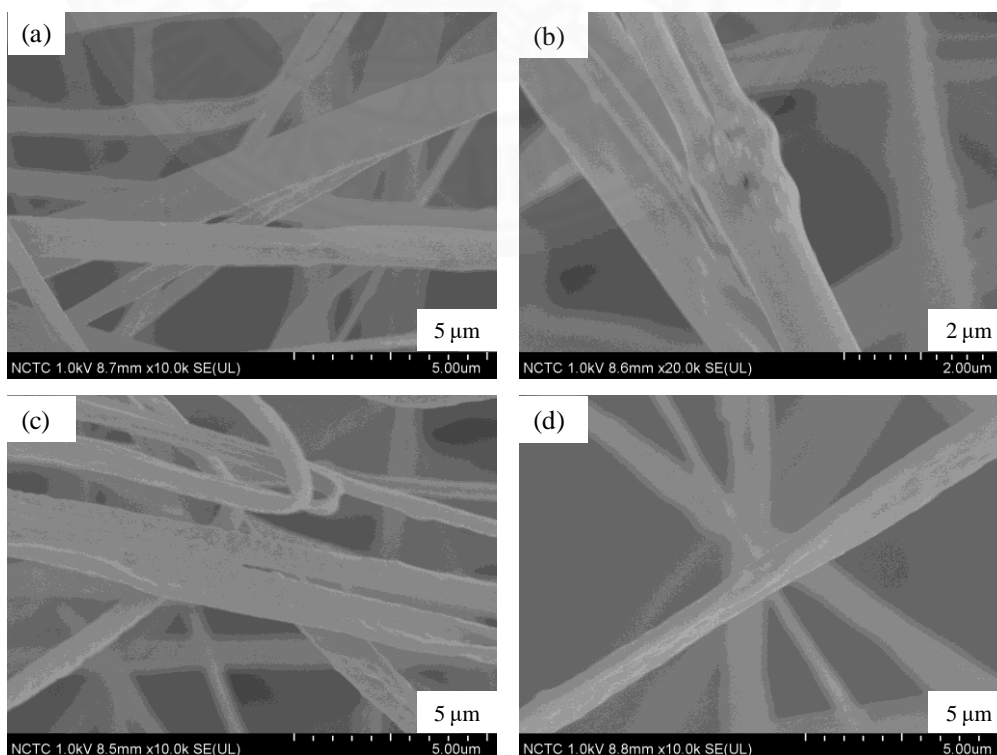
Figure 4.12: SEM images of electrospun fibers of (a) PLLA/TiO$_2$ (10 kV), (b) PLLA/TiO$_2$ (15 kV), (c) PLLA/PVP (5:1)/TiO$_2$ (10 kV), and (d) PLLA/PVP (5:1)/TiO$_2$ (15 kV).
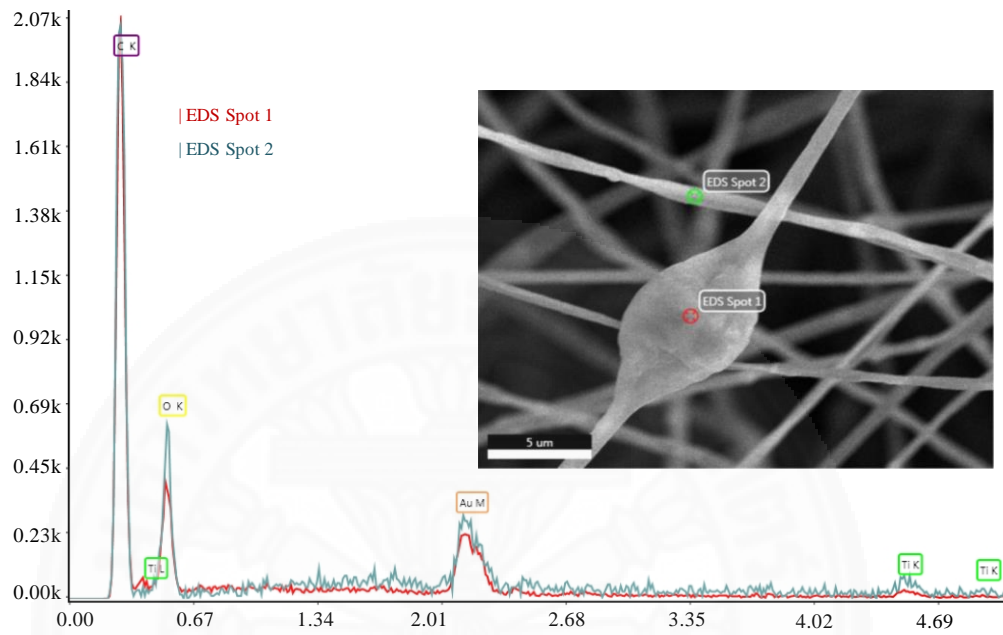
Figure 4.13: EDX spectra of bead defects with different sizes present in PLLA/PVP (5:1)/TiO2 (15kV) electrospun fibers.
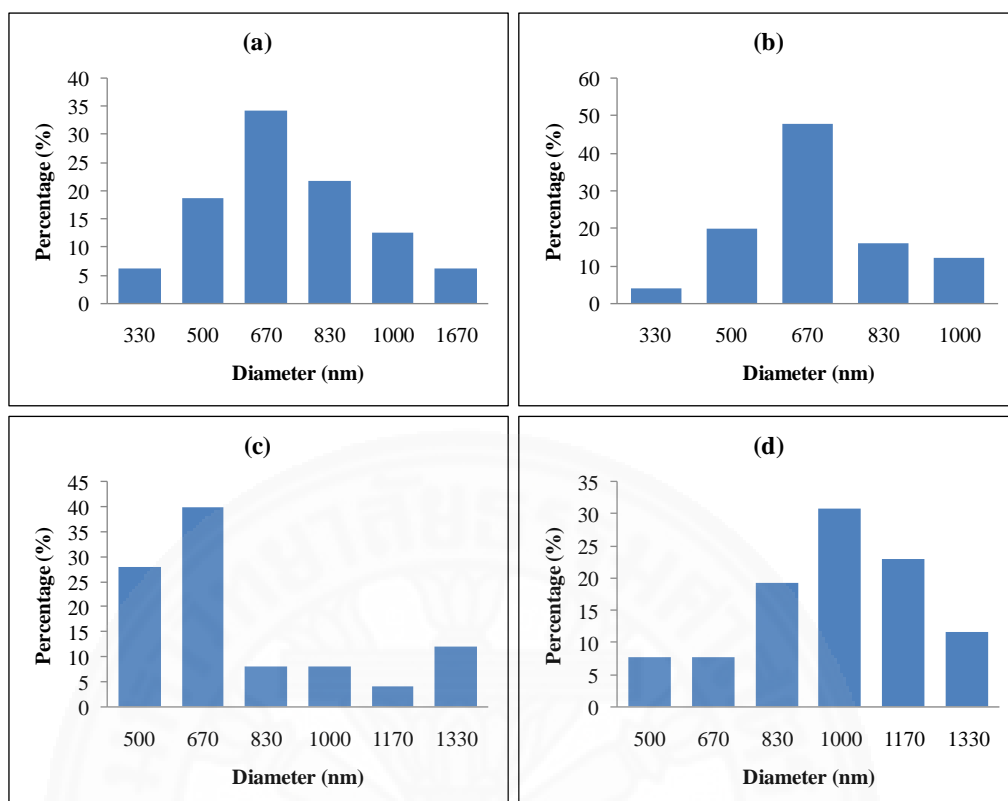
Figure 4.14: The size distribution of different electrospun nanofibers: (a) PLLA/TiO$_2$ (10 kV), (b) PLLA/TiO$_2$ (15 kV), (c) PLLA/PVP (5:1)/TiO$_2$ (10 kV), and (d) PLLA/PVP (5:1)/TiO$_2$ (15 kV).

4.2.4 **UV-Vis spectroscopy**

To validate the presence of TiO$_2$ particles on the spun fiber mats and examine the absorption behaviors of the materials, UV-Vis spectroscopy is employed, as shown in Figure 4.15. Neat PLLA, PLLA/TiO$_2$, and PLLA/PVP (5:1)/TiO$_2$ fibers fabricated at 15 kV show λ_{max} in the region below 200 nm. The corresponding fibers containing TiO$_2$ particles show a UV absorption in the region of 200-380 nm. This reflects the unique activity of the embedded TiO$_2$ particles, which should affect self degradation and catalytic efficiency of the fiber materials when UV light activator is employed.

Ref. code: 25595722040788ISO
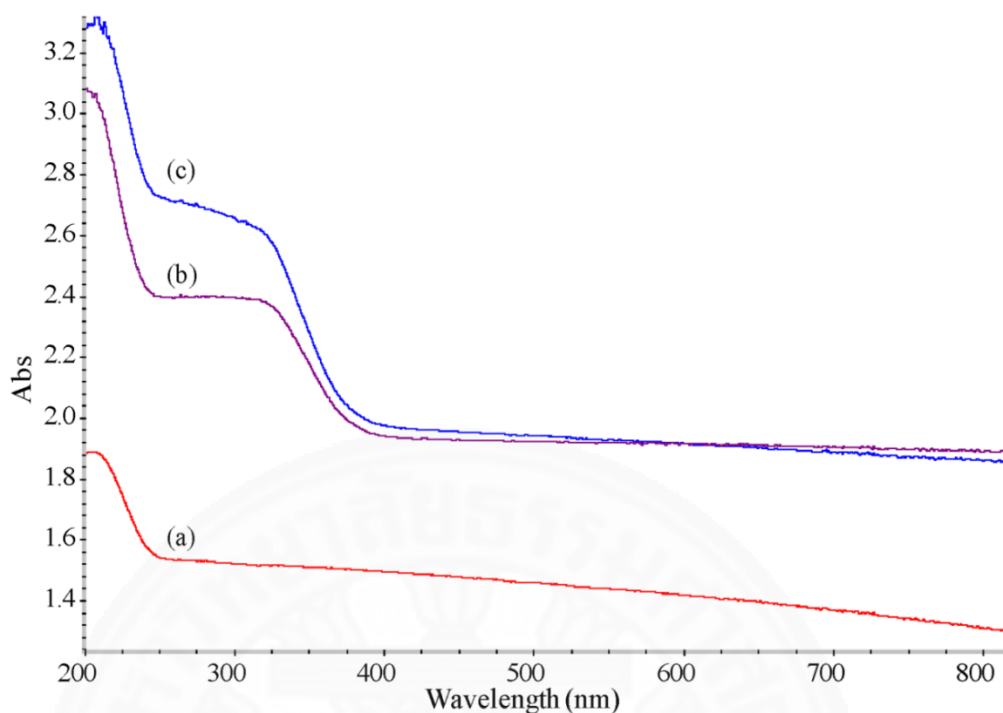
Figure 4.15: UV-Vis spectra of electrospun fibers of (a) neat PLLA (15 kV), (b) PLLA/PVP (5:1)/TiO$_2$ (15 kV), and (c) PLLA/TiO$_2$ (15 kV).

4.2.5 Degradation mechanisms

Degradation behaviors of the spun fibers are examined in PBS solutions by activating with a UVA lamp. Figure 4.16 shows FTIR spectra of PLLA fiber mats after soaking in PBS solutions at 1, 4, and 7 days, respectively. It is observed that the puffy fibers break down to small pieces and precipitated at the bottom of the container. These small pieces of fibers are, therefore, centrifuged and separated from the PBS solution. FTIR spectra of the collected materials show a disappearance of the peak at 1652 cm^{-1}, the vibration of υ(N-C=O) of PVP, compared to the original sample. This reflects the dissolution of the water-soluble PVP component from the fiber mats. An increase in the degree of degradation of PLA, as a function of time, is observed in the increase in intensities of broad bands covering 1605 cm^{-1}(C=O stretching of -COO$^-$) and 3400 cm^{-1}(–OH stretching of carboxylic acid end groups), and a sharp but weak band at 1724 cm^{-1} (C=O stretching of carboxylic acid). This indicates a conversion of ester bonds to carboxylic acid and carboxylate end groups as a result form chain scissions[131].

57

UV-Vis spectra of the remaining PBS solutions after degradation of PLLA/PVP (5:1)/TiO$_2$ (15 kV) are examined. The absorption of PLLA reported at the region of 200 nm. Figure 4.17 shows the trend of PLLA cleaving chain and absorb at the region of 202 nm. The absorption intensity of PLLA correlates with the duration of the degradation. The degradation at 7 days shows higher intensity than at 6, 5, 4, 3, 2, and 1 day, respectively. Figure 4.18 shows the absorption spectra of PBS solutions at 1, 4, and 7 days. These samples significantly absorb at region 235 nm, in which corresponding to absorption behavior of TiO$_2$ particles.

Figure 4.19 shows SEM images of the sample at 1 day and 4 days. This confirms that the surface morphology of fibers after degradation become rugged. The fiber strings break down to small fragments. It is noted that longer duration of degradation leads to higher number of small fragments. EDX is also applied to verify the components of samples after 1 day. For PLLA/PVP (5:1)/TiO$_2$ (15 kV) specimens, as shown in Figure 4.20, the smooth fiber area show a very low Ti content, compared to the bead defect area. This strongly indicates that TiO$_2$ nanoparticles are encapsulated by the polymer matrix in the bead region. After degradation experiments, these particles are released from the core beads.
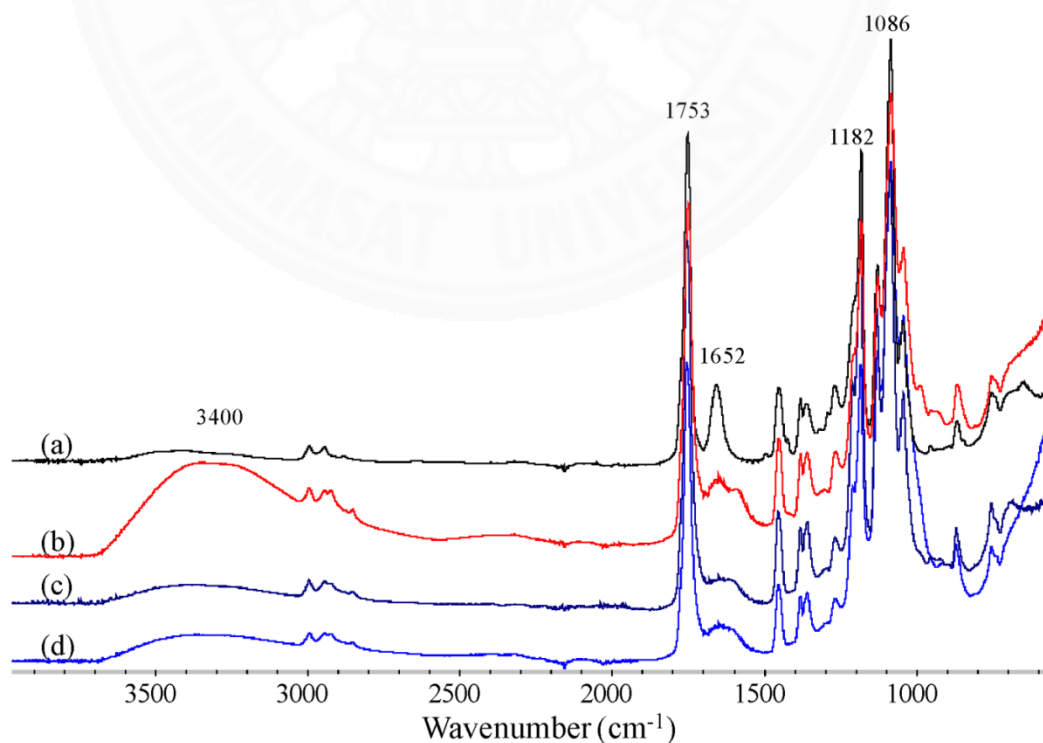
Figure 4.16: ATR-FTIR spectra of PLLA/PVP (5:1)/TiO$_2$ (15 kV) fibers as a function of degradation time, in PBS solution under UVA light at: 0 (a), 1 (b), 4 (c), 7 (d) days.
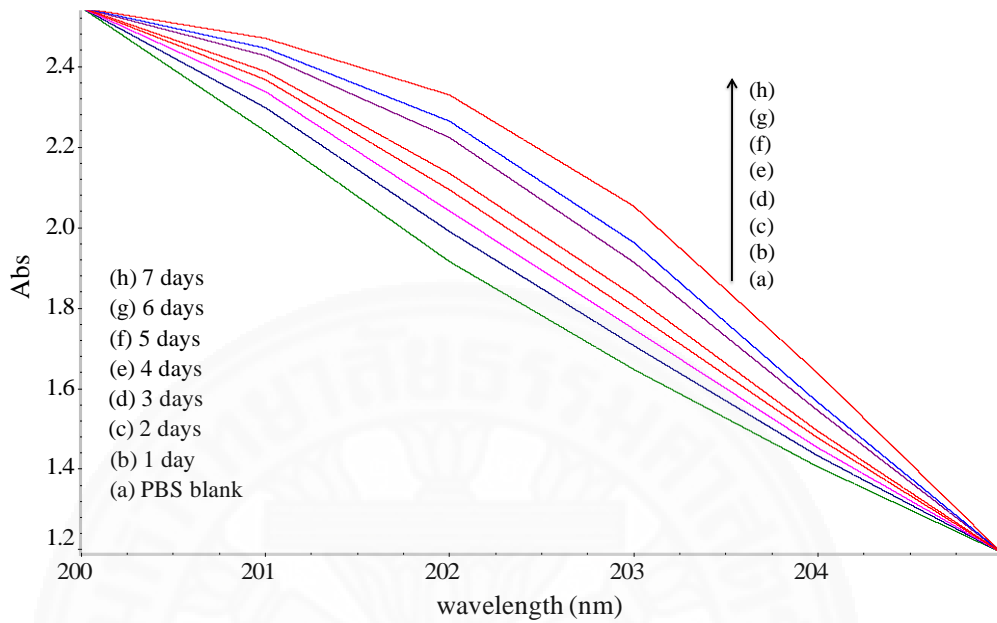
Figure 4.17: UV-Vis spectra of PBS solution of PLLA/PVP (5:1)/TiO$_2$ (15 kV) after degradation from 1-7 days.
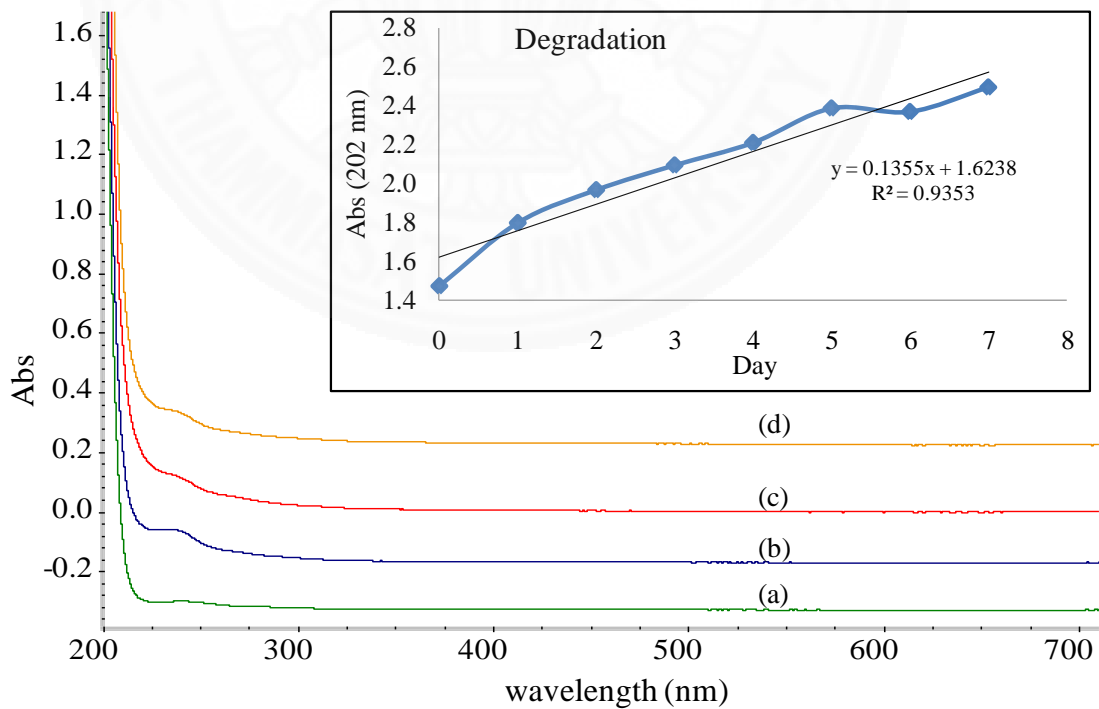
Figure 4.18: UV-Vis spectra of degradation results of PLLA/PVP (5:1)/TiO$_2$ (15 kV) in PBS solution under UVA light: PBS (a), 1 (b), 4 (c), and 7 (d) days.

59
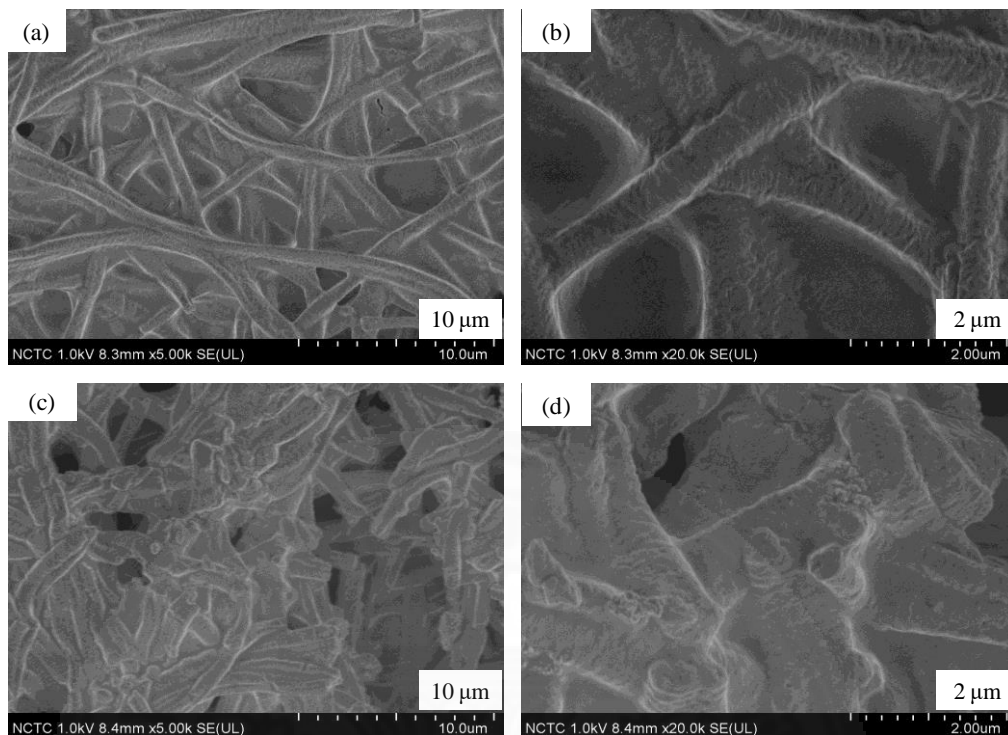
Figure 4.19: SEM images of degraded of PLLA/PVP (5:1)/TiO$_2$ (15 kV) in PBS solution under UVA light at 1day, (a)-(b), and 4days, (c)-(d).
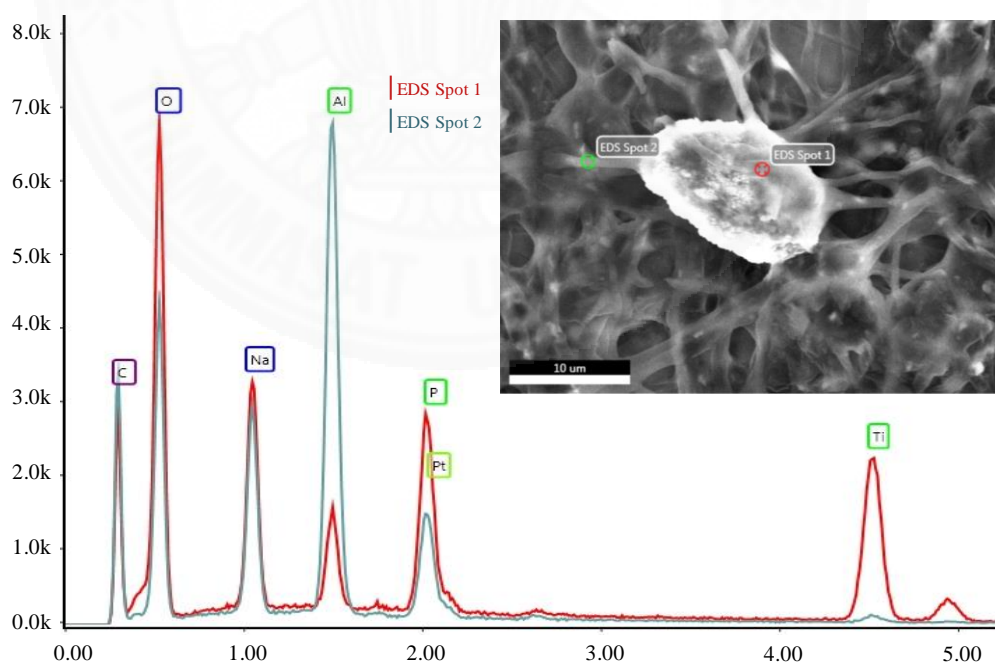
Figure 4.20: EDX spectra of bead defects with different sizes of PLLA/PVP (5:1)/TiO$_2$ (15 kV) electrospun fibers after 1 day of degradation in PBS under UVA light.

60

4.2.6 **Epoxidation of sunflower oils (SFO)**

The resulting electrospun fibers are employed as a surface-enhanced catalyst in the epoxidation reaction of SFO. HCOOH/H_2O_2 oxidizing agents are employed, whose content per 8 g of SFO are varied: 0.5/1, 0.75/1.5, and 1/2 mL. The epoxidized SFO products obtained without the fiber catalyst is denoted as ESFO-x, where x indicates the HCOOH content. The corresponding products obtained with the application of the fiber catalyst are coded as P-T-ESFO-x or P-P-T-ESFO-x. Efficiency and mechanisms of the reactions conducted at room temperature and at 65°C are evaluated. ATR-FTIR spectra of SFO and its epoxidized ESFO derivatives are compared Figure 4.21. Changes in band intensity are observed at 3007 cm^{-1} (olefinic C–H stretching), 2923 and 2853 cm^{-1} (aliphatic's $\nu_{as}CH_2$ and ν_sCH_2 stretching), 1741 ($\nu_{as}C=O$), 1465 (δ_sCH_2), and 1160 cm^{-1} ($\nu_{as}C–O$)[132].
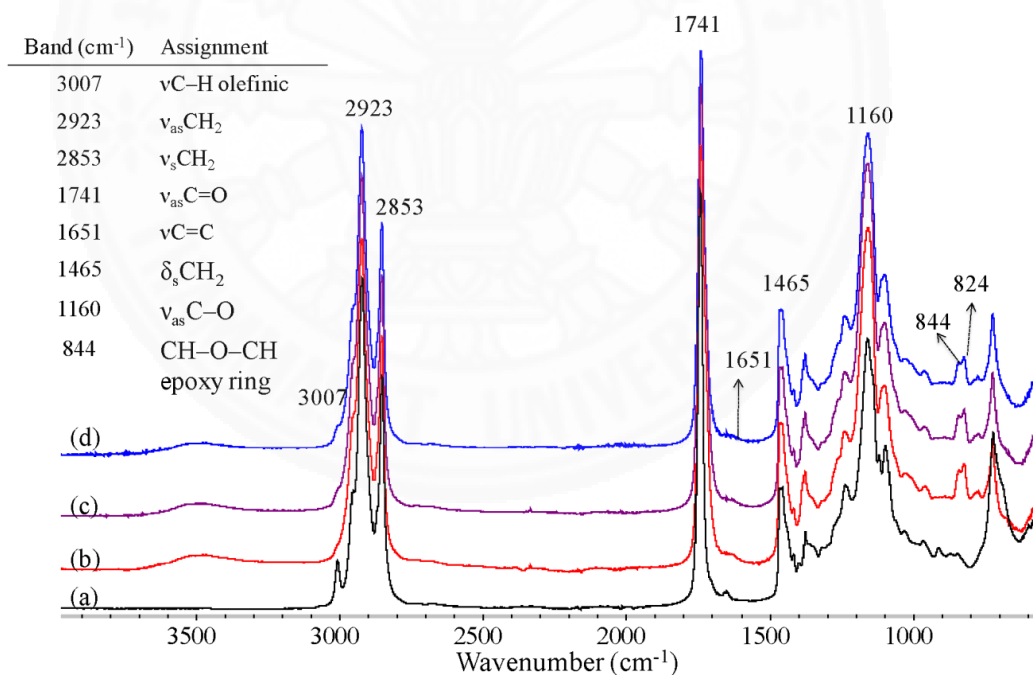
Figure 4.21: ATR-FTIR spectra of: (a) sunflower oil (SFO), (b) ESFO-1, (c) P-T-SFO-1, and (d) P-P-T-SFO-1 epoxidized at 65°C.

The mechanisms of the reaction are proposed in Figure 4.22, in which perfomic acid, generated from the reaction between formic acid and hydrogen peroxide, plays a key role as an oxygen carrier for the epoxidation process. The

61

formation of epoxide groups in the ESFO structure is confirmed by the presence of new characteristic FTIR bands at 844 and 824 cm^{-1} (C–O–C). In contrast, a decrease in intensity of the olefinic stretching mode at 3007 cm^{-1} also indicates the conversion of the double bonds to epoxide groups. The changes in intensity of these modes can be employed in the measurement of reaction efficiency.
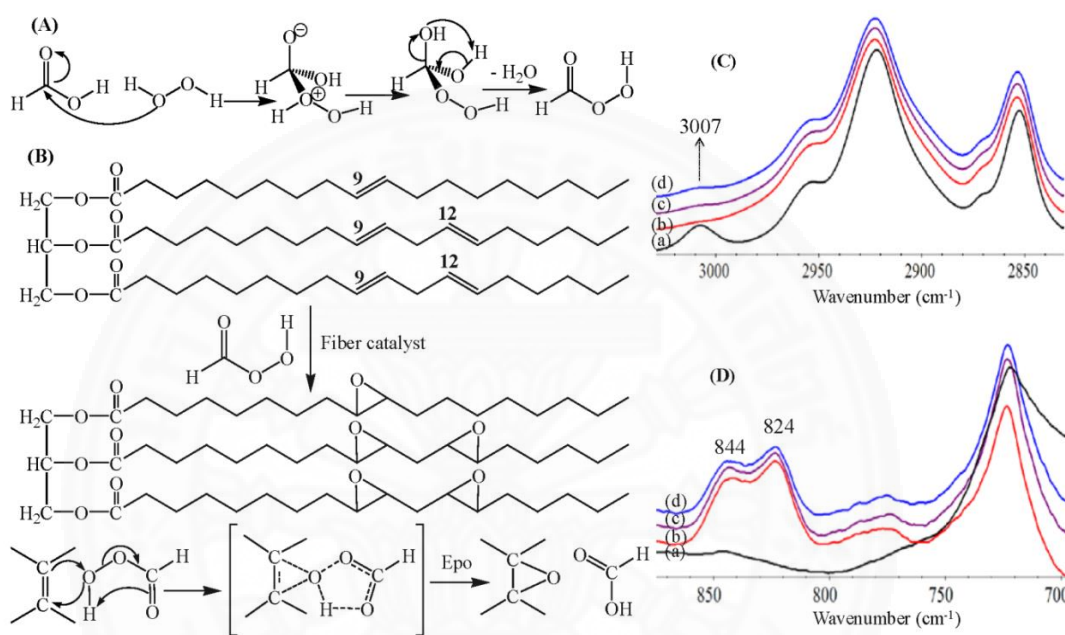
Figure 4.22: Mechanism of epoxidation and FTIR band characteristics of epoxy group of (a) SFO, (b) ESFO-1, (c) P-T-SFO-1, and (d) P-P-T-SFO-1 epoxidized at 65°C.

Interestingly, the results also show an occurrence of major side reactions, especially when the fiber catalyst is not employed, due to the extreme reaction conditions and the employment of highly reactive reagents. In addition to the conversion of olefinic bonds to oxirane groups, the performic acid reagents also liberate free fatty acids (FFAs) and glycerol by breaking ester bonds of SFO triglycerides, as shown in Figure 4.23. These undesirable FFA by-products, whose content can be directly measured from the intensity of a 1723 cm^{-1} band (C=O stretching of carboxylic acid), are not suitable for use in our proposed applications as structural-tunable plasticizer for biopolymers.

ATR-FTIR spectra of epoxidized oils products obtained at different oxidizing agent contents, with and without the fiber catalyst are compared in Figure 4.23. An

increase in the contents of HCOOH and H_2O_2 lead to an increase in intensity of the FFA band. A much higher degree of intensity increase is observed in the reaction system without the fiber catalyst. Interestingly, the presence of PVP in the P-P-T fiber catalyst results in the lowest degree of FFA liberation from SFO. The reaction temperature also plays a key role in this side reaction, in which the reaction at room temperature produces lower FFA content than that at 65°C.
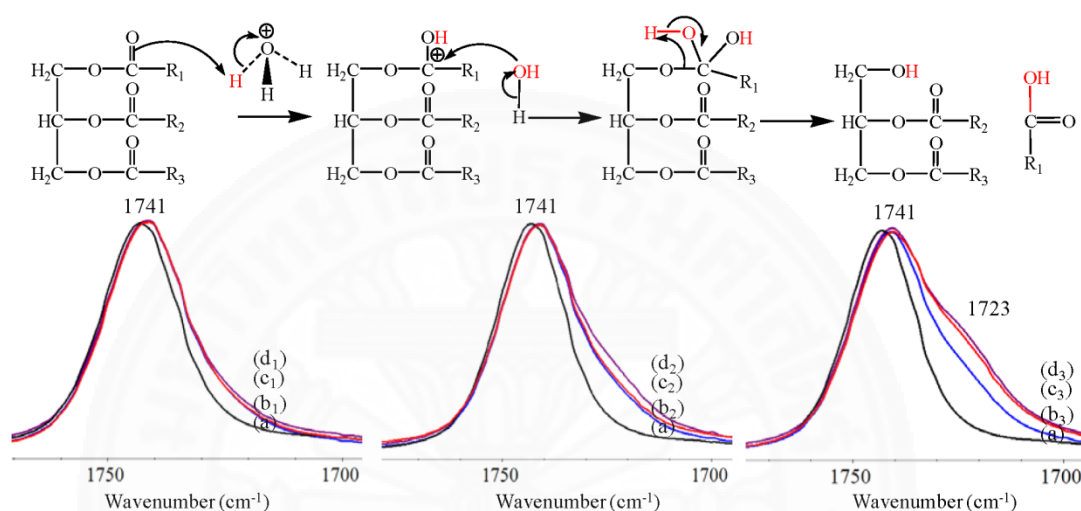
Figure 4.23: Mechanism of free fatty acid released from SFO after epoxidation and FTIR-ATR of (a) SFO, (b) P-T-ESFO-1 epoxidized at room temperature, and (c) P-T-ESFO-1 epoxidized at 65°C.

To quantitatively determine the degree of epoxidation and the contents of FFA by-products, a curve fitting process is employed to the FTIR spectra of products from each reaction, by using the OMNIC program, as shown in Figure 4.24. The conversion yield of olefinic bonds to epoxide groups is calculated from the conversion of the 3007 cm^{-1} band, while the degree of FFA liberation is measured from the ratios of 1723/1740 cm^{-1} band areas. Results from Figure 4.25(a)-(b) and Table 4.1 show that the olefinic bond conversion yield at room temperature is higher when the fiber catalysts are employed, compared to the system using oxidizing agents alone at all contents of the oxidizing agents. The yields also increase with the increase in the oxidizing agent contents. The 1723/1740 cm^{-1} band ratio also increases with the oxidizing agent content for all samples, due to more extreme conditions, which is undesirable.

63

When the reaction temperature is increased to 65°C, all reactions using the same oxidizing agent contents show comparable conversion yields, are higher than the corresponding reactions at room temperature. However, the degree of FFA liberation of the reactions using the fiber catalyst, especially P-P-T-ESFO-x, is much lower than other systems. This implies that the optimum condition for epoxidation of SFO with high yields, but low amount of FFA liberation, is at 65°C with the application of P-P-T-ESFO-x. This effective process is achieved because the PVP-containing PLA/TiO$_2$ composites provide active surfaces on the fiber that are more specific for epoxidizing double bonds, which decrease the hydrolysis reaction of ester bond cleavage, especially at higher contents of oxidizing agents and high reaction temperatures. The resulting products are effective additives for use as plasticizers or toughening agents for other biopolymers.
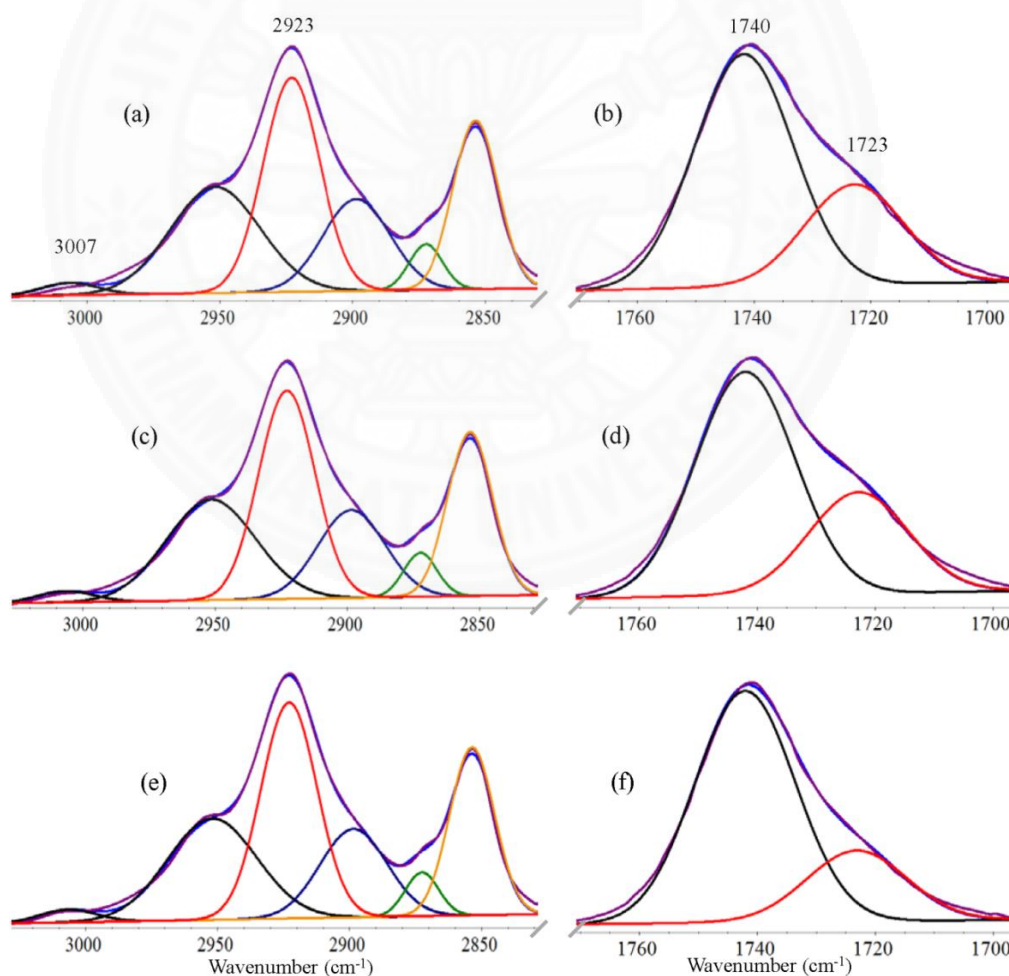
Figure 4.24: Curve fitting results from bands of olefinic bond and FFA liberation of (a)-(b) ESFO-1, (c)-(d) P-T-ESFO-1, and (e)-(f) P-P-T-ESFO-1 epoxidized at 65°C.

64
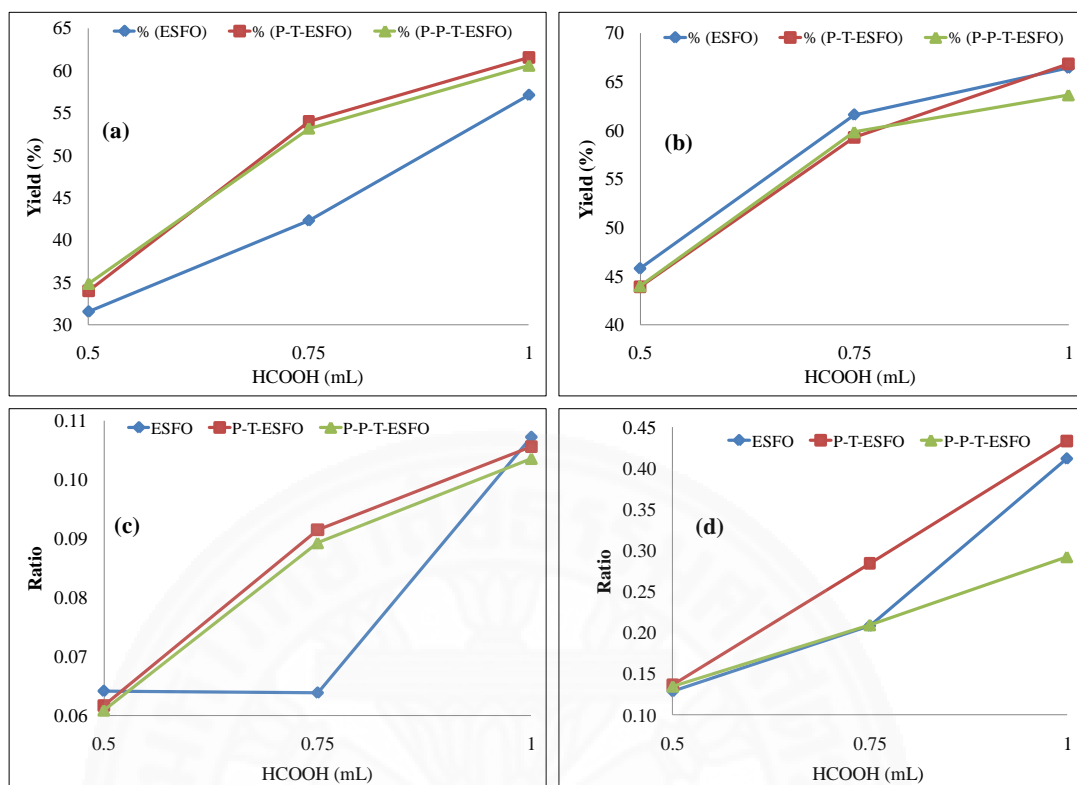
Figure 4.25: The olefinic conversion yield epoxidized at: (a) room temperature and (b) 65°C and the free fatty acid liberation ratio between peak areas of 1723/ 1740 cm^{-1} epoxidized at (c) room temperature and (d) 65°C.

Table 4.1: Epoxidation yield of SFO using HCOOH 1mL.

	Epoxidation Yield (%)	
	Room temperature (29-31°C)	65°C
ESFO-1	57.15	66.39
P-T-ESFO-1	61.55	66.81
P-P-T-ESFO-1	60.64	63.63

ATR-FTIR spectra of P-T and P-P-T, electrospun at 15 kV, catalyst before and after the epoxidation process are shown in Figure 4.26. After reaction, the catalysts show low intensity of amide group (1652 cm^{-1}, N-C=O) of PVP, as the material is dissolved by formic acid in mixture of reactor during processing. The crystalline peak of PLLA at 920 cm^{-1} increases noticeably after reaction. The mixture of SFO,

65

HCOOH, and H_2O_2 under UV light (254 nm) affects the reformation of hydrogen bonding, molecular interaction, and more order of PLLA.
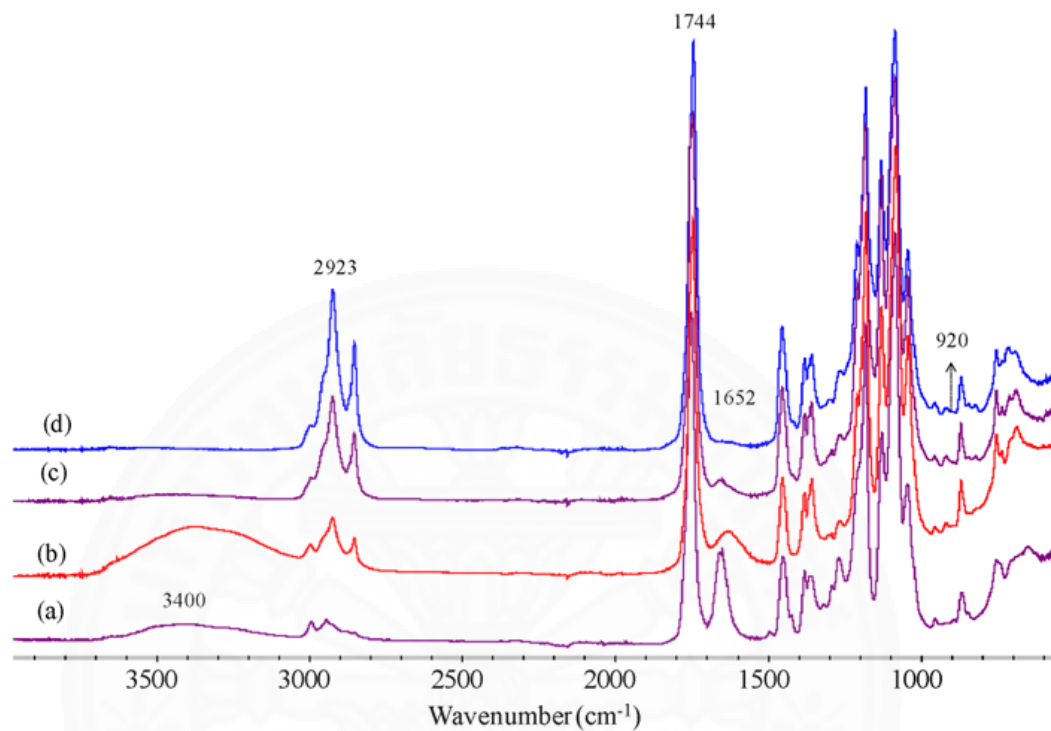
Figure 4.26: ATR-FTIR of catalyst before and after epoxidation process: (a) P-P-T (15 kV) fiber, (b) P-P-T-ESFO-0.5 (65°C), (c) P-P-T-ESFO-0.5 (room temp), and (d) P-T-ESFO-0.5(room temp).

Chapter 5

Conclusions

Conclusion, electrospun fiber mats of PLA/PVP blends loaded with TiO_2 particles, i.e., P-P-T, and P-P-I-T, are successfully fabricated by an electrospinning method. The fiber mats absorb UV light in a region of 300 nm, which enables their photo-catalytic activity. Preliminary results from degradability experiments show that degradation of the PLA component start to degrade very early, due to the presence of TiO_2 catalytic particles, and also PVP component is dissolved by water medium and is removed from the filaments. These enable the materials to possess photo-catalytic activity for use in many applications, such as epoxidation of unsaturated oils or degradation of contaminated water. These investigations will be addressed in details in a separate work.

In detailed study, nanofibers of polylactide (PLA)/poly(vinlylpyrrolidone) (PVP) blends loaded with TiO_2 nanoparticles have been successfully prepared by an electrospinning method. All spun fibers are completely amorphous in nature, in which those fabricated from PLA/PVP/$TiO_2$are smoother and more uniform than the corresponding samples without PVP. SEM images clearly show that TiO_2 particles are embedded on the filaments, and the samples show a UV absorption band covering 200-380 nm regions. The spun composite fibers have a high potential for applications as catalytic systems for epoxidation of unsaturated oils, for use as additives or plasticizers for biopolymers. The fibers, especially those containing PVP, can effectively enhance epoxidation yield of the oils, and decrease undesirable side reactions which break ester bonds of the triglyceride, to generate free fatty acid by-products. These composited fibers are promising for various applications as photo-catalyst to remove organic pollutants. This work will be extended and investigated more about acetylene degradation in order to apply as food packaging to delay fruit ripening.

References

1. Vinu, R. and G. Madras, *Environmental remediation by photocatalysis.* Journal of the Indian Institute of Science, 2010. **92:2**.

2. Zhou, Q., et al., *Applications of TiO$_2$ nanotube arrays in environmental and energy fields: A review.* Microporous and Mesoporous Materials, 2015. **202**: p. 22-35.

3. Fujishima, A., X. Zhang, and D.A. Tryk, *Heterogeneous photocatalysis: From water photolysis to applications in environmental cleanup.* International Journal of Hydrogen Energy, 2007. **32**: p. 2664 - 2672.

4. Linsebigler, A.L., G. Lu, and J. John T. Yates, *Photocatalysis on TiO$_2$ Surfaces: Principles, Mechanisms, and Selected Results.* Chem. Rev, 1995. **95**: p. 735-758.

5. Sriwong, C., SumpunWongnawa, and O. Patarapaiboolchai, *Degradation of indigo carmine by rubber sheet impregnated with TiO$_2$ particles.* ScienceAsia, 2010. **36**: p. 52–58.

6. Saggioro, E.M., et al., *Use of Titanium Dioxide Photocatalysis on the Remediation of Model Textile Wastewaters Containing Azo Dyes.* Molecules, 2011. **16**: p. 10370-10386.

7. Lin, W.-C., W.-D. Yang, and S.-Y. Jheng, *Photocatalytic degradation of dyes in water using porous nanocrystalline titanium dioxide.* Journal of the Taiwan Institute of Chemical Engineers, 2012. **43**: p. 269-274.

8. Vroman, I. and L. Tighzert, *Biodegradable Polymers.* Materials, 2009. **2**(2): p. 307-344.

9. Mekonnen, T., et al., *Progress in bio-based plastics and plasticizing modifications.* Journal of Materials Chemistry A, 2013. **1**(43): p. 13379.

10. Gupta, K.K., et al., *Hydrothermal in situ preparation of TiO$_2$ particles onto poly(lactic acid) electrospun nanofibres.* Applied Surface Science, 2013. **264**: p. 375-382.

11. Ali, N.A. and F.T.M. Noori, *Gas Barrier Properties of Biodegradable Polymer Nanocomposites Films.* Chemistry and Materials Research, 2014. **6**(1).

12. Kale, G., R. Auras, and S.P. Singh, *Comparing the degradability of commercially available biodegradable packages in composting and ambient exposure conditions.* GPEC 2006 Paper Abstract 8B, MI 48824-1223, 2006.

13. Nakayama, N. and T. Hayashi, *Preparation and characterization of poly(l-lactic acid)/TiO$_2$ nanoparticle nanocomposite films with high transparency and efficient photodegradability.* Polymer Degradation and Stability, 2007. **92**(7): p. 1255-1264.

14. Buzarovska, A. and A. Grozdanov, *Biodegradable poly(L-lactic acid)/TiO$_2$ nanocomposites: Thermal properties and degradation.* Journal of Applied Polymer Science, 2012. **123**(4): p. 2187-2193.

15. Kale, G., et al., *Biodegradability of polylactide bottles in real and simulated composting conditions.* Polymer Testing, 2007. **26**(8): p. 1049-1061.

16. Fukushima, K., et al., *Biodegradation of poly(lactic acid) and its nanocomposites.* Polymer Degradation and Stability, 2009. **94**(10): p. 1646-1655.

17. Ghaffar, T., et al., *Recent trends in lactic acid biotechnology: A brief review on production to purification.* Journal of Radiation Research and Applied Sciences, 2014. **7**(2): p. 222-229.

18. John, R.P., et al., *Direct lactic acid fermentation: Focus on simultaneous saccharification and lactic acid production.* Biotechnology Advances, 2009. **27**: p. 145-152.

19. John, R.P., K.M. Nampoothiri, and A. Pandey, *Fermentative production of lactic acid from biomass: an overview on process developments and future perspectives.* Appl Microbiol Biotechnol, 2007. **74**(3): p. 524-34.

20. Wee, Y.-J., J.-N. Kim, and H.-W. Ryu, *Biotechnological Production of Lactic Acid and Its Recent Applications.* Food Technol. Biotechnol, 2006. **44**(2): p. 163-172.

21. Khazir, S. and S. Shetty, *BIO-BASED POLYMERS IN THE WORLD.* International Journal of Life Sciences Biotechnology and Pharma Research, 2014. **3**(2).

22. Huang, L.P., et al., *Simultaneous saccharification and fermentation of potato starch wastewater to lactic acid by Rhizopus oryzae and Rhizopus arrhizus.* Biochemical Engineering Journal 2005. **23**: p. 265-276.

23. Naveena, B.J., et al., *Direct fermentation of starch to l(+) lactic acid in SSF by Lactobacillus amylophilus GV6 using wheat bran as support and substrate: medium optimization using RSM.* Process Biochemistry 2005. **40**: p. 681-690.

24. Rojan, P.J., et al., *L(+)-Lactic acid production using Lactobacillus casei in solid-state fermentation.* Biotechnology Letters, 2005. **27**: p. 1685-1688.

25. Tanaka, T., et al., *Production of D-lactic acid from defatted rice bran by simultaneous saccharification and fermentation.* Bioresour Technol, 2006. **97**(2): p. 211-7.

26. John, R.P., K.M. Nampoothiri, and A. Pandey, *Production of L(+) lactic acid from cassava starch hydrolyzate by immobilized Lactobacillus delbrueckii.* J Basic Microbiol, 2007. **47**(1): p. 25-30.

27. Maas, R.H.W., et al., *Lactic acid production from lime-treated wheat straw by Bacillus coagulans: neutralization of acid by fed-batch addition of alkaline substrate.* Applied Microbiology and Biotechnology, 2008. **78**(5): p. 751-758.

28. Lu, Z., et al., *An economical approach for d-lactic acid production utilizing unpolished rice from aging paddy as major nutrient source.* Bioresour Technol, 2009. **100**(6): p. 2026-31.

29. Guo, W., et al., *Performances of Lactobacillus brevis for producing lactic acid from hydrolysate of lignocellulosics.* Appl Biochem Biotechnol, 2010. **161**(1-8): p. 124-36.

30. Zhang, Y. and P.V. Vadlani, *D-Lactic acid biosynthesis from biomass-derived sugars via Lactobacillus delbrueckii fermentation.* Bioprocess Biosyst Eng, 2013. **36**(12): p. 1897-904.

31. Ouyang, J., et al., *Open fermentative production of L-lactic acid by Bacillus sp. strain NL01 using lignocellulosic hydrolyzates as low-cost raw material.* Bioresour Technol, 2013. **135**: p. 475-80.

32. Wang, C., et al., *Improving the lactic acid production of Actinobacillus succinogenes by using a novel fermentation and separation integration system.* Process Biochemistry, 2014. **49**(8): p. 1245-1250.

33. Liu, Y., et al., *Pilot scale demonstration of D-lactic acid fermentation facilitated by Ca(OH)$_2$ using a metabolically engineered Escherichia coli.* Bioresour Technol, 2014. **169**: p. 559-65.

34. Smerilli, M., et al., *Direct fermentation of potato starch and potato residues to lactic acid by under non-sterile conditions.* J Chem Technol Biotechnol, 2015. **90**(4): p. 648-657.

35. Castillo Martinez, F.A., et al., *Lactic acid properties, applications and production: A review.* Trends in Food Science & Technology, 2013. **30**(1): p. 70-83.

36. Narayanan, N., P.K. Roychoudhury, and A. Srivastava, *L (+) lactic acid fermentation and its product polymerization.* Electronic Journal of Biotechnology, 2004. **7**(2).

37. Abdel-Rahman, M.A., Y. Tashiro, and K. Sonomoto, *Lactic acid production from lignocellulose-derived sugars using lactic acid bacteria: overview and limits.* J Biotechnol, 2011. **156**(4): p. 286-301.

38. Wang, Y., Y. Tashiro, and K. Sonomoto, *Fermentative production of lactic acid from renewable materials: recent achievements, prospects, and limits.* J Biosci Bioeng, 2015. **119**(1): p. 10-8.

39. Hu, J., et al., *High-titer lactic acid production from NaOH-pretreated corn stover by Bacillus coagulans LA204 using fed-batch simultaneous saccharification and fermentation under non-sterile condition.* Bioresour Technol, 2015. **182**: p. 251-7.

40. Zhang, Y., et al., *Improving lactic acid productivity from wheat straw hydrolysates by membrane integrated repeated batch fermentation under non-sterilized conditions.* Bioresour Technol, 2014. **163**: p. 160-6.

41. Bendix, D., *Chemical synthesis of polylactide and its copolymers for medical applications.* Polymer Degradatioann and stability, 1998. **59**: p. 129-135.

42. Gupta, A.P. and V. Kumar, *New emerging trends in synthetic biodegradable polymers – Polylactide: A critique.* European Polymer Journal, 2007. **43**(10): p. 4053-4074.

43. Lunt, J., *Large-scale production, properties and commercial applications of polylactic acid polymers.* Polymer Degradation and Stability, 1998. **59**: p. 145-152.

44. Achmad, F., et al., *Synthesis of polylactic acid by direct polycondensation under vacuum without catalysts, solvents and initiators.* Chemical Engineering Journal, 2009. **151**(1-3): p. 342-350.

45. SP, P., et al., *Synthesis of ciprofloxacin-conjugated poly (L-lactic acid) polymer for nanofiber fabrication and antibacterial evaluation.* 2014. **9**(1): p. 1463—1477.

46. Yanling Wang, R.Q., C. Xiong, and M. Huang, *Effects of Coupling Agent and Interfacial Modifiers on Mechanical Properties of Poly(lactic acid) and Wood Flour Biocomposites.* Iranian Polymer Journal, 2011. **20**(4): p. 281-294.

47. Ryner, M., et al., *Mechanism of Ring-Opening Polymerization of 1,5-Dioxepan-2-one and L-Lactide with Stannous 2-Ethylhexanoate. A Theoretical Study.* Macromolecules, 2001. **34**: p. 3877-3881.

48. Albertsson, A.-C. and I. K.Varma, *Recent Developments in Ring Opening Polymerization of Lactones for Biomedical Applications.* Biomacromolecules, 2003. **4**(6): p. 1466-1486.

49. Carp, O., *Photoinduced reactivity of titanium dioxide.* Progress in Solid State Chemistry, 2004. **32**: p. 33–177.

50. Fujishima, A. and K. Honda, *Nature.* 1972. **37**: p. 238.

51. Kumar, J. and A. Bansal, *Photocatalysis by Nanoparticles of Titanium Dioxide for Drinking Water Purification: A Conceptual and State-of-Art Review.* Materials Science Forum, 2013. **764**: p. 130-150.

52. Lu, N., et al., *Nano titanium dioxide photocatalytic protein tyrosine nitration: A potential hazard of TiO_2 on skin.* Biochemical and Biophysical Research Communications, 2008. **370**: p. 675–680.

53. Ibhadon, A.O. and P. Fitzpatrick, *Heterogeneous Photocatalysis: Recent Advances and Applications.* Catalysts, 2013. **3**: p. 1-x.

54. Fujishima, A., T.N. Rao, and D.A. Tryk, *Titanium dioxide photocatalysis.* Journal of Photochemistry and Photobiology C: Photochemistry Reviews, 2000. **1**: p. 1-21.

55. Han, F., et al., *Tailored titanium dioxide photocatalysts for the degradation of organic dyes in wastewater treatment: A review.* Applied Catalysis A: General, 2009. **359**: p. 25–40.

56. Li, Y., et al., *Photocatalytic degradation of methyl orange by TiO_2-coated activated carbon and kinetic study.* Water Res, 2006. **40**(6): p. 1119-26.

57. Chang, C.-C., et al., *Photocatalytic properties of porous TiO_2/Ag thin films.* Thin Solid Films, 2008. **516**(8): p. 1743-1747.

58. Mousanejad, T., et al., *Photocatalytic ozonation for degradation of 2-sec-butyl-4,6-dinitrophenol (DNBP) using titanium dioxide: effect of operational parameters and wastewater treatment.* Research on Chemical Intermediates, 2013. **40**(2): p. 711-722.

59. Fischer, K., et al., *Photoactive microfiltration membranes via directed synthesis of TiO_2 nanoparticles on the polymer surface for removal of drugs from water.* Journal of Membrane Science, 2015. **478**: p. 49-57.

60. Habibi, M.H., M.N. Esfahani, and T.A. Egerton, *Photochemical Characterization and Photocatalytic Properties of a Nanostructure CompositeTiO_2 Film.* INTERNATIONAL JOURNAL OF PHOTOENERGY, 2007. **2007**: p. 1-8.

61. Panagopoulos, I., et al., *A CFD Simulation Study of VOC and Formaldehyde Indoor Air Pollution Dispersion in an Apartment as Part of an Indoor Pollution Management Plan.* Aerosol and Air Quality Research, 2011. **11**: p. 758 – 762.

62. Han, Z., et al., *Preparation of TiO_2-Coated Polyester Fiber Filter by Spray-Coating and Its Photocatalytic Degradation of Gaseous Formaldehyde.* Aerosol and Air Quality Research, 2012. **12**: p. 1327–1335.

63. Ao, C.H., et al., *Photodegradation of volatile organic compounds (VOCs) and NO for indoor air purification using TiO_2: promotion versus inhibition effect of NO.* Applied Catalysis B: Environmental, 2003. **42**(2): p. 119-129.

64. Ao, C.H. and S.C. Lee, *Indoor air purification by photocatalyst TiO_2 immobilized on an activated carbon filter installed in an air cleaner.* Chemical Engineering Science, 2005. **60**(1): p. 103-109.

65. Jo, W.K. and J.T. Kim, *Application of visible-light photocatalysis with nitrogen-doped or unmodified titanium dioxide for control of indoor-level volatile organic compounds.* J Hazard Mater, 2009. **164**(1): p. 360-6.

66. Chun, H.-H. and W.-K. Jo, *Polymer material-supported titania nanofibers with different polyvinylpyrrolidone to TiO₂ ratios for degradation of vaporous trichloroethylene.* Journal of Industrial and Engineering Chemistry, 2014. **20**(3): p. 1010-1015.

67. Sano, T., et al., *Degradation of C₂H₂ with modified-TiO₂ photocatalysts under visible light irradiation.* Journal of Molecular Catalysis A: Chemical, 2008. **284**(1-2): p. 127-133.

68. Youssef, C., et al., *Photocatalytic Efficiency of Au/TiO₂ on the Degradation of Acetylene.* Scientific Journal of Environment Pollution and Protection, 2014. **3**(3): p. 38-45.

69. Thevenet, F., C. Guillard, and A. Rousseau, *Acetylene photocatalytic oxidation using continuous flow reactor: Gas phase and adsorbed phase investigation, assessment of the photocatalyst deactivation.* Chemical Engineering Journal, 2014. **244**: p. 50-58.

70. Thevenet, F., et al., *Photocatalytic degradation of acetylene over various titanium dioxide-based photocatalysts.* Applied Catalysis B: Environmental, 2005. **61**(1-2): p. 58-68.

71. Chawengkijwanich, C. and Y. Hayata, *Development of TiO₂ powder-coated food packaging film and its ability to inactivate Escherichia coli in vitro and in actual tests.* International Journal of Food Microbiology, 2008. **123**: p. 288-292.

72. Benabbou, A.K., et al., *Photocatalytic inactivation of Escherischia coli. Effect of concentration of TiO2 and microorganism, nature, and intensity of UV irradiation.* Applied Catalysis B: Environmental, 2007. **76**(3-4): p. 257-263.

73. Fu, G., P.S. Vary, and C.-T. Lin, *Anatase TiO₂ Nanocomposites for Antimicrobial Coatings.* J. Phys. Chem. B, 2005. **109**(18): p. 8889-8898.

74. Zhang, H. and G. Chen, *Potent Antibacterial Activities of Ag/TiO₂ Nanocomposite Powders Synthesized by a One-Pot Sol-Gel Method.* Environ. Sci. Technol, 2009. **43**(8): p. 2905-2910.

75. Wang, R.-M., et al., *Preparation of composited Nano-TiO₂ and its application on antimicrobial and self-cleaning coatings.* Polymers for Advanced Technologies, 2009. **21**(5): p. 331-336.

76. Son, B., et al., *Antibacterial electrospun chitosan/poly(vinyl alcohol) nanofibers containing silver nitrate and titanium dioxide.* Journal of Applied Polymer Science, 2009. **111**(6): p. 2892-2899.

77. Lee, K. and S. Lee, *Multifunctionality of poly(vinyl alcohol) nanofiber webs containing titanium dioxide.* Journal of Applied Polymer Science, 2012. **124**(5): p. 4038-4046.

78. Wang, T., et al., *Potential application of functional porous TiO₂ nanoparticles in light-controlled drug release and targeted drug delivery.* Acta Biomaterialia, 2015. **13**: p. 354-363.

79. Ma, X., et al., *Modulation of drug-resistant membrane and apoptosis proteins of breast cancer stem cells by targeting berberine liposomes.* Biomaterials, 2013. **34**: p. 4452-4465.

80. Zhang, X.-X., H.S. Eden, and X. Chen, *Peptides in cancer nanomedicine: Drug carriers, targeting ligands and protease substrates.* Journal of Controlled Release, 2012. **159**: p. 2-13.

81. Adams, G.P. and L.M. Weiner, *Monoclonal antibody therapy of cancer.* Nature Biotechnology, 2005. **23**: p. 1147 - 1157.

82. Devanand Venkatasubbu, G., et al., *Folate targeted PEGylated titanium dioxide nanoparticles as a nanocarrier for targeted paclitaxel drug delivery.* Advanced Powder Technology, 2013. **24**(6): p. 947-954.

83. Gabizon, A., et al., *Tumor cell targeting of liposome-entrapped drugs with phospholipid-anchored folic acid–PEG conjugates.* Advanced Drug Delivery Reviews, 2004. **56**: p. 1177- 1192.

84. Gormley, A.J., et al., *Guided delivery of polymer therapeutics using plasmonic photothermal therapy.* Nano Today, 2012. **7**: p. 158-167.

85. Xu, J., et al., *Photokilling cancer cells using highly cell-specific antibody-TiO₂ bioconjugates and electroporation.* Bioelectrochemistry, 2007. **71**(2): p. 217-22.

86. Liu, L., et al., *Study of Pt/TiO₂ nanocomposite for cancer-cell treatment.* J Photochem Photobiol B, 2010. **98**(3): p. 207-10.

87. Naghibi, S., et al., *Mortality response of folate receptor-activated, PEG–functionalized TiO₂ nanoparticles for doxorubicin loading with and without ultraviolet irradiation.* Ceramics International, 2014. **40**: p. 5481-5488.

88. Liew, C.-W. and S. Ramesh, *Studies on ionic liquid-based corn starch biopolymer electrolytes coupling with high ionic transport number.* Cellulose, 2013. **20**(6): p. 3227-3237.

89. Wei, Q.F., et al., *Surface functionalisation of polymer nanofibres by sputter coating of titanium dioxide.* Applied Surface Science, 2006. **252**(22): p. 7874-7877.

90. Drew, C., et al., *The Effect of Viscosity and Filler on Electrospun Fiber Morphology.* Journal of Macromolecular Science, Part A:Pure and Applied Chemistry, 2003. **40**(12): p. 1415-1422.

91. Kedem, S., et al., *Composite Polymer Nanofibers with Carbon Nanotubes and Titanium Dioxide Particles.* Langmuir, 2005. **21**(12): p. 5600-5604.

92. Xin, Y., et al., *Preparation and photoluminescence of single conjugated polymer–TiO₂ composite nanofibers.* Journal of Luminescence, 2012. **132**(3): p. 738-742.

93. Im, J.S., M.I. Kim, and Y.-S. Lee, *Preparation of PAN-based electrospun nanofiber webs containing TiO₂ for photocatalytic degradation.* Materials Letters, 2008. **62**(21-22): p. 3652-3655.

94. Kedem, S., et al., *Enhanced Stability Effect in Composite Polymeric Nanofibers Containing Titanium Dioxide and Carbon Nanotubes.* J. Phys. Chem. C, 2009. **113**: p. 14893-14899.

95. Hamid, N.A.A., et al., *Morphological and separation performance study of polysulfone/titanium dioxide (PSF/TiO2) ultrafiltration membranes for humic acid removal.* Desalination, 2011. **273**(1): p. 85-92.

96. Pant, H.R., et al., *Photocatalytic TiO₂–RGO/nylon-6 spider-wave-like nano-nets via electrospinning and hydrothermal treatment.* Journal of Membrane Science, 2013. **429**: p. 225-234.

97. Kang, S.-J., et al., *Fabrication and photocatalytic activity of electrospun nylon-6 nanofibers containing tourmaline and titanium dioxide nanoparticles.* Ceramics International, 2013. **39**(6): p. 7143-7148.

98. Neppalli, R., et al., *Polystyrene/TiO₂ composite electrospun fibers as fillers for poly(butylene succinate-co-adipate): Structure, morphology and properties.* European Polymer Journal, 2014. **50**: p. 78-86.

99. Daels, N., et al., *Functionalisation of electrospun polymer nanofibre membranes with TiO₂ nanoparticles in view of dissolved organic matter photodegradation.* Separation and Purification Technology, 2014. **133**: p. 282-290.

100. Zhuang, W., et al., *Preparation, characterization, and properties of TiO₂/PLA nanocomposites by in situ polymerization.* Polymer Composites, 2009. **30**(8): p. 1074-1080.

101. Wadsworth, L.C., et al., *Evaluation of Degradable Spun-Melt 100% Polylactic Acid Nonwoven Mulch Materials in a Greenhouse Environment.* Journal of Engineered Fibers and Fabrics, 2013. **8**(4).

102. Colomines, G., et al., *Barrier properties of poly(lactic acid) and its morphological changes induced by aroma compound sorption.* Polymer International, 2010. **59**: p. 818-826.

103. Carosio, F., et al., *Efficient Gas and Water Vapor Barrier Properties of Thin Poly(lactic acid) Packaging Films: Functionalization with Moisture Resistant Nafion and Clay Multilayers.* Chemistry of Materials, 2014. **26**(19): p. 5459-5466.

104. Song, M., et al., *The application of new nanocomposites: Enhancement effect of polylactide nanofibers/nano-TiO₂ blends on biorecognition of anticancer drug daunorubicin.* Applied Surface Science, 2008. **255**(2): p. 610-612.

105. Hong, Y., et al., *Electrospinning of multicomponent ultrathin fibrous nonwovens for semi-occlusive wound dressings.* Journal of Biomedical Materials Research Part A, 2009. **89A**(2): p. 345-354.

106. Dural-Erem, A., et al., *Anatase titanium dioxide loaded polylactide membranous films: preparation, characterization, and antibacterial activity assessment.* The Journal of The Textile Institute, 2014: p. 1-6.

107. Man, C., et al., *Poly (lactic acid)/titanium dioxide composites: Preparation and performance under ultraviolet irradiation.* Polymer Degradation and Stability, 2012. **97**(6): p. 856-862.

108. Silva, K.I.s.M.d., et al., *Structural stability of photodegradable poly(l-lactic acid)/PE/TiO₂ nanocomposites through TiO₂ nanospheres and TiO₂ nanotubes incorporation.* Polymer Bulletin, 2014. **71**(5): p. 1205-1217.

109. Torres, F., et al., *Mechanical properties and bioactivity of porous PLGA/TiO₂ nanoparticle-filled composites for tissue engineering scaffolds.* Composites Science and Technology, 2007. **67**(6): p. 1139-1147.

110. Luo, Y.-B., X.-L. Wang, and Y.-Z. Wang, *Effect of TiO₂ nanoparticles on the long-term hydrolytic degradation behavior of PLA.* Polymer Degradation and Stability, 2012. **97**(5): p. 721-728.

111. Wang, W.-W., et al., *Stability of poly(l-lactide)/TiO₂ nanocomposite thin films under UV irradiation at 254 nm.* Polymer Degradation and Stability, 2013. **98**(4): p. 885-893.

112. Buzarovska, A., et al., *Effect of TiO$_2$ nanoparticle loading on Poly(l-lactic acid) porous scaffolds fabricated by TIPS.* Composites Part B: Engineering, 2015. **81**: p. 189-195.

113. Sharifah Nafisah, S.I., et al., *Epoxidation of Palm Oil Catalyzed by Titanium-Grafted Silica Catalyst.* Advanced Materials Research, 2013. **812**: p. 30-37.

114. Guidotti, M., et al., *Epoxidation of unsaturated FAMEs obtained from vegetable source over Ti(IV)-grafted silica catalysts: A comparison between ordered and non-ordered mesoporous materials.* Journal of Molecular Catalysis A: Chemical, 2006. **250**(1-2): p. 218-225.

115. Kumar, D. and A. Ali, *Ti/SiO$_2$ as a Nanosized Solid Catalyst for the Epoxidation of Fatty Acid Methyl Esters and Triglycerides.* Energy & Fuels, 2012. **26**(5): p. 2953-2961.

116. Rubio, M., G. Ramírez-Galicia, and L.J. López-Nava, *Mechanism formation of peracids.* Journal of Molecular Structure: THEOCHEM, 2005. **726**(1-3): p. 261-269.

117. Di Serio, M., et al., *Valuation of Nb$_2$O$_5$–SiO$_2$ catalysts in soybean oil epoxidation.* Catalysis Today, 2012. **192**(1): p. 112-116.

118. Sharma, R.V. and A.K. Dalai, *Synthesis of bio-lubricant from epoxy canola oil using sulfated Ti-SBA-15 catalyst.* Applied Catalysis B: Environmental, 2013. **142-143**: p. 604-614.

119. Somidi, A.K.R., R.V. Sharma, and A.K. Dalai, *Synthesis of Epoxidized Canola Oil Using a Sulfated-SnO$_2$ Catalyst.* Industrial & Engineering Chemistry Research, 2014. **53**(49): p. 18668-18677.

120. Turco, R., et al., *Influence of preparation methods and structure of niobium oxide-based catalysts in the epoxidation reaction.* Catalysis Today, 2015. **254**: p. 99-103.

121. Silvestre-Alberó, J., et al., *Spectroscopic, calorimetric, and catalytic evidences of hydrophobicity on Ti-MCM-41 silylated materials for olefin epoxidations.* Applied Catalysis A: General, 2015. **507**: p. 14-25.

122. Zhang, D. and J. Chang, *Electrospinning of Three-Dimensional Nanofibrous Tubes with Controllable Architectures.* Nano Lett 2008. **8**(10).

123. Wang, X., et al., *Electro-spinning/netting: A strategy for the fabrication of three-dimensional polymer nano-fiber/nets.* Progress in Materials Science, 2013. **58**(8): p. 1173-1243.

124. Bhardwaj, N. and S.C. Kundu, *Electrospinning: a fascinating fiber fabrication technique.* Biotechnol Adv, 2010. **28**(3): p. 325-47.

125. Balu, R., S. Singaravelu, and N. Nagiah, *Bioceramic Nanofibres by Electrospinning.* Fibers, 2014. **2**(3): p. 221-239.

126. Li, D. and Y. Xia, *Electrospinning of Nanofibers: Reinventing the Wheel? .* Advanced Materials, 2004. **16**(14): p. 1151-1170.

127. Thammawong, C., et al., *Electrospinning of poly(l-lactide-co-dl-lactide) copolymers: Effect of chemical structures and spinning conditions.* Polymer Engineering and Science, 2014. **54**(2): p. 472-480.

128. Sriromreun, P., et al., *Standard methods for characterizations of structure and hydrolytic degradation of aliphatic/aromatic copolyesters.* Polymer Degradation and Stability, 2013. **98**: p. 169-176.

129. Silva, K.I.M.d., et al., *Structural stability of photodegradable poly(l-lactic acid)/PE/TiO₂ nanocomposites through TiO₂ nanospheres and TiO₂ nanotubes incorporation.* Polymer Bulletin, 2014. **71**(5): p. 1205-1217.

130. Pakorn, O., O. Mantana, and T. Pramaun, *Crystallization of Polylactide and Its Stereocomplex Investigated by Two-Dimensional Fourier Transform Infrared Correlation Spectroscopy Employing Carbonyl Overtones.* Society for Applied Spectroscopy, 2007. **61**(12): p. 1352-1358.

131. Sriromreun, P., et al., *Standard methods for characterizations of structure and hydrolytic degradation of aliphatic/aromatic copolyesters.* Polymer Degradation and Stability, 2013. **98**(1): p. 169-176.

132. Shimamoto, G.G., M.M.A. Favaro, and M. Tubino, *Simple Methods via Mid-IR or1H NMR Spectroscopy for the Determination of the Iodine Value of Vegetable Oils.* Journal of the Brazilian Chemical Society, 2015. **26**(7): p. 1431-1437.

Appendices

Appendix A
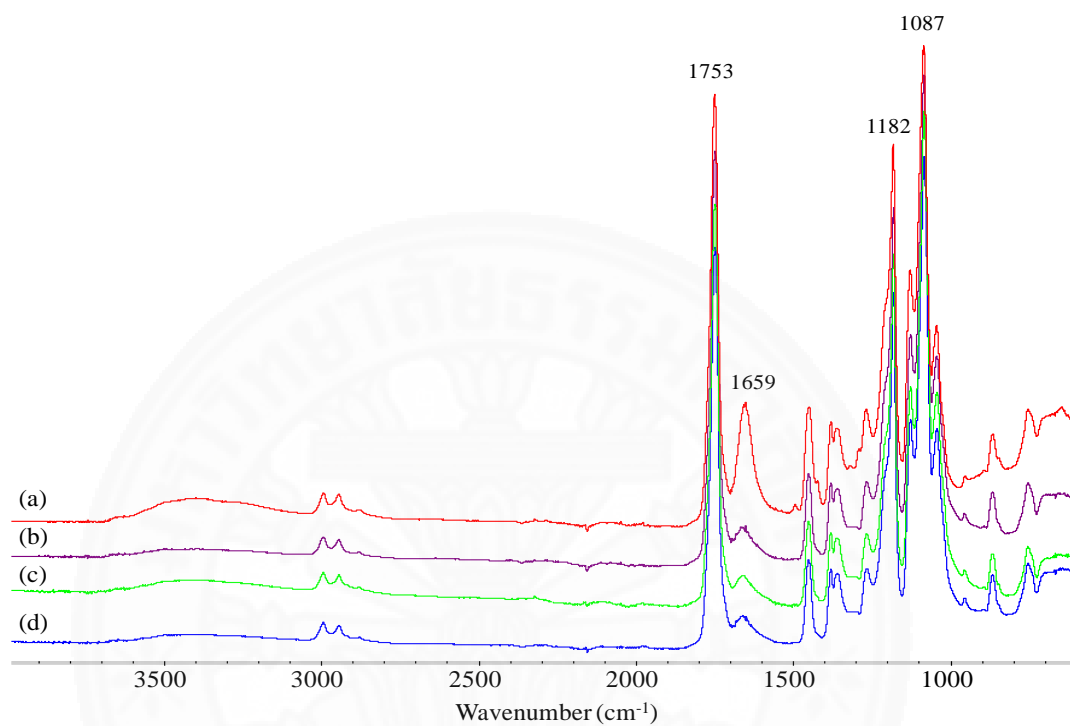
Appendix A.1: FTIR-ATR spectra of electrospun P-P-T (10 kV) fiber soaking in PBS solution at: (a) 0, (b) 1, (c) 4, and (d) 6 days.

Appendix B
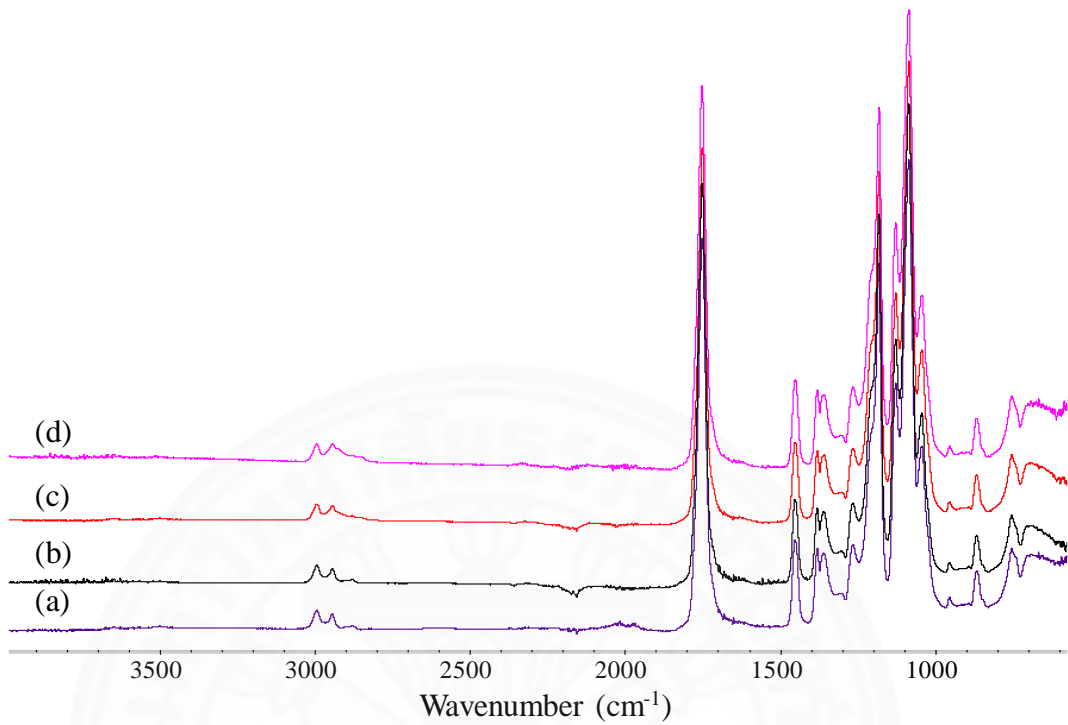
Appendix B.1: FTIR of PLLA/TiO$_2$ 5% electrospun fiber at: (a) 10, (b) 11, (c) 13, and (d) 14 kV.
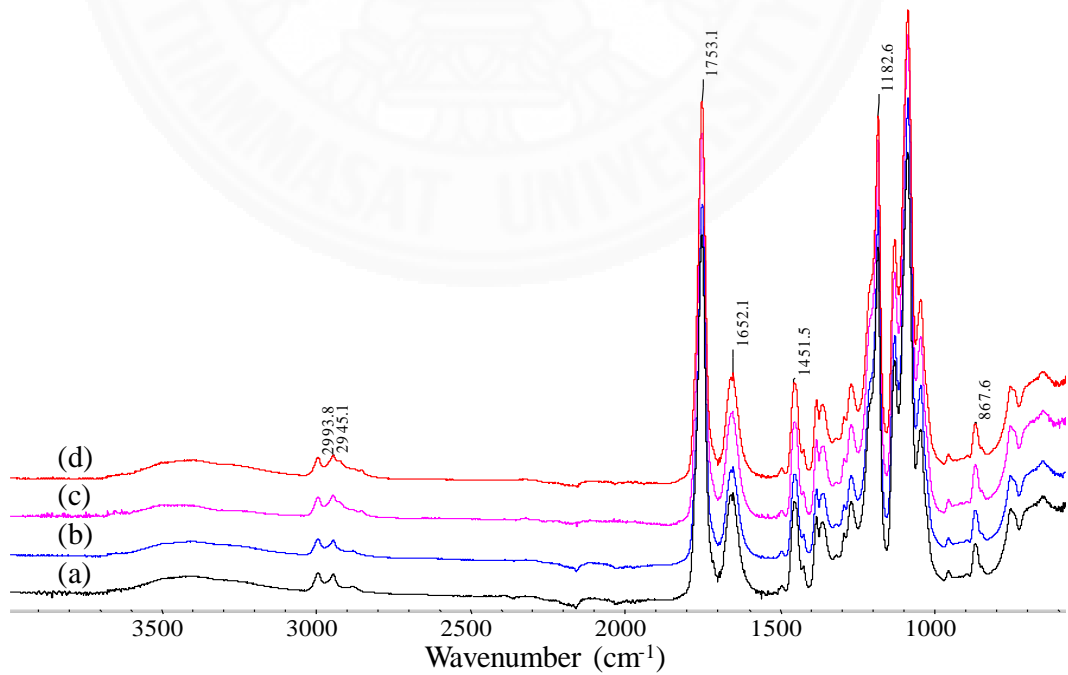
Appendix B.2: FTIR of PLLA/PVP (5:1)/TiO$_2$ 5% electrospun fiber at: (a) 10, (b) 11, (c) 13, and (d) 14 kV.

78
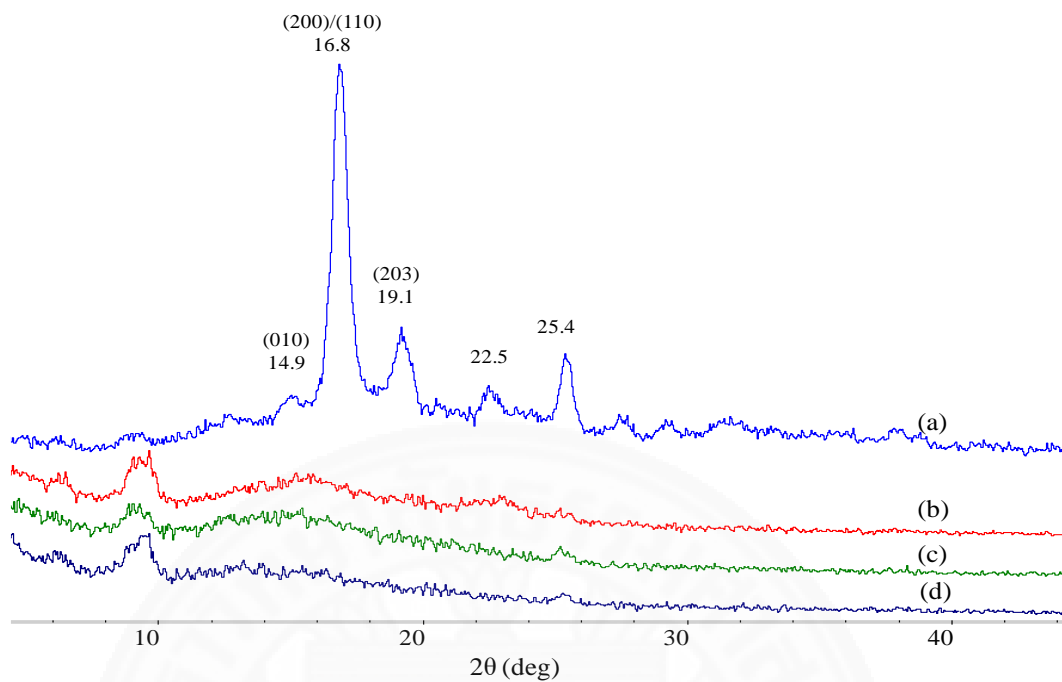
Appendix B.3: XRD of PLLA/PVP(5:1)/TiO$_2$ 5% : (a) film, (b)10, (c) 11, (c) 13, and (d) 15 kV
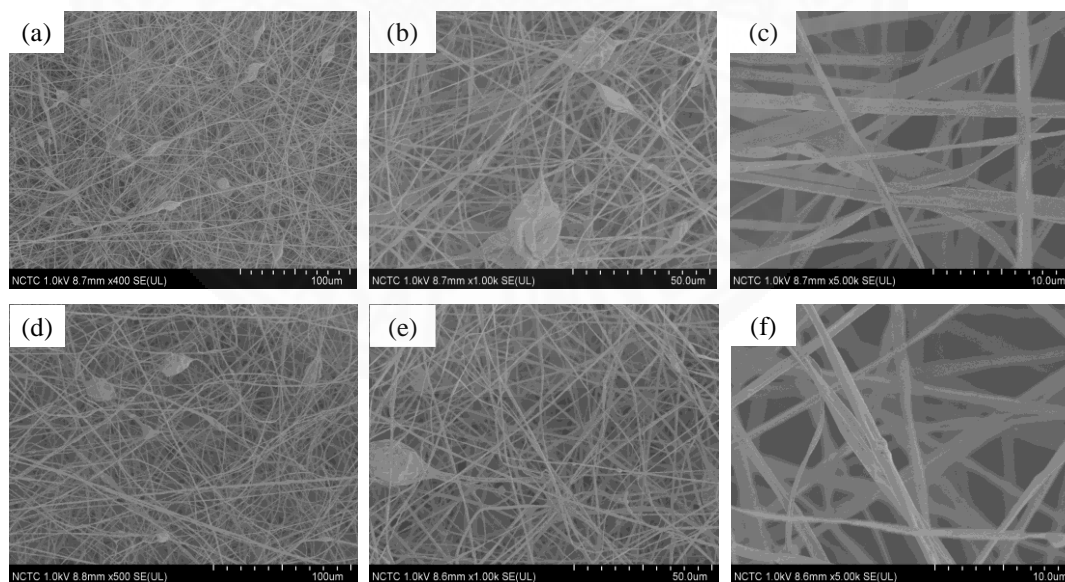
Appendix B.4: SEM images of (a)-(c) PLLA/TiO$_2$ 5% 10kV and (d)-(f) PLLA/TiO$_2$ 5% 15 kV.
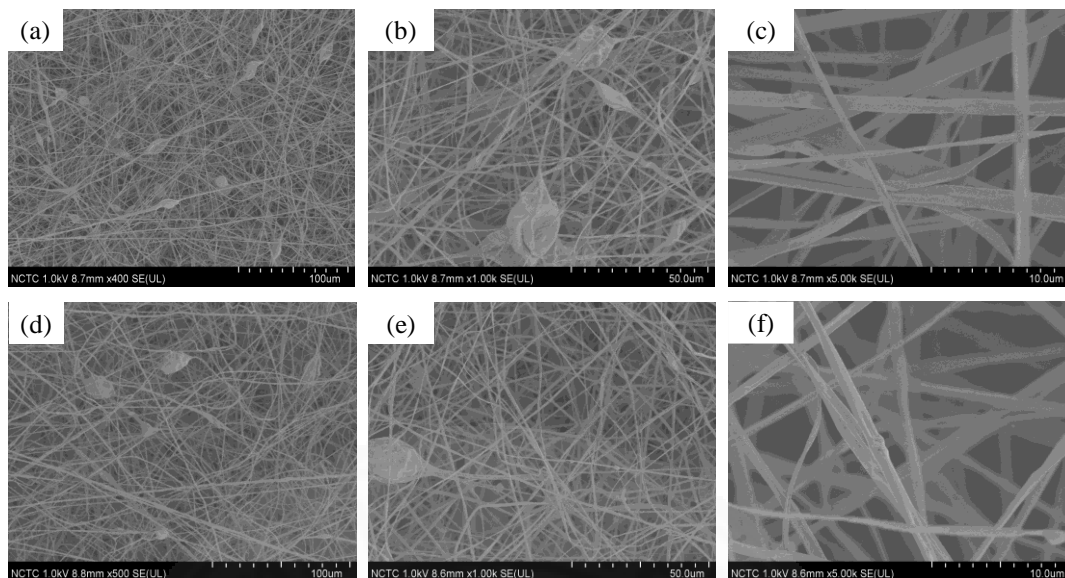
Appendix B.5: SEM images of (a)-(c) PLLA/PVP (5:1)/TiO$_2$ 5% 10kV and (d)-(f) PLLA/PVP (5:1)/TiO$_2$ 5% 15 kV.
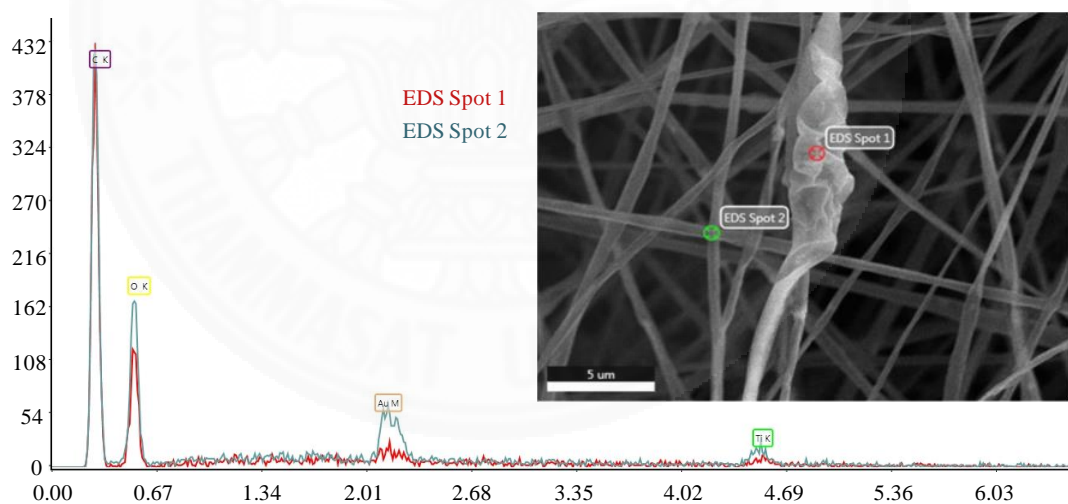
Appendix B.6: EDX of PLLA/TiO$_2$ 5% (15kV).
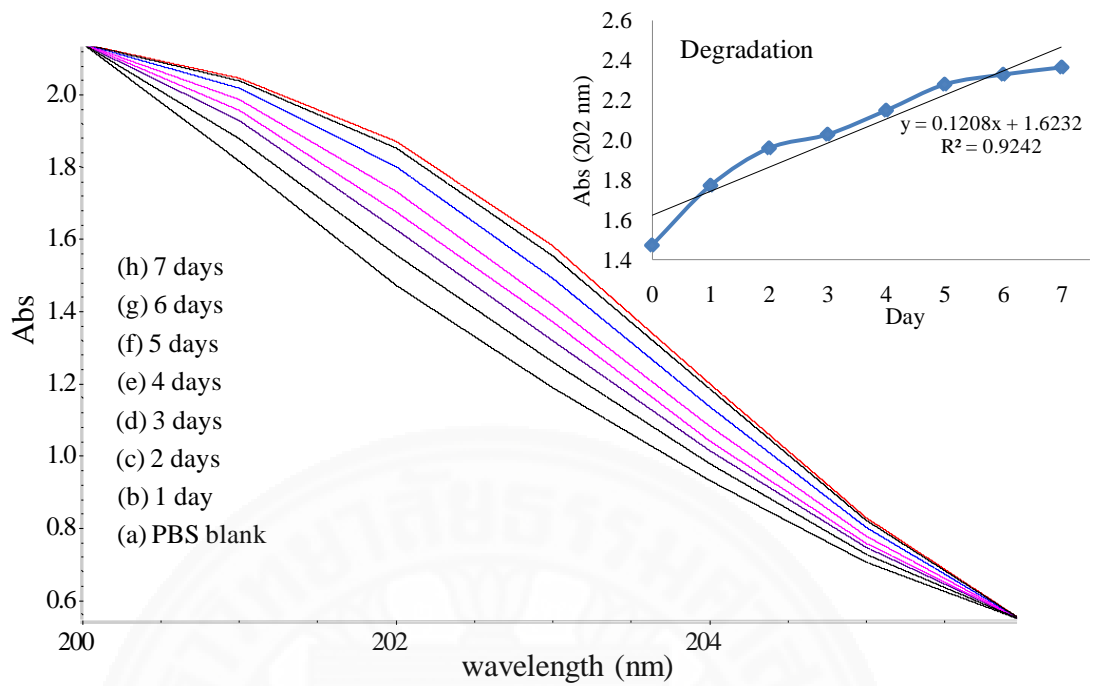
Appendix B.7: UV-Vis spectra of PBS solution of PLLA/TiO$_2$ (15 kV) after degradation from 1-7 days.
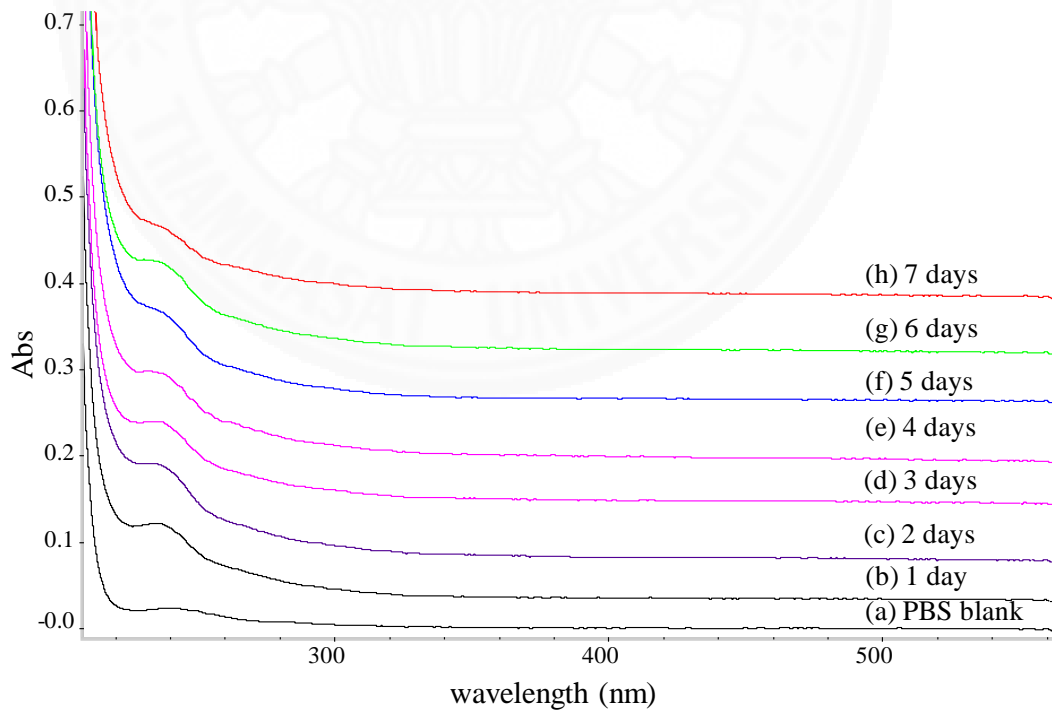
Appendix B.8: UV-Vis spectra of degradation results of PLLA/TiO$_2$ (15 kV) in PBS solution under UVA light from 1-7 days.
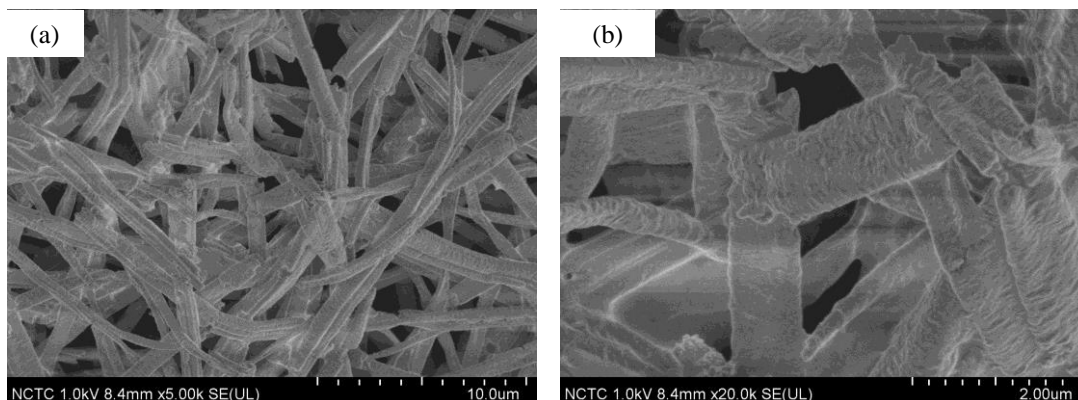
Appendix B.9: SEM images of degradation of PLLA/TiO$_2$ (15 kV) in PBS solution under UVA light at 1day.
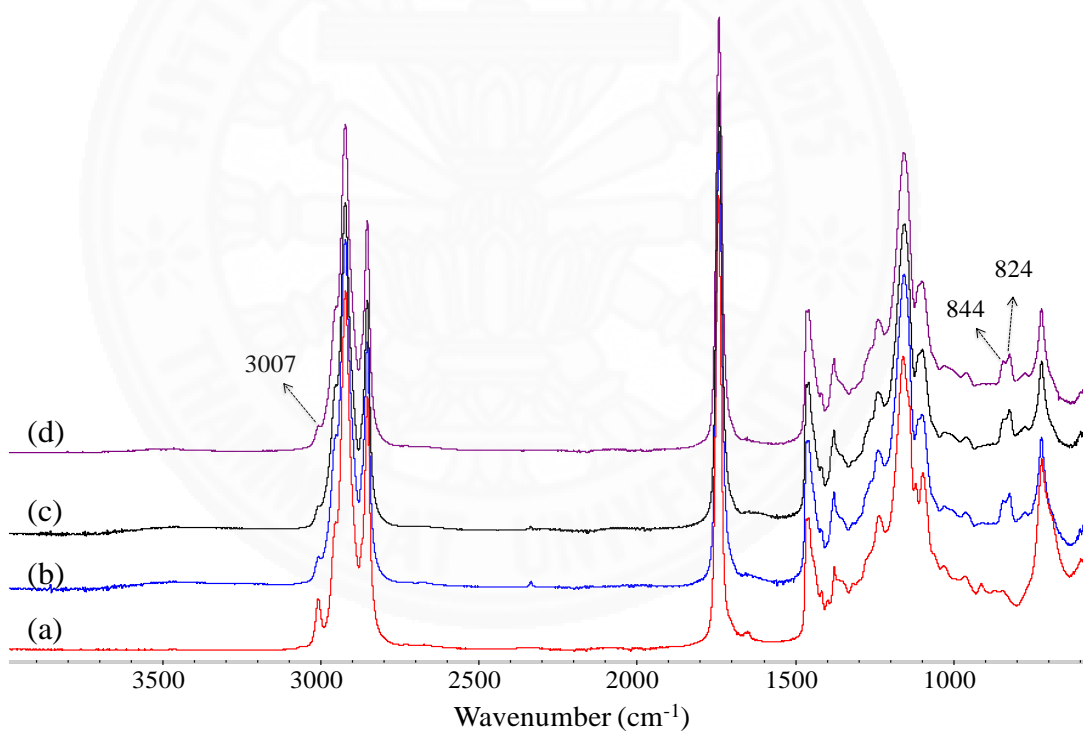
Appendix B.10: FTIR-ATR of: (a) sunflower oil (SFO), (b) ESFO-1, (c) P-T-SFO-1, and (d) P-P-T-SFO-1 epoxidized at 29-33°C.

Appendix C

1. International Conference: "The 26th National Thai Institute of Chemical Engineering and Applied Science Conference (TIChE2016) and The 6th International Thai Institute of Chemical Engineering and Applied Science Conference (ITIChE2016)". The paper in the title of "Preparation and Properties of Electrospun Fibers of Titanium Dioxide-Loaded Polylactide/Poly(vinylpyrrolidone) Blends" was forwarded to "KMUTNB Int J Appl Sci Technol" and under review.

2. International Conference: "The Pure and Applied Chemistry International Conference 2017 (PACCON2017)". Entitle "Property modifications of polylactide/polyvinylpyrrolidone blends loaded with TiO_2 by dielectric barrier discharge (DBD) plasma treatment".

3. International Journal: This manuscript has been submitted to "Industrial Crops and Products-Journal Elsevier". Entitle "Preparation of TiO_2-Loaded Electrospun Fibers of Polylactide/Poly(vinylpyrrolidone)Blends for Use as Catalysts in Epoxidation of Unsaturated Oils".

Preparation and Properties of Electrospun Fibers of Titanium Dioxide-Loaded Polylactide/Poly(vinylpyrrolidone) Blends

Bunthoeun Nim, Paiboon Sreearunothai, and Pakorn Opaprakasit*

School of Bio-Chemical Engineering and Technology, Sirindhorn International Institute of Technology (SIIT), Thammasat University, Pathum Thani 12121, Thailand

* Corresponding author. E-mail: pakorn@siit.tu.ac.th

Abstract
Nanofibers of polylactide (PLA)/poly(vinylpyrrolidone) (PVP) blends loaded with TiO_2 particles have been prepared by an electrospinning technique. TiO_2 particles are formed by sol-gel mechanisms from titanium (IV) isopropoxide (TTIP) precursor. Effect of TiO_2 formation rate on properties of the fibers are examined by adding isopropyl alcohol (IPPA) to slow down the TiO_2 precipitation process. The use of IPPA produces fiber mats consisting of slightly bigger and smoother filaments, but smaller-sized embedded TiO_2 particles. Both materials show a distinct UV absorption characteristic of TiO_2 at λ_{max} 300 nm, which can be applied in many catalytic applications. Degradation behaviors of the materials in phosphate buffer solutions have also been investigated.

Keywords: Polylactide, Poly(vinylpyrrolidone), Titanium dioxide, Electrospinning, Degradation

1 Introduction

Polylactide (PLA) is a widely used biodegradable polymer, which can be synthesized from renewable resources. This polymer is derived from lactic acid monomers, commonly obtained from fermentation of agricultural products, such as corn, rice, wheat, and cassava starch [1]. PLA is recently applied in a wide range of applications, including packaging [2, 3] , tissue engineering [4], scaffold engineering [5] , wound dressing, drug delivery, and anti-microbial materials [6], due to its good mechanical properties, ease of processibility, biodegradability [7, 8], biocompatibility [9] , and high transparency [10]. Therefore, PLA is a promising alternate to non-degradable petroleum-based plastics to solve serious plastic waste problems.

Polymer blends and composites have attracted vast attention from the research community and industrial sectors to further improve properties of the materials and expand their applications. Various blends and composites of PLA have been developed and used for many specific applications. Recently, composites of PLA with titanium dioxide (TiO_2) particles were prepared and their properties and potentials were examined. TiO_2 nanoparticles possess a unique photo-catalytic activity that can be applied in environmental remediation, especially degradation of organic pollutants and bacteria with high efficiency [11, 12].

The major advantages of using TiO_2 particles include inexpensive cost, non-toxicity, high chemical stability, and high resistant to solvents. Various preparation methods of PLA/TiO_2 composites were reported, such as in situ polymerization, electrospinning [6], spin coating [13], solution casting [9], and a surface modified method [10]. In addition, several PLA-based blends were used to prepare various composites, including poly(vinylpyrrolidone) (PVP) [14], polyethylene (PE) [15], polystyrene (PS) [16], and poly(butylene succinate) (PBS) [17]. Among these, PVP shows interesting properties, as it is water soluble, with low toxicity and high physiological compatibility [18]. This polymer is also considered as a conventional polymer for safe use in pharmaceutical, cosmetic, and food industries [19].

Blends of PLA and PVP loaded with TiO_2 nanoparticles ($PLA/PVP/TiO_2$) are a promising nanocomposite for use in improving PLA's properties and introducing specific catalytic activities. These composites exhibited enhanced properties compared to their neat material counterparts, such as higher Young's modulus, improved thermal stability, higher photo-degradability and biodegradability, and higher gas barrier properties [20, 21]. Nanocomposite fibres of

1

PLA/TiO$_2$/PVP/ZnCl$_2$ were fabricated by an electrospinning technique and used in a wound dressing application [14].

In this work, TiO$_2$-loaded PLA/PVP nanofibers are fabricated by an electrospinning method. The loaded TiO$_2$ particles are formed by sol-gel mechanisms by employing their precursor solution mixed with the solutions of the polymer matrix during the electrospinning process. Effects of TiO$_2$ particles formation rate on properties of the fibers are examined by adding isopropyl alcohol (IPPA). Morphology and properties of the resulting fiber mats are investigated. The materials have high potential for use as a degradable catalytic system. Their degradability is then examined in phosphate buffer solutions (PBS), under UVA light activator [22].

2 Methodology

2.1 Materials

Poly(L-lactide) 4043D (PLA) was supplied by NatureWork®. Poly(vinlylpyrrolidone) K29-32 (Mw=58,000 g/mol) and Titanium (IV) Isopropoxide, Ti(O*i*Pr)$_4$ (TTIP), precursor (98+ %) were purchased from Acros. Chloroform RPE (>99%), N,N-Dimethy formamide (DMF) (99.8%), and Isopropyl alcohol (99.7%) (IPPA) solvents were purchased from Carlo Erba. Sodium dihydrogen phosphate monohydrate (NaH$_2$PO$_4$;H$_2$O) and disodium hydrogen phosphate heptahydrate (Na$_2$HPO$_4$;7H$_2$O) were supplied by Carlo Erba and PANREAC, respectively.

2.2 Preparation of PLA/PVP Blends and TiO$_2$ composites

PLA/PVP blends were prepared by mixing PLA (0.84 g) with PVP at a ratio of 5:1 wt./wt., in chloroform (9 g), stirring until completely dissolved. A TiO$_2$ precursor mixture was prepared from TTIP (200 µL), mixed with DMF (3 g) and IPPA (1.5 g), followed by adding DI water (100 µL) drop wise. The mixture was stirred at room temperature for 1 h. IPPA was used to slow down the precipitation rate of TiO$_2$ particles. The polymer mixture was then mixed with the precursor mixture and stirred at room temperature for 1 h to generate suitable solutions for electrospinning. A summary of the samples compositions and sample names is listed in Table 1.

2.3 Electrospinning

The fiber mats were fabricated by an electrospinning technique. The composited mixture was placed in a syringe (capacity 3 mL) connected to a syringe-stainless needle. The syringe was placed on a flow controller (KD Scientific KD 100 Syringe Pump), with a flow rate of 1 mL/h. The distance between the collector and the needle tip was 15 cm. A voltage of 10 kV was applied by using a Gamma high voltage (0-40 kV) power supply. The electrospun fibers were gathered on an aluminum foil collector.

Table 1: Summary of sample compositions and sample names.

Samples	PLA (g)	PVP (g)	TTIP (µL)	IPPA (g)
P-P-T	0.84	0.168	200	0
P-P-I-T	0.84	0.168	200	1.5

2.4 Characterization

Fourier Transform Infrared (FTIR) spectroscopy, equipped with an attenuated total reflectance (ATR) accessory (Nicolet iS5 Spectrometer), was employed to determine functional groups and interactions of the electrospun fiber mats. Scanning electron microscopy (SEM-SU8030) was used to investigate size and surface morphology of the samples. Energy-dispersive X-ray (EDX-SU8030) was employed to observe surface compositions of each component. A UV-Vis spectrophotometer (Genesys 10S) was uesed to examine the absorption behaviors of the fiber mats.

2.5 Degradation Experiments

Degradation behaviors of the fiber mats were examined in phosphate buffer solutions (PBS at pH 7.4) at ambient temperature. Neat PLA, P-P-T, and P-P-I-T fiber mats were cut into 2×2 cm^2. Each specimen was immersed into 50 mL PBS and placed at a 22 cm distance under UVA light (UVA 15WT8 lamp). The experiments were conducted for 6 days, and after that the specimens were removed from the solution and washed with DI water and dried at 40°C in a vacuum oven for overnight. FTIR and UV-Vis spectroscopy were used to examine the structures of the samples as a function of degradation time.

3 Results and Discussion

3.1 ATR-FTIR Spectroscopy

2

ATR-FTIR spectra of spun fiber samples of neat PLA, P-P-T, and P-P-I-T are shown in Figure 1. Band characteristics of PLA and PVP are observed, indicating the presence of the 2 components on a filament's surface. A strong band at 1753 cm^{-1} is assigned to the vibration of C=O of PLA chains, whereas that at 1659 cm^{-1} corresponds to the amide (N-C=O) vibration. Both P-P-T and P-P-I-T show similar FTIR spectra pattern. This reflects that the technique may not be able to differentiate the nature of the two samples. Nonetheless, a broad band centered at 3400 cm^{-1} (O-H stretching), observed in these 2 samples but not in neat PLA, indicates the presence of remaining isopropyl alcohol after the TiO_2 particle formation, and also bound water molecules due to the hygroscopic nature of PVP.

Figure 1: ATR-FTIR of fiber mats: (a) Neat PLA, (b) P-P-T, and (c) P-P-I-T.

3.2 *Scanning Electron Microscopy*

Figure 2 shows surface morphology of P-P-T and P-P-I-T mats examined by SEM. Significant differences between the 2 samples are observed. Both sample mats show rough and irregular surface morphology, which is different from that of neat PLA, as reported earlier [23]. This is likely due to the interplay between the 2 polymeric components during electrospinning. Nonetheless, it is clearly observed that the surface of P-P-I-T fibers is smoother than that of P-P-T. The fiber mats of P-P-I-T show embedded TiO_2 beads more uniform than P-P-T, as the addition of IPPA slows down the TiO_2 precipitation rate. The regions of irregular fiber (beads) shape are caused by agglomeration of TiO_2 particles present as beads embedded in the filaments. This is confirmed by EDX results, as illustrated in Figure 3. The Ti content in the beads is very high compared to that in the regular fiber region. The size distribution of the filaments is compared in Figure 4. The P-P-T fibers have an average diameter of 800 nm, slightly smaller than that of P-P-I-T (827 nm).

3

86
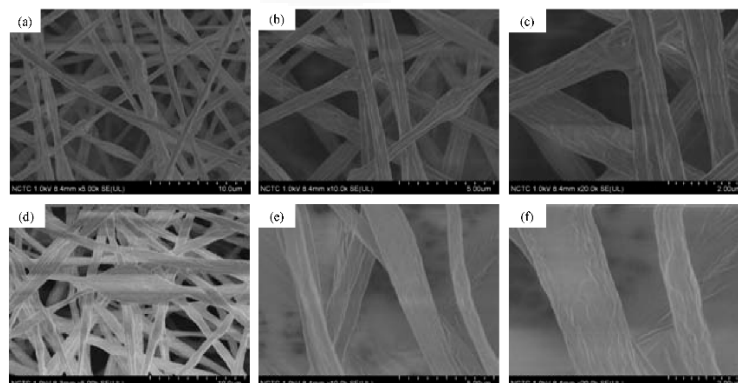
Figure 2: SEM images of electrospun fibers (a)-(c) P-P-T and (d)-(f) P-P-I-T at 5,000×, 10,000×, and 20,000× magnifications.
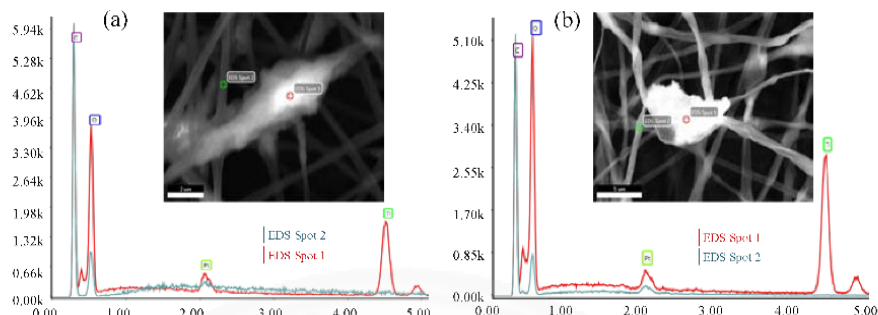
Figure 3: EDX spectra illustrating atomic compositions of bead defects with different sizes present in (a) P-P-T and (b) P-P-I-T fibers.
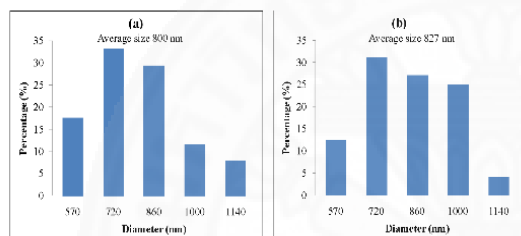
Figure 4: Size distribution of (a) P-P-T and (b) P-P-I-T fiber mats.

3.3 *UV-Vis absorption*

UV-Vis spectroscopy is used to examine absorption behaviors of the materials, as shown in Figure 5. P-P-T and P-P-I-T fibers show major absorption bands at λ_{max} 214 nm. This is due to the n→π* transition of the carbonyl groups in PLA, in which is similar to that observed in spun fibers of neat PLA. All samples also show a broad absorption covering the full visible region, likely due to the opaque nature of the fiber mats. A distinct absorption band is observed at 300 nm for P-P-T and P-P-I-T fiber mats, indicating the presence of TiO₂ particles. This enables the materials to possess photo-catalytic activity for use in many applications, such as epoxidation of unsaturated oils or degradation of contaminated water. Due to space limitations, this will be addressed in details in a separate work.

3.4 *Degradation Mechanisms*

Degradation behaviors of the spun fiber mats are examined in PBS solutions by activation with UVA light. The fiber samples were soaked in PBS at 1, 4, and 6 days, and their FTIR and UV-Vis spectra were recorded (Figure 6). ATR-FTIR and UV-Vis spectroscopy show evidence of PLA degradation as a function of time, similar to those reported in our previous work [24]. Both P-P-T and P-P-I-T mats show similar FTIR changes, and the latter is chosen to show the changes. A decrease in intensity of the 1659 cm⁻¹ band of the amide group of PVP reflects that during the degradation, PVP present on the surface of the filaments is released and dissolves in PBS solutions. However, a weak band in the same region is observed at 1650 cm⁻¹, associated with carboxylate of degraded PLA.
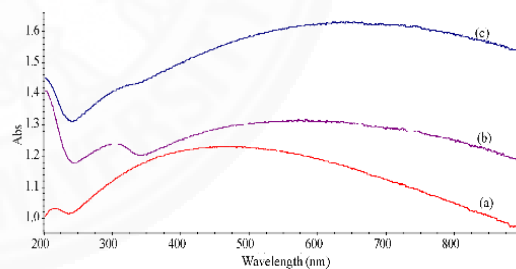
Figure 5: UV-Vis spectra of fibers mats of (a) neat PLA, (b) P-P-T, and (c) P-P-I-T.
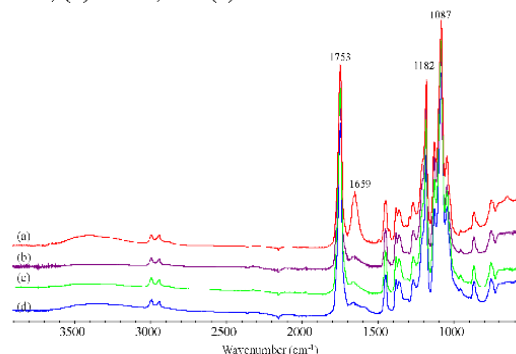
Figure 6: FTIR-ATR spectra of electrospun P-P-I-T (10 kV) fiber soaked in PBS solution at: (a) 0, (b) 1, (c) 4, and (d) 6 days.

Results from UV-Vis spectra of the PBS solutions after P-P-I-T fiber mats are soaked for 1, 4, and 6 days, as shown in Figure 7, illustrates an absorption band of lactate oligomers, products from the degradation of PLA, at 202 nm. The intensity of the band increases with the degradation time, indicating that degradation of the PLA component takes place very early. This is likely because of the presence of TiO_2 catalytic particles and the dissolubility of PVP from the filaments, which in turn, exposes the PLA component to a higher degree of hydrolysis.
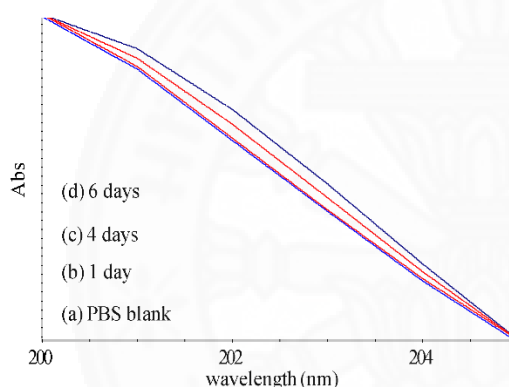
Figure 7: UV-Vis spectra of P-P-I-T fiber mats as a function of degradation time from 1, 4, and 6 days.

4   Conclusions

Fiber mats of PLA/PVP blends loaded with TiO_2 particles, i.e., P-P-T, and P-P-I-T, are successfully fabricated by an electrospinning method. The fiber mats absorb UV light in a region of 300 nm, which enables their photo-catalytic activity. Preliminary results from degradability experiments show that degradation of the PLA component takes place very early, due to the presence of TiO_2 catalytic particles and the dissolubility of PVP from the filaments.

Acknowledgements

### References

[1].   Mekonnen, T., et al., *Progress in bio-based plastics and plasticizing modifications.* Journal of Materials Chemistry A, 2013. **1**(43): p. 13379.

[2].   Carosio, F., et al., *Efficient Gas and Water Vapor Barrier Properties of Thin Poly(lactic acid) Packaging Films: Functionalization with Moisture Resistant Nafion and Clay Multilayers.* Chemistry of Materials, 2014. **26**(19): p. 5459-5466.

[3].   Colomines, G., et al., *Barrier properties of poly(lactic acid) and its morphological changes induced by aroma compound sorption.* Polymer International, 2010. **59**: p. 818-826.

[4].   Torres, F., et al., *Mechanical properties and bioactivity of porous PLGA/TiO₂ nanoparticle-filled composites for tissue engineering scaffolds.* Composites Science and Technology, 2007. **67**(6): p. 1139-1147.

[5].   Buzarovska, A., et al., *Effect of TiO₂ nanoparticle loading on Poly(l-lactic acid) porous scaffolds fabricated by TIPS.* Composites Part B: Engineering, 2015. **81**: p. 189-195.

[6].   Gupta, K.K., et al., *Hydrothermal in situ preparation of TiO₂ particles onto poly(lactic acid) electrospun nanofibres.* Applied Surface Science, 2013. **264**: p. 375-382.

[7].   Kale, G., et al., *Biodegradability of polylactide bottles in real and simulated composting conditions.* Polymer Testing, 2007. **26**(8): p. 1049-1061.

[8].   Fukushima, K., et al., *Biodegradation of poly(lactic acid) and its nanocomposites.* Polymer Degradation and Stability, 2009. **94**(10): p. 1646-1655.

[9].   Buzarovska, A. and A. Grozdanov, *Biodegradable poly(L-lactic acid)/TiO₂ nanocomposites: Thermal properties and degradation.* Journal of Applied Polymer Science, 2012. **123**(4): p. 2187-2193.

[10]. Nakayama, N. and T. Hayashi, *Preparation and characterization of poly(l-lactic*

5

88

acid)/TiO₂ nanoparticle nanocomposite films with high transparency and efficient photodegradability. Polymer Degradation and Stability, 2007. **92**(7): p. 1255-1264.

[11]. Lin, W.-C., W.-D. Yang, and S.-Y. Jheng, *Photocatalytic degradation of dyes in water using porous nanocrystalline titanium dioxide.* Journal of the Taiwan Institute of Chemical Engineers, 2012. **43**: p. 269-274.

[12]. Chawengkijwanich, C. and Y. Hayata, *Development of TiO₂ powder-coated food packaging film and its ability to inactivate Escherichia coli in vitro and in actual tests.* International Journal of Food Microbiology, 2008. **123**: p. 288-292.

[13]. Man, C., et al., *Poly (lactic acid)/titanium dioxide composites: Preparation and performance under ultraviolet irradiation.* Polymer Degradation and Stability, 2012. **97**(6): p. 856-862.

[14]. Hong, Y., et al., *Electrospinning of multicomponent ultrathin fibrous nonwovens for semi-occlusive wound dressings.* Journal of Biomedical Materials Research Part A, 2009. **89A**(2): p. 345-354.

[15]. Silva, K.I.s.M.d., et al., *Structural stability of photodegradable poly(l-lactic acid)/PE/TiO₂ nanocomposites through TiO₂ nanospheres and TiO₂ nanotubes incorporation.* Polymer Bulletin, 2014. **71**(5): p. 1205-1217.

[16]. Shimpi, N.G., M. Borane, and S. Mishra, *TiO₂/polystyrene core–shell nanoparticles as fillers for LLDPE/PLA blend: development, and morphological, thermal and mechanical properties.* Polymer Bulletin, 2016.

[17]. Buasri, A., et al., *Effect of Titanium Dioxide Nanoparticles on Mechanical and Thermal Properties of Poly(Lactic Acid) and Poly(Butylene Succinate) Blends.* Advances in Science and Technology, 2014. **96**: p. 33-38.

[18]. Hsiao, C.N. and K.S. Huang, *Synthesis, characterization, and applications of polyvinylpyrrolidone/SiO2 hybrid materials.* Journal of Applied Polymer Science, 2005. **96**(5): p. 1936-1942.

[19]. Haaf, F., A. Sanner, and F. Straub, *Polymers of N-Vinylpyrrolidone: Synthesis, Characterization and Uses.* Polymer Journal, 1985 **17**(1): p. 143-152.

[20]. Zhuang, W., et al., *Preparation, characterization, and properties of TiO₂/PLA nanocomposites by in situ polymerization.* Polymer Composites, 2009. **30**(8): p. 1074-1080.

[21]. Ali, N.A. and F.T.M. Noori, *Gas Barrier Properties of Biodegradable Polymer Nanocomposites Films.* Chemistry and Materials Research, 2014. **6**(1).

[22]. Luo, Y.-B., X.-L. Wang, and Y.-Z. Wang, *Effect of TiO₂ nanoparticles on the long-term hydrolytic degradation behavior of PLA.* Polymer Degradation and Stability, 2012. **97**(5): p. 721-728.

[23]. Thammawong, C., et al., *Electrospinning of poly(l-lactide-co-dl-lactide) copolymers: Effect of chemical structures and spinning conditions.* Polymer Engineering and Science, 2014. **54**(2): p. 472-480.

[24]. Sriromreun, P., et al., *Standard methods for characterizations of structure and hydrolytic degradation of aliphatic/aromatic copolyesters.* Polymer Degradation and Stability, 2013. **98**: p. 169-176.

Property modifications of polylactide/polyvinylpyrrolidone blends loaded with TiO₂ by dielectric barrier discharge (DBD) plasma treatment

Bunthoeun Nim[1], Paiboon Sreearunothai[1], Thawatchai Onjun[2] and Pakorn Opaprakasit[1,*]

1 School of Bio-Chemical Engineering and Technology, Sirindhorn International Institute of Technology (SIIT), Thammasat University, Pathum Thani 12121, Thailand
2School of Manufacturing Systems and Mechanical Engineering, Sirindhorn International Institute of Technology (SIIT), Thammasat University, Pathum Thani 12121, Thailand

*e-mail: pakorn@siit.tu.ac.th

Abstract: Polylactide/polyvinylpyrrolidone blends loaded with TiO₂ nanoparticles in the forms of cast films and electrospun nanofibers have been fabricated by solution casting and electrospinning methods. The materials are intended for use as a catalytic system in epoxidation of unsaturated oils for applications in plasticizing of biopolymers. The properties of the spun fibers are optimized by dielectric barrier discharge (DBD) plasma treatments. Properties of the materials before and after treatments are characterized, in terms of UV-Vis absorption, surface wettability, and crystallinity, by employing contact angle measurements, ATR-FTIR and UV-Vis spectroscopy. The results reveal that the TiO₂-loaded fibers show an absorption band in the region of 250-350 nm, which is suitable for activating epoxidation reactions. The original amorphous fibers show a large increase in their crystalline contents after the plasma treatments, as a result from an annealing effect. The plasma treatments also impose strong effect on hydrophilicity enhancements of the fibers, as the contact angle values are largely decreased. This will enhance the efficiency of the epoxidation reactions.

1. Introduction

Polylactide (PLA) is biodegradable and biocompatible polymer, widely used in packaging, pharmaceutical, and agricultural applications[1]. The material has attracted vast attention, due to its high Young's modulus, tensile strength, and optical plasticity.

Some properties of PLA can be improved by blending with various polymers, i.e. polyvinylpyrrolidone (PVP)[2], polycaprolactone (PCL)[3], and poly (butylene succinate) (PBS)[4]. PVP is also a biodegradable polymer with high hydrophilicity. The material has been widely used in pharmaceutical and cosmetic applications. Composites of PLA with inorganic particles, especially TiO₂ nanoparticles, are also promising to using in many applications. TiO₂ is employed as photo-catalyst in many fields, i.e. water treatment, air purification, anti-bacterial, cosmetic, anti-cancer cells, pigments[5,6] and solar cell systems[7,8].

Electrospinning is a promising method for preparation of polymeric nanofibers. This technique is widely used in order to control structures, porosity, orientations, and dimensions of materials. Modern nanotechnology employing nanofibers has become attractive in various applications, such as high efficiency filters[9], biomaterials, drug delivery, sensors, and photo-degradation catalysts[10-12].

Dielectric barrier discharge (DBD) is commonly employed for surface treatment of materials[13]. This process can produce free radicals to react with various species, especially reactive monomer or polymer chains, on materials surface. Therefore, the DBD plasma treatment is applied for

surface enhancements by improving adhesion and wettability properties[14].

This work aims to fabricate polylactide/ polyvinylpyrrolidone blends composited with TiO₂ particles by an electrospinning method for use as catalyst for photo-catalytic reactions. Effects of DBD plasma treatment on properties of the materials are examined. Properties enhancements, in terms of crystallinity of the PLA matrix and the fibers' surface wettability are achieved, which can further enhance the materials' catalytic reactivity.

2. Methods
2.1 Materials
Polylactide (PLA) 4043D, poly vinlylpyrrolidone K29-32 (Mw=58,000 g/mol), TiO₂ particles (>99.5%, average particle size of 21 nm) were purchased from NatureWork, Acros company, and Sigma Aldrich, respectively. Chloroform RPE (>99%) and N,N-Dimethyformamide (DMF) (99.8%) solvents were purchased from Carlo Erba.

2.2 Preparation of composited blends
Composited blends of PLA/TiO₂ (PT), and PLA/PVP/TiO₂ (PPT) were prepared with a constant PLA:PVP weight ratio of 1:0.2. TiO₂ particles (5 wt% of PLA) were then added. Chloroform (9 g) was employed as a solvent for each mixture, by stirring overnight at ambient condition. DMF (3 g) was then added, and the mixture was further stirred at room temperature for 4 hours. Film samples were prepared by casting the solutions on a glass surface, in which the solvent was evaporated at room temperature for 2 days, followed by vacuum drying for a week.

2.3 Electrospinning of composited blends
Nonwoven composited fibers were prepared by an electrospinning technique. The polymeric mixture was pumped into a syringe (5 mL capacity) connected with a stainless steel needle (22 mm × 1½ mm). A flow controller (KD Scientific KD100

Syringe Pump) was employed in the spinning process, with a flow rate of 1 mL/h. The distance between the needle tip and the collector was fixed at 15 cm. A voltage of 15 kV (Gamma High Voltage Research 0-40 kV) was applied. The resulting nonwoven fiber mats were finally collected on an aluminum foil connected to a ground electrode.

2.4 Characterization
The electrospun fibers and cast films of neat PLA, PT, and PPT composites were characterized by Fourier Transform Infrared (FTIR) spectroscopy in an Attenuated Total Reflectance (ATR) mode on a Nicolet iS5 spectrometer. Each sample was recorded at 64 scans, with a resolution of 2 cm⁻¹. An Ultraviolet-Visible (UV-Vis) spectrophotometer (Genesys 10S) was used to observe absorption characteristics of the fiber mats.

2.5 Plasma treatments
The cast films and fibers were treated with DBD plasma to modify their surface properties. The samples were placed between two electrodes (copper plates) at a fixed distance of 2 mm. The electrodes were covered by petri dish glass plates. The plasma was generated at a frequency of 5.5 Hz, 40 V output voltage, at atmospheric room temperature. The treatment times were varied from 1, 2, 3, 4 and 5 min. After the plasma treatment, the materials were characterized by ATR-FTIR spectroscopy and water contact angle measurements.

3. Results & Discussion
### 3.1 ATR-FTIR and UV-Vis spectroscopy
ATR-FTIR spectra of the resulting materials are shown in Figure 1. The carbonyl (C=O) vibration mode is located at 1752 cm⁻¹ [15]. Characteristic bands of PVP are observed at 1659 (N-C=O stretching)[2], 1453 (–CH₃ asym stretching), and 1382 cm⁻¹ (C-H bending). A C-O vibration mode of PLA is found at 1182-1085 cm⁻¹ [15]. A crystalline characteristic

band of PLA is observed at 920 cm^{-1} [16,17]. This is clearly found in the cast film samples, i.e. neat PLA, PT, and PPT films. However, the electrospun fiber samples do not exhibit this crystalline band, because the rapid solvent evaporation during electrospinning retards chain orientation[18]. To confirm this, the C=O bands of cast films and fibers are closely examined, as shown in Figure 2. The crystalline C=O band of PLA is located at 1756 cm^{-1}, whereas that at 1748 cm^{-1} is corresponding to amorphous structure[19]. The spectra of

cast films clearly show a combination of these 2 bands, indicating their semi-crystalline nature. In contrast, the corresponding spun fibers do not exhibit the crystalline band, while the amorphous mode is dominant. This reflects a complete amorphous nature.

UV-Vis spectra of the TiO2-embedded materials are examined, as shown in Figure 3. The absorption behaviors of PLA matrix is characterized by an absorption in a region of 200 nm. An additional absorption band is observed in a region of 200-380
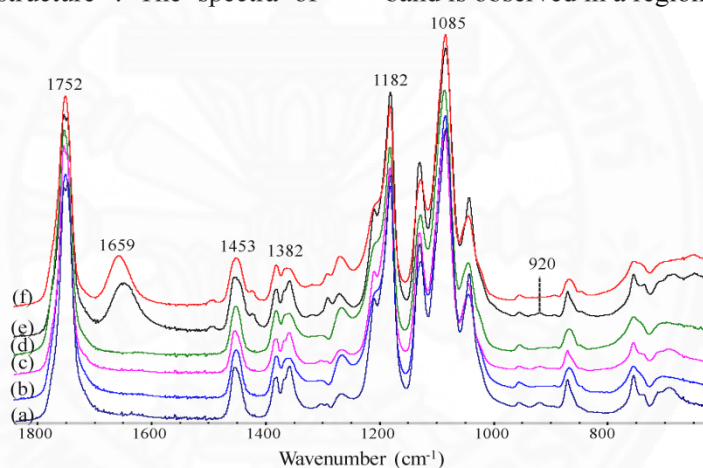
Figure 1. ATR-FTIR spectra of: (a)-(b) neat PLA, (c)-(d) PT and (e)-(f) PPT cast films and electrospun fibers.
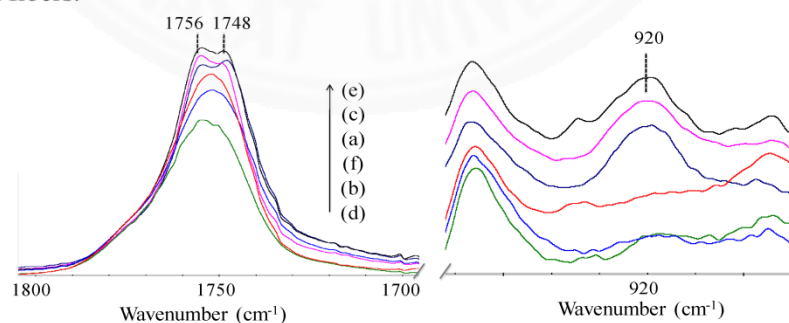
**Figure 2.** ATR-FTIR spectra in the C=O stretching mode and PLA's crystalline characteristics region of: (a)-(b) neat PLA, (c)-(d) PT and (e)-(f) PPT cast films and electrospun fibers.

nm, which confirms the presence of the TiO$_2$ particles embedded on the fiber materials[2]. This enables the use of these

materials in various photo-catalytic applications, especially the degradation of pollutant species and epoxidation of

unsaturated compounds or oils, which will be further discussed in a separate communication.
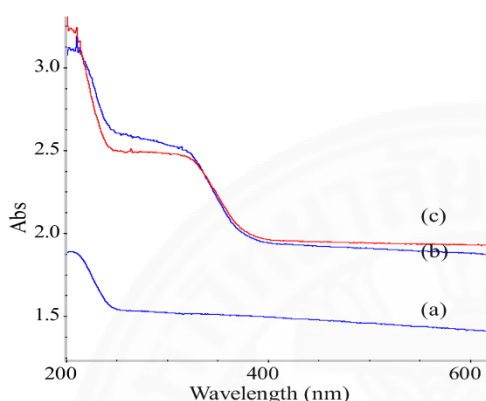

Figure 3. UV-Vis spectra of (a) neat PLA, (b) PT and (c) PPT electrospun fibers.

3.2 DBD plasma treatment

Effect of DBD plasma treatment on properties of the electrospun fibers are characterized by ATR-FTIR spectroscopy, as shown in Figure 4. Band intensity changes are observed in the C=O mode and the PLA crystalline band, as a function of treatment times. The intensities of both 1756 and 920 cm^{-1} bands increase with the treatment time, reflecting crystalline formation of PLA chains[19].

The correlation between the degree of crystal formation, in terms of normalized band area of the crystalline mode, as a function of plasma treatment time are shown in Figure 5. ATR-FTIR spectra are normalized against a reference band at 870 cm^{-1} (C-C), and the curve fitting program is employed to determine the band area of the 920 cm^{-1} mode. The results reveal that after plasma treatments, neat PLA, PT, and PPT cast films show a drastic increase in the crystal content, and reaches a constant level after 1 min of treatment time. This is likely because the original films samples already possess high crystalline content. Upon plasma treatment, induction of further crystallization occurs at the surface as a

result of high surface temperature. Interestingly, PPT and PT samples show higher total crystalline content compared to that of neat PLA films. This is likely because of the presence of TiO$_2$. However, the mechanisms of this crystallization enhancement are unclear and require further examination.
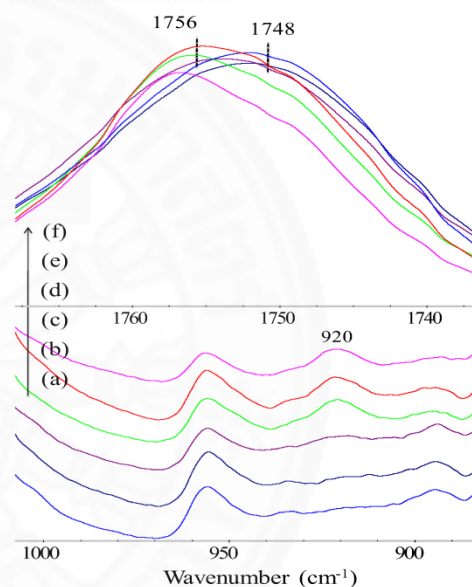
Figure 4. ATR-FTIR spectra of PPT electrospun fibers treated with plasma at: (a) 0, (b) 1, (c) 2, (d) 3, (e) 4 and (f) 5 min.

In contrast, all of the corresponding fiber mats show a linear increase in the crystalline content as a function of time. A rough increase of about ten folds is observed at 5 min. This large increase in crystallinity is because the original fibers are completely amorphous. The increase in temperature from the plasma treatment, therefore, provides PLA chains more flexibility for chain arrangement. As the fiber filaments are in nanometer sizes, the effect of the plasma treatment can be experienced homogeneously across the filaments, leading to a linear increase in the content, which still does not reach a

93

constant level within 5 min of treatment time.
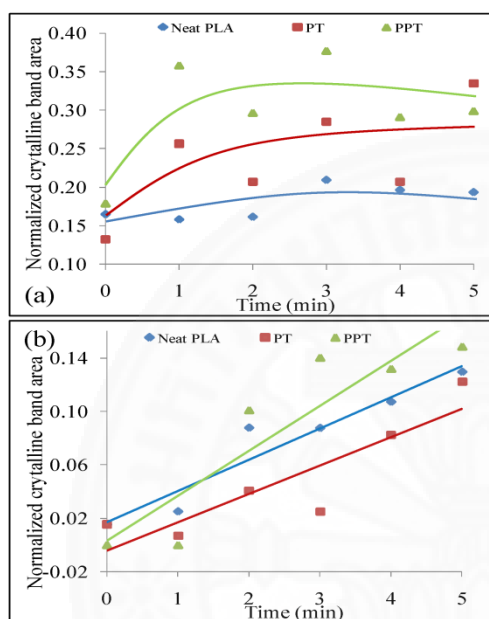
Figure 5. Normalized crystalline band area of: (a) cast films and (b) electrospun fibers after plasma treatment, as a function of time.

3.3 Surface Wettability

Hydrophilicity of the materials before and after plasma treatments are examined by water contact angle measurements, as shown in Figure 6. The contact angle values of neat PLA films decrease as a function of time, reflecting it more hydrophilicity due to a generation of hydrophilic groups on the surface [20]. In contrast, treated PT and PPT cast films show increasing hydrophobicity as a function of time, probably because of the presence of TiO₂ on their surface [21].
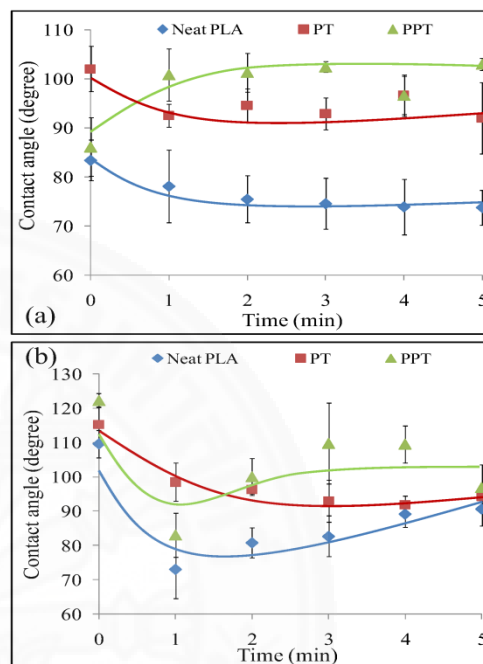
Figure 6. Water contact angle of: (a) cast films and (b) fiber mats of neat PLA, PT and PPT before and after treatment, as a function of time.

A different pattern is observed, however, in the electrospun fibers. All original fiber mats exhibit similar contact angle values at around 110-120°, due to the nanostructure filament nature. Upon plasma treatment, all samples show a drastic decrease in the value, reflecting a large hydrophilicity of the materials, especially at 1 min treatment time. This is likely due to a formation of polar groups on the large surface area of the fiber mats [20].

4. Conclusions

Polylactide and polyvinylpyrrolidone/ polylactide composited with TiO₂ nano particles in a form of electrospun fiber mats are successfully prepared for use as catalytic materials. Properties of the fibers are different from those of their cast film counterparts, due to their nano-filament structures. The spun fibers mats are subject

to plasma treatments to further modify their surface properties and crystallinity. The information is essential in further optimization of the materials' properties for enhancement in their catalytic activity.

Acknowledgements

References

1. Carosio, F.; Colonna, S.; Fina, A.; Rydzek, G.; Hemmerlé, J.; Jierry, L.; Schaaf, P.; Boulmedais, F. *Chemistry of Materials* **2014**, *26*, 5459.
2. Hong, Y.; Li, Y.; Zhuang, X.; Chen, X.; Jing, X. *Journal of Biomedical Materials Research Part A* **2009**, *89A*, 345.
3. Chavalitpanya, K.; Phattanarudee, S. *Energy Procedia* **2013**, *34*, 542.
4. Bhatia, A.; Gupta, R. K.; Bhattacharya, S. N.; Choi, H. J. *Korea-Australia Rheology Journal* **2007**, *19*, 125.
5. El-Sherbiny, S.; Morsy, F.; Samir, M.; Fouad, O. A. *Applied Nanoscience* **2013**, *4*, 305.
6. Kumar, S.; Verma, N. K.; Singla, M. L. *Digest Journal of Nanomaterials and Biostructures* **2012**, *7*, 607.
7. Rashad, M. M.; Shalan, A. E.; Lira-Cantú, M.; Abdel-Mottaleb, M. S. A. *Applied Nanoscience* **2012**, *3*, 167.
8. Tasić, N.; Marinković Stanojević, Z.; Branković, Z.; Lačnjevac, U.; Ribić, V.; Žunić, M.; Novaković, T.; Podlogar, M.; Branković, G. *Electrochimica Acta* **2016**, *210*, 606.
9. Hamid, N. A. A.; Ismail, A. F.; Matsuura, T.; Zularisam, A. W.; Lau, W. J.; Yuliwati, E.; Abdullah, M. S. *Desalination* **2011**, *273*, 85.
10. Pant, H. R.; Pant, B.; Pokharel, P.; Kim, H. J.; Tijing, L. D.; Park, C. H.; Lee, D. S.; Kim, H. Y.; Kim, C. S. *Journal of Membrane Science* **2013**, *429*, 225.
11. Daels, N.; Radoicic, M.; Radetic, M.; Van Hulle, S. W. H.; De Clerck, K. *Separation and Purification Technology* **2014**, *133*, 282.
12. Kang, S.-J.; Tijing, L. D.; Hwang, B.-s.; Jiang, Z.; Kim, H. Y.; Kim, C. S. *Ceramics International* **2013**, *39*, 7143.
13. Kogelschatz, U. *Plasma Chemistry and Plasma Processing* **2003**, *23*.
14. Sun, X.; Zang, B.; Sun, B. *International Journal of Engineering Innovation & Research* **2016**, *5*.
15. Kister, G.; Cassanas, G.; Vert, M. *Polymer* **1998**, *39*, 267.
16. Zhang, J. M.; Tsuji, H.; Noda, I.; Ozaki, Y. *J. Phys. Chem. B* **2004**, *108*, 11514.
17. Kang, S. H.; Hsu, S. L.; Stidham, H. D.; Smith, P. B.; Leugers, M. A.; Yang, X. Z. *Macromolecules* **2001**, *34*, 4542.
18. Thammawong, C.; Buchatip, S.; Petchsuk, A.; Tangboriboonrat, P.; Chanunpanich, N.; Opaprakasit, M.; Sreearunothai, P.; Opaprakasit, P. *Polymer Engineering & Science* **2014**, *54*, 472.
19. Opaprakasit, P.; Opaprakasit, M.; Tangboriboonrat, P. *Applied Spectroscopy* **2007**, *61*.
20. Hergelová, B.; Zahoranová, A.; Kováčik, D.; Stupavská, M.; Černák, M. *Open Chemistry* **2014**, *13*.
21. Zhang, L.; Wan, M. *J. Phys. Chem. B* **2003**, *107*, 6748.

Preparation of TiO₂-Loaded Electrospun Fibers of Polylactide/Poly(vinylpyrrolidone)Blends for Use as Catalysts in Epoxidation of Unsaturated Oils

Bunthoeun Nim [a], Paiboon Sreearunothai [a], Atitsa Petchsuk [b], and Pakorn Opaprakasit [a,*]

[a] School of Bio-Chemical Engineering and Technology, Sirindhorn International Institute of Technology (SIIT),
Thammasat University, Pathum Thani 12121, Thailand

[b] National Metal and Materials Technology Center (MTEC), National Science and Technology Development Agency,
Pathum Thani, 12120, Thailand

E-mail:nimbunthoeun@gmail.com, paiboon_sree@siit.tu.ac.th, atitsp@mtec.or.th

*Corresponding author: pakorn@siit.tu.ac.th

Abstract

Nanofibers of polylactide (PLA)/poly(vinylpyrrolidone) (PVP) blends loaded with TiO₂nanoparticles have been prepared by an electrospinning method. The electrospun fiber mats were characterized by ATR-FTIR, X-ray diffraction (XRD), SEM, EDX, and UV-Visible spectroscopy to examine structures, functional groups, crystallinity, surface morphology, and UV absorptivity. It is clearly observed that TiO₂ particles are embedded on the filaments. All PLA-based spun fibers are completely amorphous in nature, in which surface morphology of those blended with PVP are smoother and more uniform than the corresponding samples without PVP. Neat PLA fibers shows a UV absorption band at around 200 nm, whereas the fibers loaded with TiO₂nanoparticles show an additional absorption band covering the 200-380 nm region. Photo-degradation of the fiber samples are conducted in phosphate buffer solution (PBS) under UVA light. The results indicate that the PVP component is dissolved into PBS solution, and the PLA matrix is degraded as a function of time. The fibers are then applied as a catalytic system for

1

epoxidation of unsaturated sunflower oil (SFO) for use as additives or plasticizers for biopolymers, employing a performic acid oxidizing agent. The fibers, especially those containing PVP, can effectively enhance the epoxidation yield of oils with a slow rate of undesirable side reactions, which break ester bonds of the triglyceride to generate free fatty acids.

Keywords: Polylactide, Poly(vinylpyrrolidone), TiO$_2$, Electrospinning, Degradation, Epoxidation.

2

1. Introduction

Biopolymers have attracted vast attention, due to their excellent characteristics, such as renewability, degradability, and biocompatibility. These materials can be degraded by various mechanisms, e.g. oxidation, photo-degradation, enzymatic activity, and biodegradation by microorganisms. Biopolymers can also be called bio-based polymers, as these are synthesized from renewable bio sources[1]. Some examples of biopolymers that are widely investigated and used are polylactide (PLA), polyglycolic acid (PLGA), polycaprolactone (PCL), silk, gelatin, and chitosan.

PLA is one of the most promising biopolymers for commercial use in various fields, e.g. packaging, agricultural, electronic, automobile, textile, tissue engineering, wound dressing, drug delivery, and anti-microbial applications. The polymer is synthesized from agricultural resources, such as cassava, rice, and corn. These raw materials are converted to lactic acid monomer, through fermentation using microorganisms. The polymer possesses many excellent characteristics, such as good mechanical properties, thermal plasticity, fabric ability, high water resistance, good transparency[2], biocompatibility[3], and degradability [4, 5].

Titanium dioxide (TiO_2) is a heterogeneous photocatalyst widely used in various applications, especially in environmental fields. The material is a strong oxidizing agent, commonly applied in photo-degradation of organic contaminants in wastewater treatment[6, 7], drinking water disinfection, air purification[8], anti-microbial activity[9], cancer cell treatment[10, 11], and drug delivery [12, 13].In addition, TiO_2 possesses inexpensive cost, non-toxicity, high chemical stability, long durability, and high resistance to acid-alkali and organic solutions.

3

Recently, various composites materials derived from PLA have been developed.It is suggested that nanocomposites containing particles have improved the properties of the PLA matrix. The nanocomposites exhibited higher Young's modulus, improved thermal stability, and higher gas barrier properties than neat PLA [14].Preparation of composites of PLA and TiO_2 particles is a promising approach for improvement of this biopolymer's properties. The composites show higher biodegradability and photo-degradability, especially under UV radiation with the presence of an activator, compared to neat PLA. The materials are widely used as packaging products to extend shelf-life of food products[15].PLA/TiO_2composite is also a promising choice for use as a wound dressing material and catalyst. It can be used for drug delivery, anti-microbial activity, and gas barrier packaging. To further enhance specific properties, the composites have been fabricated into the form of nanofibers, which possess high surface area. Gupta et al. reported a preparation of PLA/TiO_2 fibers by an electrospinnig technique for use as an anti-microbial material[16]. Honget al.developednanocomposite fibres of PLA/TiO_2/poly(vinyl pyrrolidone)/zinc chloride by electrospinning and used them as wound dressing materials[17]. Degradability of this composite system and its mechanisms have been examined in phosphate buffer solution (PBS) [18].

Vegetable oils (VO) are one of the major dietary and also valuable raw materials for utilization in many applications. This group of triglyceride, such as palm oils, sunflower oils, soybean oils, olive oils, and canola oils, has different contents of unsaturated and saturated fatty acids, in which the former contains at least one double bond in their molecules. The compounds can undergo several reactions, such as epoxidation, carboxylation, hydroxylation, hydrogenation, halogenation, and oxidation by using suitable reagents and catalysts [19]. These olefinic bonds present in VO are promising functional groups for converting to epoxy groups, which can be

4

applied as non-metallic co-plasticizers or heat stabilizers in bioplastic processing. These epoxidized oils have been added to polymers to improve their elasticity, elongation, softness, and decrease the glass transition temperature (T_g). For instance, epoxidized sunflower oil (ESFO) was used as an organic co-plasticizer and thermal co-stabilizer for plasticized PVC [20-22]. Sunflower oil (SFO) consists of approximately 11% saturated and 89% unsaturated fatty acids. Several catalysts have been designed and used in the epoxidation of this oil. It was reported that Ti (IV)-grafted silica [19, 23], Ti/SiO$_2$[24], and Ti-MCM-41 [25] catalysts exhibited high activities and stabilities for epoxidation of different olefinic compounds.

This work aims to fabricate polylactide/poly (vinylpyrrolidone)/TiO$_2$ (PLA/PVP/TiO$_2$) composite nanofibers via an electrospinning method for use as surface-enhanced immobilized photocatalytic materials in the epoxidation of SFO. Miscibility of the composite components and their role in the dispersing of TiO$_2$ particles, and properties of the resulting nanofiber composites are investigated. Self-degradation of the materials in PBS buffer solutions under UV light is examined to gain insights into the degradation mechanisms. The nanofiber composites are then applied as a catalytic system in the epoxidation of SFO, in which the reaction efficiency and mechanisms are examined. The epoxidized triglycerides, which contain reactive epoxide functional groups for further structural modifications, have high potential use as a plasticizer for property enhancements of various biopolymers.

2. Methodology

2.1. Materials

Polylactide (PLA) 4043D was purchased from NatureWork[R]. Poly(vinylpyrrolidone) K29-32 (Mw=58,000 g/mol) was supplied from Acros company. TiO$_2$ (>99.5%), average particle size

5

of 21 nm, was supplied by Sigma Aldrich. Chloroform RPE (>99%) and N,N-Dimethyformamide (DMF) (99.8%) solvents were purchased from Carlo Erba. Sodium dihydrogen phosphate monohydrate ($NaH_2PO_4.H_2O$) and disodium hydrogen phosphate heptahydrate ($Na_2HPO_4.7H_2O$) were obtained from Carlo Erba and PANREAC, respectively. Sunflower oil (SFO) (Big C sunflower oil) was used in epoxidation experiments. Formic acid (90%) and sodium carbonate anhydrous (99.8%) were supplied by AJAX. Hydrogen peroxide (35%) was purchased from Chem Supply. All chemicals were used without further purification.

2.2. Preparation of composited blends

Two different composited mixtures were prepared, i.e., PLA/TiO_2 5% (P-T), and PLA/PVP (5:1)/TiO_2 5% (P-P-T) by keeping the weight of PLA constant at 0.7g. TiO_2 particles were then added to each mixture at a constant weight composition of 5wt% of PLA. The polymer mixtures were dissolved in chloroform (9 g) and stirred overnight at room temperature. After the polymers were completely dissolved, DMF (3 g) was added, and the mixture was further stirred at room temperature for 4 h to generate a suitable solution for electrospinning. Cast film samples were also prepared by casting the solutions on a glass surface, in which the solvents were evaporated at room temperature for 2 days, followed by vacuum drying for a week.

2.3. Fabrication of electrospun composited fibers

A horizontal electrospinning setup was employed to prepare nonwoven composited fibers. The electrospinning apparatus consists of a high voltage power supply (Gamma High Voltage Research0-40 kV), a flow controller (KD Scientific KD100 Syringe Pump), an aluminum collector, a syringe (5mL), a stainless steel needle (22×1½ mm), and aluminum foil. Essentially, the polymer mixture was pumped into a syringe connected with a stainless needle, at a flow rate of 1 mL/h. The distance between the needle tip and the collector was fixed at 15 cm, whereas the

6

101

voltage was varied at 10 and 15kV. The nonwoven fiber mats were collected on an aluminum foil connected to a ground electrode.

2.4. Characterization

The electrospun fibers of PLA/TiO$_2$ and PLA/PVP/TiO$_2$composites were characterized by Fourier Transform Infrared (FTIR) spectroscopy in an Attenuated Total Reflectance (ATR) mode on a Nicolet iS5 spectrometer. Each sample was recordedat64 scans, with a resolution of 2 cm^{-1}. X-ray diffraction (XRD) spectroscopy was used to measure the crystalline characteristics of all fiber mats and solution cast film samples. The measurements were conducted on an X'Pert PRO spectrometer using the following conditions: Cu/K-alpha radiation (λ=1.54056 Å) at 40kV, 30mA, and a scanning rate of 2°/min from 2θ= 4° to 45°. Scanning electron microscopy (SEM-SU8030) and energy-dispersive X-ray (EDX-SU8030) were employed to examine surface morphology and surface composition of each component. A Genesys 10S UV-Vis spectrometer was used to observe the absorption characteristics of the fiber mats, and phosphate buffer solutions(PBS)obtained from degradation experiments of the electrospun fiber samples.

2.5. Degradation experiments

The nonwoven fiber mats were cut into 2×2 cm^2 specimens for degradation experiments. Each specimen was pre-weighed (W$_0$) and placed in a beaker filled with 50 mL of PBS (pH 7.4) at room temperature. The buffer solutions were prepared by the mixing of NaH$_2$PO$_4$.H$_2$O and Na$_2$HPO$_4$.7H$_2$Owithdistilled water. The fiber specimens were immersed in PBS and irradiated with UVA light (UVA 15WT8 lamp, with wavelength 315-400 nm). The samples were placed at a 22 cm distance from the lamp. Each specimen was removed from the PBS solution at an interval of 1 day and washed with a large amount of distilled water to remove residue buffer solution. The specimens were wiped with Whatman filter papers to remove surface water and

7

then dried at 37°C until a constant weight (W_d) was reached. The experiment was conducted for a duration of 7 days.

2.6. Epoxidation of Sunflower oil (SFO)

The composite nanofibers were applied as a surface-enhanced catalyst in the epoxidation of SFO in the presence of formic acid and hydrogen peroxide at room temperature and 65°C. The fiber catalyst was soaked in the reaction flask containing the oil and formic acid. Hydrogen peroxide was, then, added dropwise with continuous stirring. The mixture was irradiated with UV light (254 nm), using a UV lamp Spectroline® (ENF-260C/FE) at a 10 cm distance, with continued stirring for 3 h. The fibers were then removed, and the organic layer of the epoxidized oil was transferred to a separatory funnel. The epoxidized oil was washed by Na_2CO_2 (0.1M) solution for 3 times, followed by distilled water for 5 times, to remove residue aqueous phase. The organic layer was finally dried overnight at 65°C.

The effects of contents of oxidizing agents and the application of nanofiber catalyst on efficiency of the epoxidation reaction were examined by varying of the $HCOOH/H_2O_2$ ratios from 0.5/1, 0.75/1.5, and 1/2 mL. This was conducted by fixing the amount of SFO at 5 g and the amount of electrospun fibers at 10.8 g.

3. Results and Discussion

3.1. ATR-FTIR spectroscopy

Solution-cast films and fiber samples electrospun at 15 kV of $PLLA/TiO_2$ (P-T15) and $PLLA/PVP$ (5:1)$/TiO_2$ (P-P-T15) are characterized by ATR-FTIR, as shown in Figure 1. The characteristic band at 3400 cm^{-1} corresponds to the stretching mode of -OH group. Bands at 2994, 2944, 1455, and 1359 cm^{-1} belong to vibrations of –CH$_3$ asymmetric, –CH$_3$ symmetric,

8

bending of –CH$_3$ asymmetric, and –CH$_3$ symmetric modes, respectively. Absorption modes at 1753, 1652, 1381, 1182-1086, and 871 cm^{-1} are assigned to the vibration of υ(C=O), υ(N-C=O), C-H bending, υ(C-O), and υ(C-C), respectively [26]. The characteristic band located at 920 cm^{-1} indicates the appearance of crystalline domains of PLA [27]. This band has high intensity in the film samples, but disappears in the electrospun fibers, reflecting their complete amorphous nature, as the rapid solvent evaporation during the spinning process inhibits the polymer chain's crystallization. This is confirmed by the carbonyl stretching mode, υ(C=O), in which the semi-crystalline film samples show two clearly separate bands at 1747and 1755 cm^{-1}. In contrast, the electrospun fibers show only 1broad band at 1753 cm^{-1}.The vibrational mode of Ti-O-Ti is observed at 802 cm^{-1}, indicating the presence of TiO$_2$ particles on the fibers.
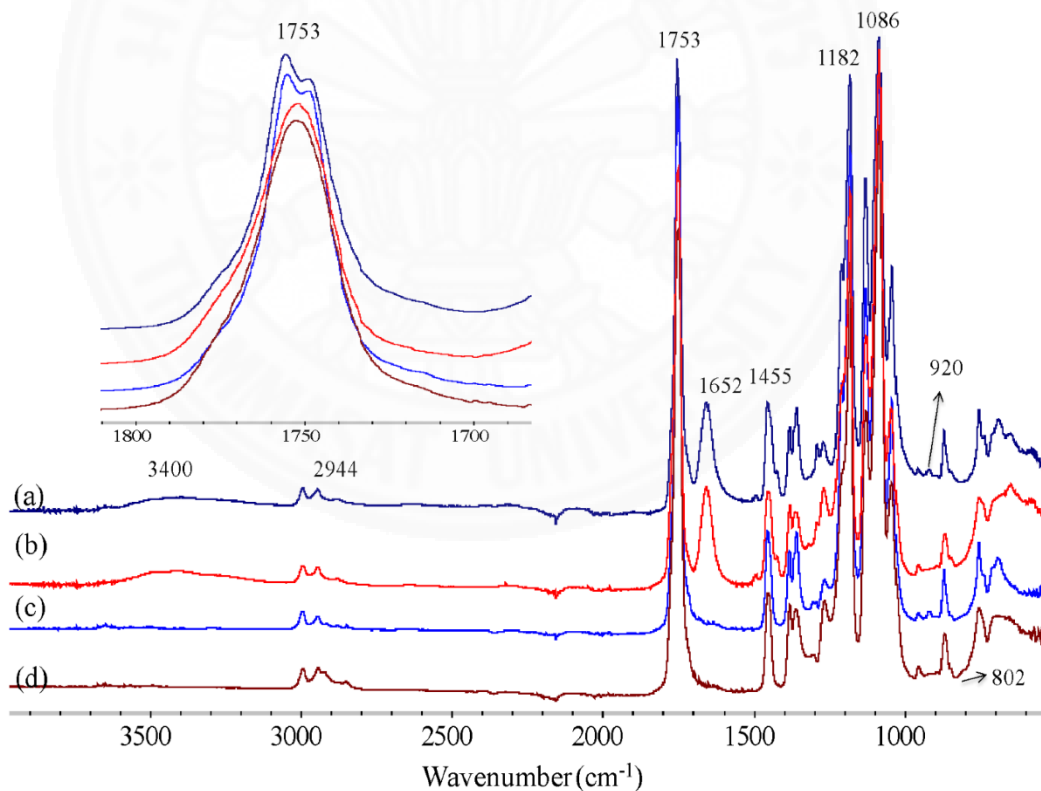
Figure 1: ATR-FTIR spectra of P-T: (a) film and (b) electrospun fiber (15 kV), and P-P-T: (c) film and (d) electrospun fiber (15 kV).

3.2. X-ray diffraction (XRD)

XRD spectra of P-T and P-P-T solution-cast films and fiber samples are compared in Figure 2. Signals at 2θ= 14.9°, 16.8°, 19.1° are observed in the spectra of film samples, corresponding to crystalline planes (010), (110/200), and (203) of PLA, respectively. The sharpest band at 16.8°and that at 19.1° reflect the orthorhombic lattice of the α-form[11, 28]. The electrospun fiber samples, however, show only a broad signal covering a 9-22° region, reflecting amorphous domains. Both samples either with PVP or without PVP show similar characteristic spectra. The solution cast samples show only characteristic signals of PLA, reflecting that the PVP minor phase cannot form separate crystalline domains. However, a slight shift to a lower d-spacing value is observed in the signal of (200)/(100) planes, likely indicating an interruption of PLA's crystalline structure by the presence of PVP.

The effect of electrospinning voltage on crystalline formation of the fibers is investigated. It was expected that higher potentials could break down the surface tension of the solution jets more effectively, leading to smaller-size filaments with different degrees of crystallinity. However, similar XRD spectra are observed for all spun samples. This similar crystalline characteristic likely indicates that the lowest critical voltage has been reached at 10 kV, in which the solidifying rate of the solution jets has already been faster than the required rate of crystallization. A small signal located at 25.4° is associated with crystalline characteristic of TiO_2 nanoparticles[28]. This band appears with high intensity for film samples, but with lower intensity for electrospun fibers. This likely reflects the higher degrees of dispersion of the nanoparticles along the fibers during the electrospinning process.
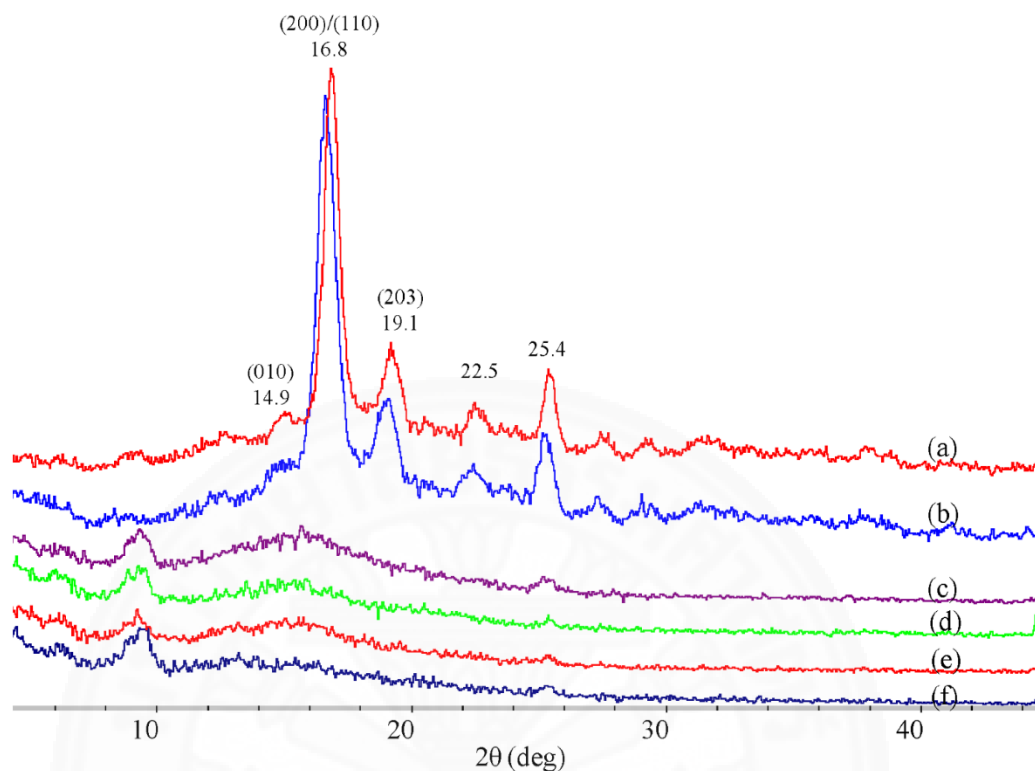
10

105

Figure **2**: XRD spectra of (a) P-P-T film, (b) P-T film, P-T fibers spun at: (c) 15 kV, (d) 13 kV, and (e) 10 kV, and (f) P-P-T fibers spun at 15kV.

3.3. Scanning Electron Microscopy (SEM)

Surface morphology and size distribution of the electrospun composited fibers are examined by SEM, as shown in Figure 3. Smooth filaments containing several beads are obtained. The spinning operation at 10kV produces fibers with more beads than those at 15kV. The surfaces of both fibers electrospun at 15 kV, either with or without PVP, are more uniform than those at 10kV.It is also clearly observed that TiO_2 nanoparticles are present as isolated beads on the filaments, especially in the region of irregular shaped fibers. It is noted that, however, most bead defects with larger sizes are not caused by the agglomeration of TiO_2 particles. This is confirmed

11

106

by the EDX results, as shown in Figure 4, in which the Ti content measured at small-sized isolated beads, located in a fine fiber region, is higher than that of a large-sized bead defect. The average diameter and size distribution, of the spun nanofibers of P-T and P-P-T fibers spun at 10 and 15 kV, are examined. The average sizes for P-T10, P-T15, P-P-T10, and P-P-T15 are 754, 686, 759, and 980 nm, respectively. The results reflect incorporation of PVP into PLA, leading to an increase in average size of the spun fibers.
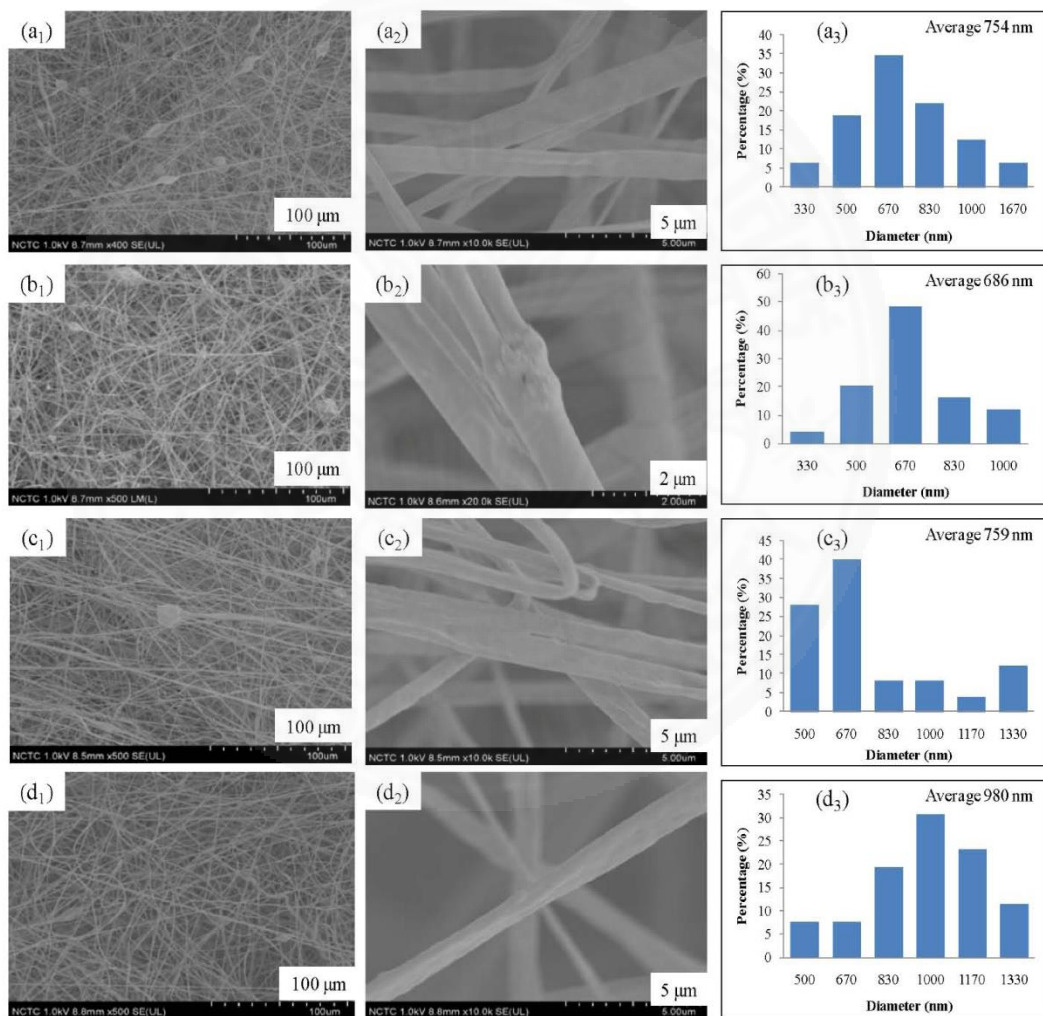

12

Figure **3**: SEM images and size distribution of electrospun fibers of P-T: (a_1)-(a_3) spun at 10kV and (b_1)-(b_3) 15kV, and P-P-T fibers: (c_1)-(c_3) spun at 10kVand (d_1)-(d_3)15kV, with 500× and 10,000×magnifications.
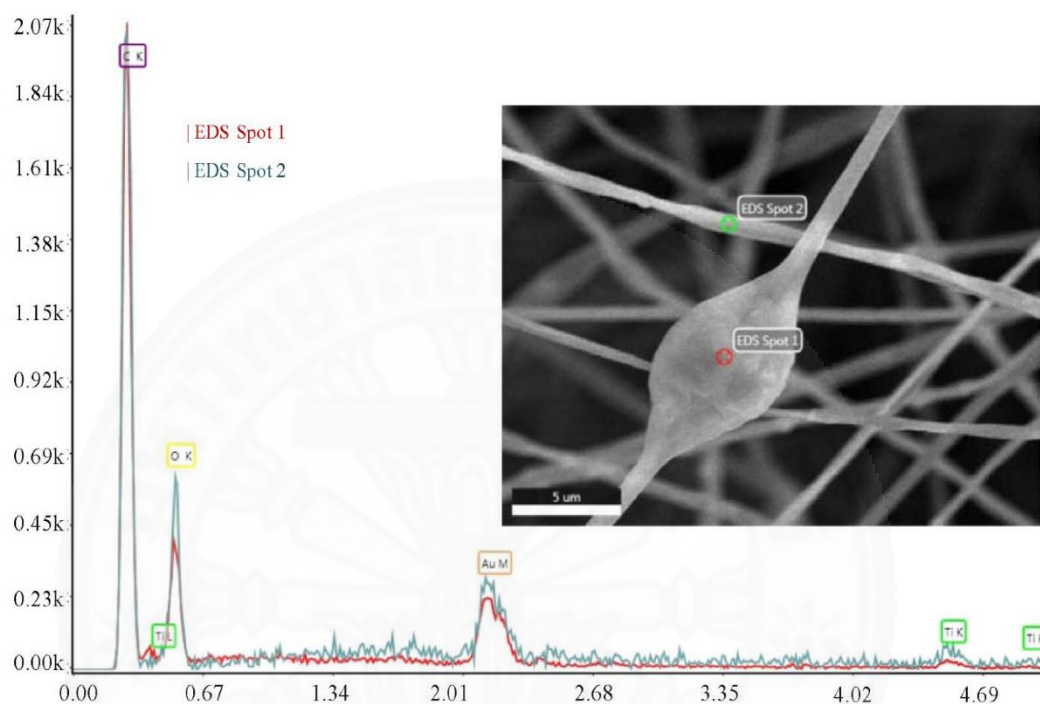

Figure 4: EDX spectra measured at different bead defect regions, i.e., TiO_2 containing beads (spot 1) and common irregular beads generated from the spinning process (spot 2), onP-P-T15 electrospun fibers.

3.4. UV-Visible spectroscopy

To validate the presence of TiO_2 particles on the spun fiber mats and examine the absorption behaviors of the fabricated materials, UV-Vis spectroscopy is employed, as shown in Figure 5. Neat PLA, P-T15, and P-P-T15 fibers show a similar λ_{max} in the region below 200 nm. The latter 2 fibers, which containTiO_2 particles, however, show an additional distinct absorption band in the region of 200-380 nm. This reflects the activity of the embedded TiO_2 particles,

13

108

which can affect photo-degradability and catalytic efficiency of the fiber materials, when UV light activator is employed.
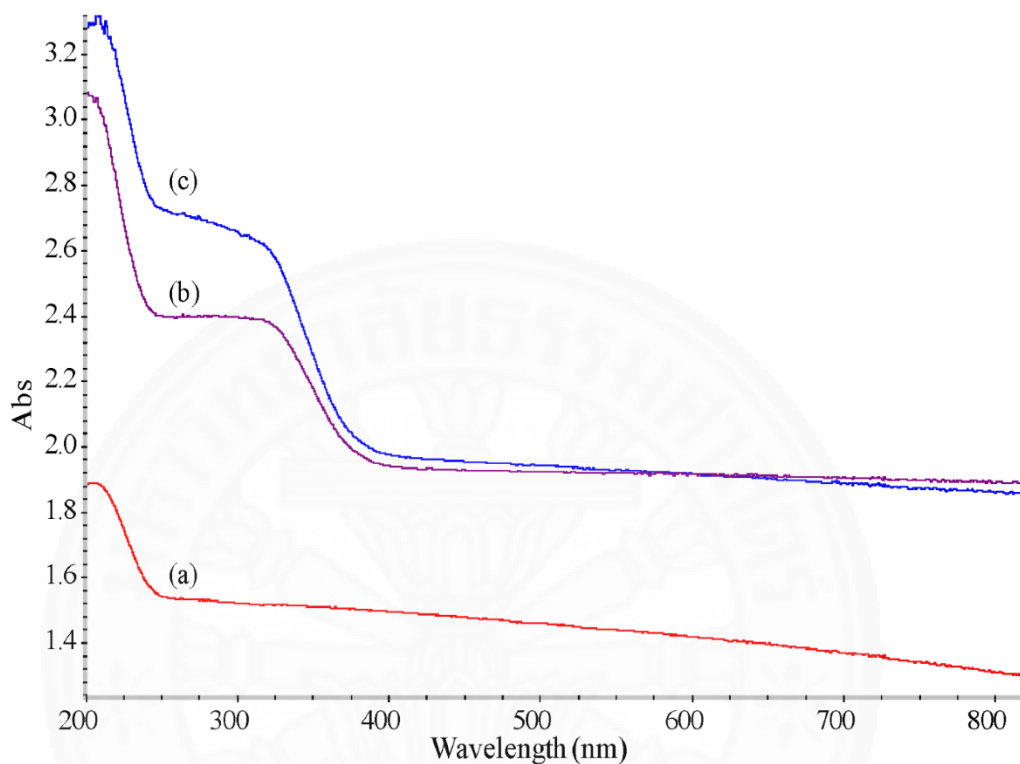

Figure **5**: UV-Vis spectra of: (a) neat PLA, (b) P-T15, and (c) P-P-T15 electrospun fibers.

3.5. Photo-degradation mechanisms

Photo-degradation behaviors, as a function of time, of the spun fibers are examined in PBS solutions with a UVA lamp. It is observed that the puffy fibers break down to small pieces and precipitate at the bottom of the container. These small pieces of fibers are centrifuged and separated from the PBS. ATR-FTIR spectra of the remaining P-P-T15 fiber mat after soaking in PBS at 1, 4, and 7 days are compared in Figure 6. A distinct υ(N-C=O) band of PVP at 1652 cm^{-1} decreases in intensity and completely disappears at 4 days, reflecting a fast rate of PVP dissolution, as the polymer is a water-soluble component of the fibers. An increase in the degree

14

109

of degradation of PLA, as a function of time, is observed in the increase in intensities of broad bands covering 1605 cm^{-1}(C=O stretching of -COO^{-}) and 3400 cm^{-1}(–OH stretching of carboxylic acid end groups), and a sharp but weak band at 1724 cm^{-1} (C=O stretching of carboxylic acid). This indicates a conversion of ester bonds to carboxylic acid and carboxylate end groups as a result form chain scissions[29].

UV-Vis spectra of the remaining PBS solutions after degradation of P-P-T15 are also examined, as shown in Figure 7. An absorption band at 202 nm is clearly observed, whose intensity increases with degradation time. This is associated with absorption of carboxylate end groups of soluble PLA's fragments [29].Another unique band is observed at 235 nm, corresponding to the absorption of TiO$_2$ particles. This confirms that the embedded TiO$_2$ particles are released to PBS, along with the fragmented PLA matrix.

SEM images, as shown in Figure 8, of the remaining fiber samples after1and 4daysof degradation, confirm that the surface morphology becomes rugged. The fiber strings break down to small fragments. The longer degradation time leads to a higher number of small fragments.EDX is also applied to verify the chemical composition of different regions on the remaining P-P-T15 fibers, as shown in Figure 9. After 1 day, the Ti content measured at a smooth fiber area is very low, compared to that of a bead defect area. This strongly indicates that TiO$_2$ nanoparticles are embedded in the polymer matrix. After degradation of the polymer matrix shell, these particles are exposed at the filaments surface, and released into the solution medium when the degree of degradation further increased.
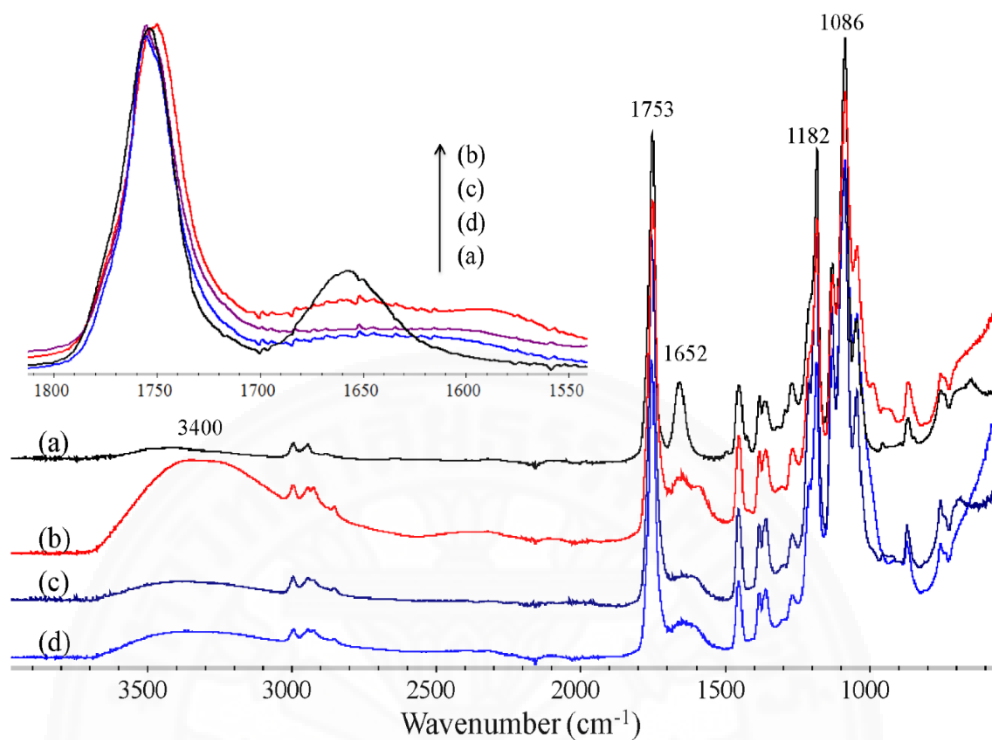
15

Figure 6: ATR-FTIR spectra of P-P-T15fibers as a function of degradation time in PBS solution under UVA light at: (a) 0, (b) 1, (c) 4, and (d) 7 days.
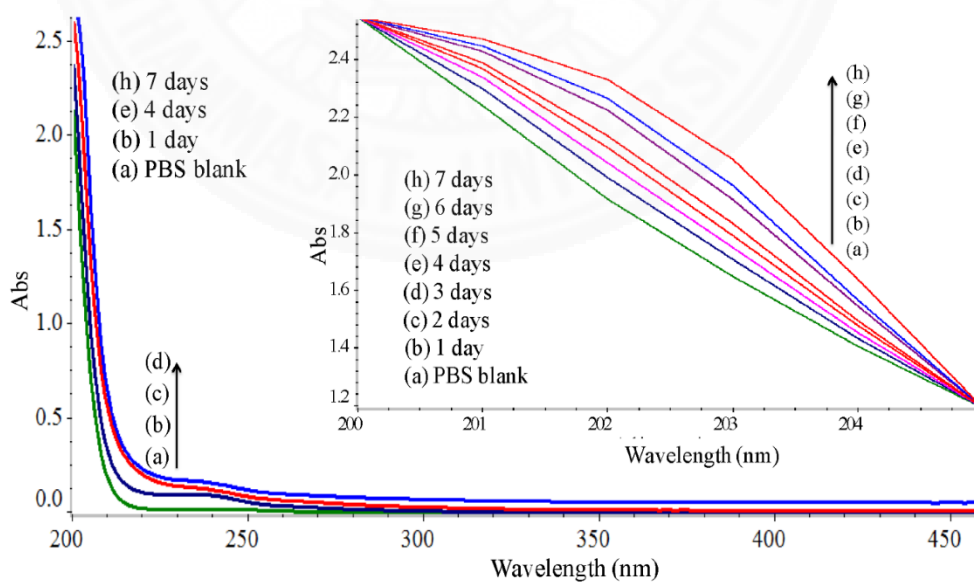

16

111

Figure 7: UV-Vis spectra of PBS solutions obtained from the photo-degradation of P-P-T15fibers as a function of time.
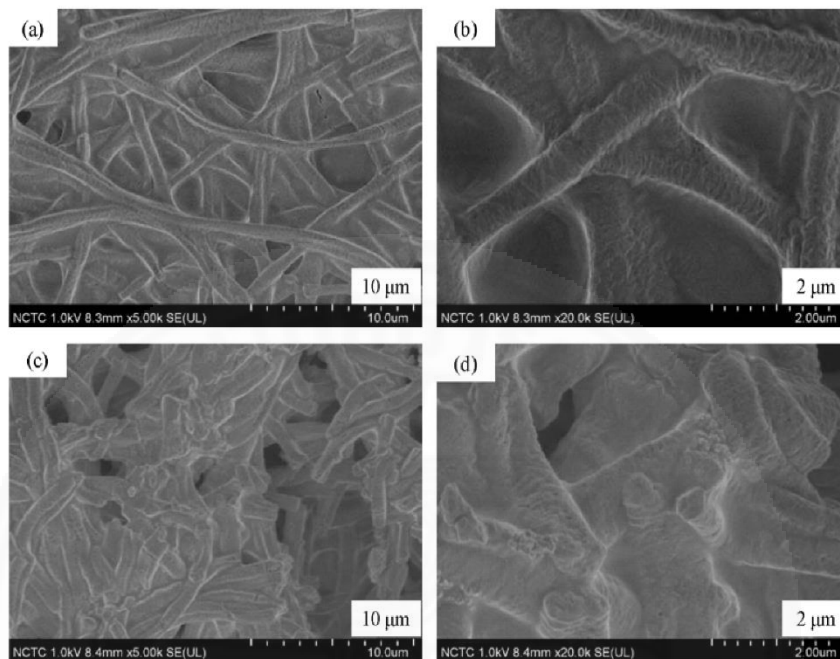

Figure 8: SEM images of photo-degraded products of P-P-T15fibers in PBS solution under UVA light after: 1day, (a)-(b), and 4days, (c)-(d).
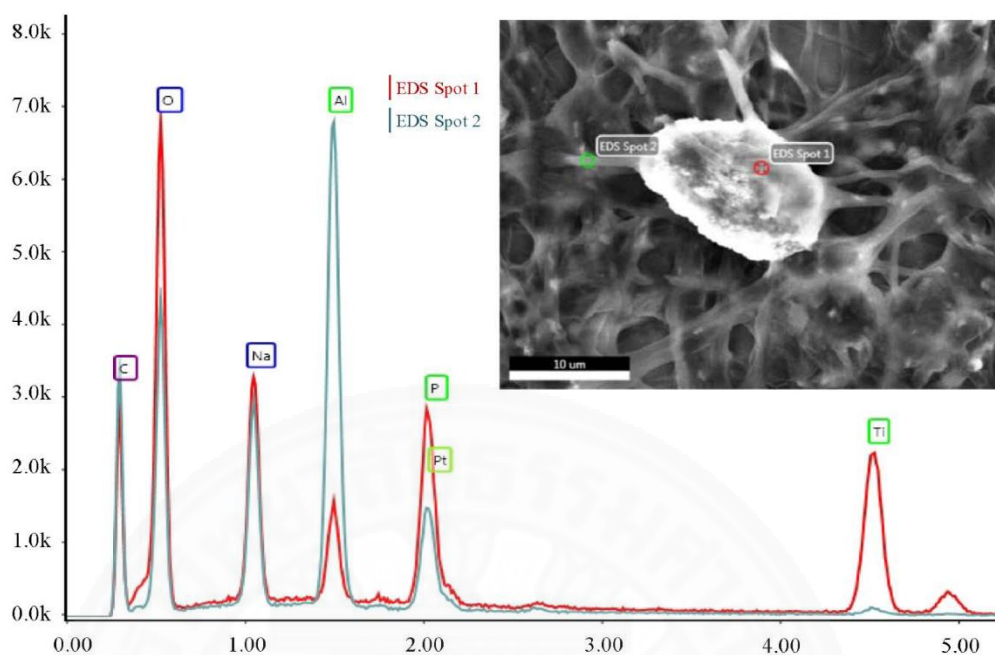
17

Figure 9: EDX spectra measured at different regions on P-P-T15 electrospun fibers, after 1 day of photo-degradation in PBS under UVA light.

3.6. Catalytic Efficiency for Epoxidation of SFO

The resulting electrospun fibers are employed as a surface-enhanced catalyst in the epoxidation reaction of SFO. $HCOOH/H_2O_2$ oxidizing agents are employed, whose content per 8 g of SFO are varied: 0.5/1, 0.75/1.5, and 1/2 mL. The epoxidized SFO products obtained without the fiber catalyst is denoted as ESFO-x, where x indicates the HCOOH content. The corresponding products obtained with the application of the fiber catalyst are coded as P-T-ESFO-x or P-P-T-ESFO-x. Efficiency and mechanisms of the reactions conducted at room temperature and at $65°C$ are evaluated. ATR-FTIR spectra of SFO and its epoxidized ESFO derivatives are compared (Supplement data1). Changes in band intensity are observed at 3007 cm^{-1} (olefinic C–H stretching), 2923 and 2853 cm^{-1} (aliphatic's $v_{as}CH_2$ and v_sCH_2 stretching),

18

113

1741 (ν_{as}C=O), 1465 (δ_sCH$_2$), and 1160 cm^{-1}(ν_{as}C–O)[30]. The mechanisms of the reaction are proposed in Figure 10, in which perfomic acid, generated from the reaction between formic acid and hydrogen peroxide, plays a key role as an oxygen carrier for the epoxidation process. The formation of epoxide groups in the ESFO structure is confirmed by the presence of new characteristic FTIR bands at 844 and 824 cm^{-1} (C–O–C). In contrast, a decrease in intensity of the olefinic stretching mode at 3007 cm^{-1} also indicates the conversion of the double bonds to epoxide groups. The changes in intensity of these modes can be employed in the measurement of reaction efficiency.
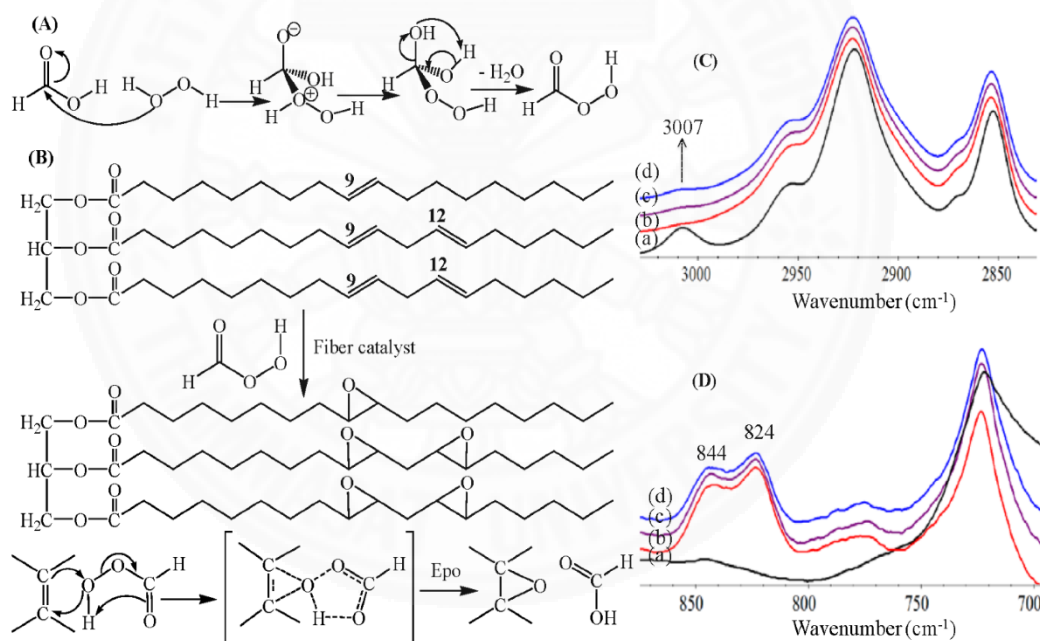

Figure 10: Proposed mechanism of epoxidation reaction and ATR-FTIR spectra in the region of epoxide characteristics of: (a) SFO, (b) ESFO-1, (c) P-T-ESFO-1, and (d) P-P-T-ESFO-1.

19

Interestingly, the results also show an occurrence of major side reactions, especially when the fiber catalyst is not employed, due to the extreme reaction conditions and the employment of highly reactive reagents. In addition to the conversion of olefinic bonds to oxirane groups, the performic acid reagents also liberate free fatty acids (FFAs) and glycerol by breaking ester bonds of SFO triglycerides, as shown in Figure 11. These undesirable FFA by-products, whose content can be directly measured from the intensity of a 1723 cm^{-1} band (C=O stretching of carboxylic acid), are not suitable for use in our proposed applications as structural-tunable plasticizer for biopolymers.

ATR-FTIR spectra of epoxidized oils products obtained at different oxidizing agent contents, with and without the fiber catalyst are compared in Figure 11. An increase in the contents of HCOOH and H_2O_2 lead to an increase in intensity of the FFA band. A much higher degree of intensity increase is observed in the reaction system without the fiber catalyst. Interestingly, the presence of PVP in the P-P-T fiber catalyst results in the lowest degree of FFA liberation from SFO. The reaction temperature also plays a key role in this side reaction, in which the reaction at room temperature produces lower FFA content than that at 65°C.
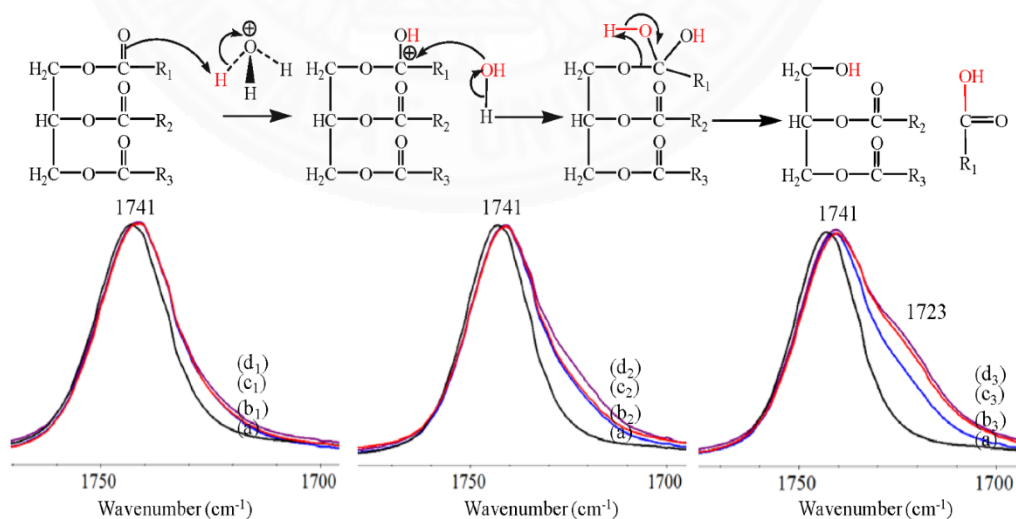

20

115

Figure 11: Proposed mechanisms of ester bond cleavage and ATR-FTIR spectra of epoxidized oil products obtained at 65°C:(a) SFO, (b$_1$)-(b$_3$) P-P-T-ESFO-0.5, 0.75, and 1, (c$_1$)-(c$_3$) ESFO-0.5, 0.75, and 1, and (d$_1$)-(d$_3$) P-T-ESFO-0.5, 0.75, and 1.

To quantitatively determine the degree of epoxidation and the contents of FFA by-products, a curve fitting process is employed to the FTIR spectra of products from each reaction, by using the OMNIC program (Supplement Data 2). The conversion yield of olefinic bonds to epoxide groups is calculated from the conversion of the 3007 cm^{-1}band, while the degree of FFA liberation is measured from the ratios of 1723/1740 cm^{-1} band areas. Results from Figure 12(a)-(b) and Table 1 show that the olefinic bond conversion yield at room temperature is higher when the fiber catalysts are employed, compared to the system using oxidizing agents alone at all contents of the oxidizing agents. The yields also increase with the increase in the oxidizing agent contents. The 1723/1740 cm^{-1} band ratio also increases with the oxidizing agent content for all samples, due to more extreme conditions, which is undesirable.

When the reaction temperature is increased to 65°C, all reactions using the same oxidizing agent contents show comparable conversion yields, are higher than the corresponding reactions at room temperature. However, the degree of FFA liberation of the reactions using the fiber catalyst, especially P-P-T-ESFO-x, is much lower than other systems. This implies that the optimum condition for epoxidation of SFO with high yields, but low amount of FFA liberation, is at 65°C with the application of P-P-T-ESFO-x. This effective process is achieved because the PVP-containing PLA/TiO$_2$ composites provide active surfaces on the fiber that are more specific for epoxidizing double bonds, which decrease the hydrolysis reaction of ester bond cleavage, especially at higher contents of oxidizing agents and high reaction temperatures. The resulting

21

116

products are effective additives for use as plasticizers or toughening agents for other biopolymers.
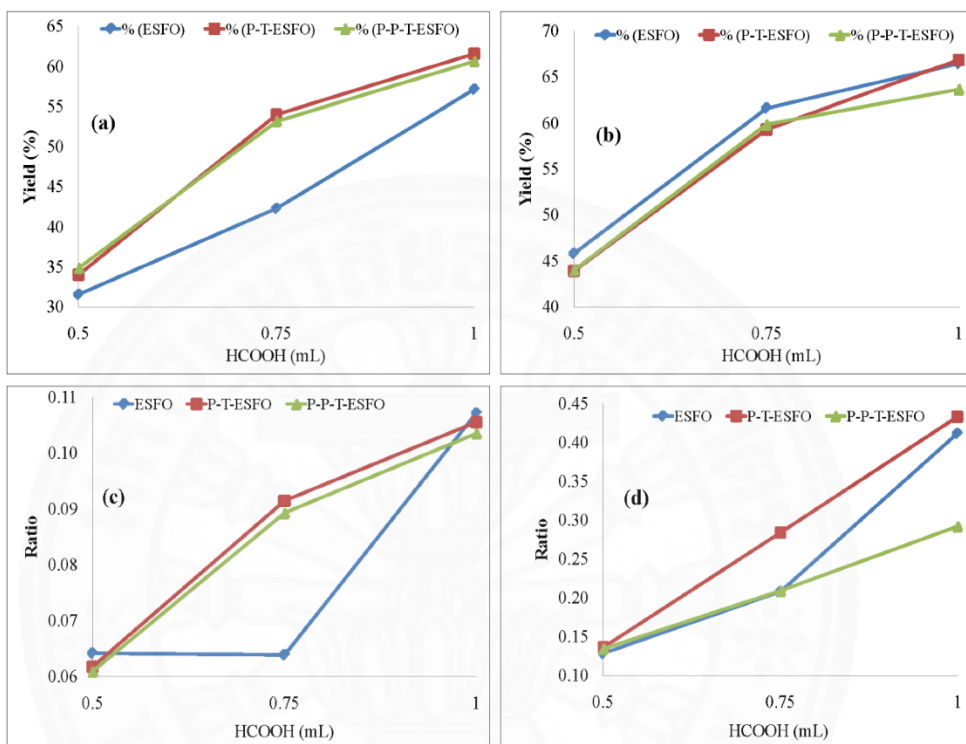

Figure 12: The olefinic conversion yields at: (a) room temperature and (b) 65°C, and the degree of FFA liberation calculated from ratios of 1723/ 1740 cm⁻¹ band areas at: (c) room temperature and (d) 65°C.

Table 1: Epoxidation yields of SFO using HCOOH 1 mL, with and without the fiber catalysts.

	Epoxidation Yield (%)	
	Room temperature (29-31°C)	65°C
ESFO-1	57.15	66.39
P-T-ESFO-1	61.55	66.81
P-P-T-ESFO-1	60.64	63.63

22

117

ATR-FTIR spectra of P-T15 and P-P-T15 fiber catalyst before and after the epoxidation process are also examined (Supplement Data 3). After reaction, FTIR spectra of the catalysts are similar to those obtained from the photo-degradation experiments. Interestingly, a crystalline band of PLA at 920 cm^{-1} appears and increases in intensity as a function of time. This reflects that under these reaction conditions, the dissolution of PVP component to PBS and the penetration of oil molecules into the PLA matrix may generate more free volume for PLA chain rearrangements, leading to an increase in the crystalline contents.

4. Conclusions

Nanofibers of polylactide (PLA)/poly(vinlylpyrrolidone) (PVP) blends loaded with TiO_2 nanoparticles have been successfully prepared by an electrospinning method. All spun fibers are completely amorphous in nature, in which those fabricated from PLA/PVP/$TiO_2$are smoother and more uniform than the corresponding samples without PVP. SEM images clearly show that TiO_2 particles are embedded on the filaments, and the samples show a UV absorption band covering 200-380 nm regions. The spun composite fibers have a high potential for applications as catalytic systems for epoxidation of unsaturated oils, for use as additives or plasticizers for biopolymers. The fibers, especially those containing PVP, can effectively enhance epoxidation yield of the oils, and decrease undesirable side reactions which break ester bonds of the triglyceride, to generate free fatty acid by-products.
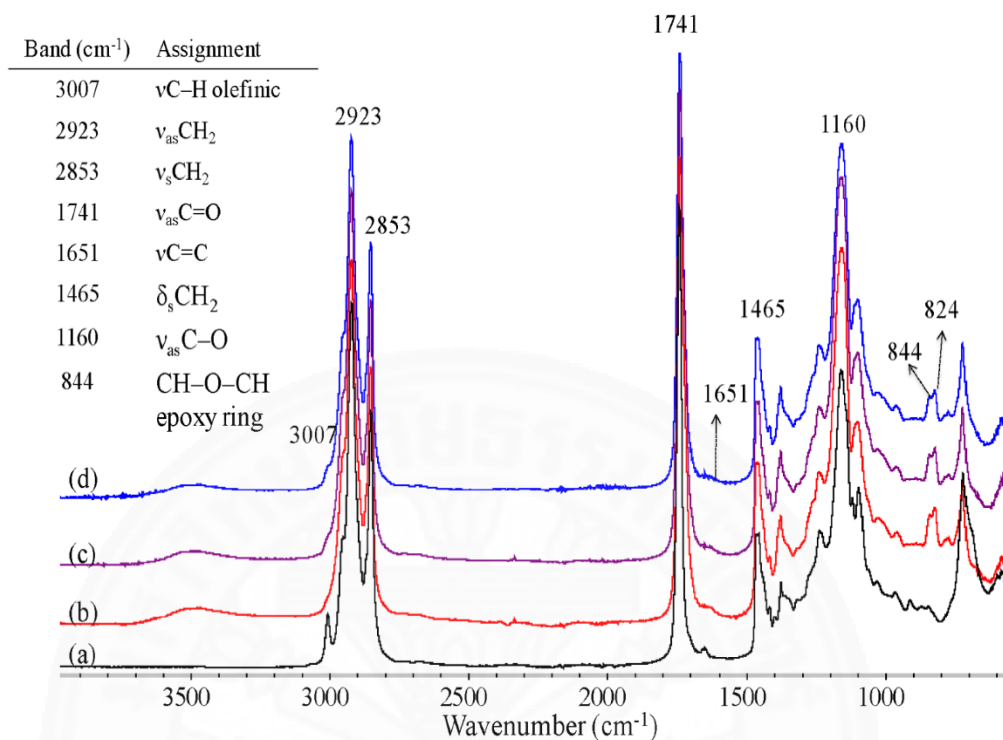
23

References

[1]   Mekonnen, T., et al., *Progress in bio-based plastics and plasticizing modifications.* Journal of Materials Chemistry A, 2013. **1**(43): pp. 13379.

http://dx.doi.org/10.1039/c3ta12555f

[2]   Nakayama, N. and T. Hayashi, *Preparation and characterization of poly(l-lactic acid)/TiO$_2$ nanoparticle nanocomposite films with high transparency and efficient photodegradability.* Polymer Degradation and Stability, 2007. **92**(7): pp. 1255-1264.

http://dx.doi.org/10.1016/j.polymdegradstab.2007.03.026

[3]   Buzarovska, A. and A. Grozdanov, *Biodegradable poly(L-lactic acid)/TiO$_2$ nanocomposites: Thermal properties and degradation.* Journal of Applied Polymer Science, 2012. **123**(4): pp. 2187-2193.

http://dx.doi.org/10.1002/app.34729

[4]   Kale, G., et al., *Biodegradability of polylactide bottles in real and simulated composting conditions.* Polymer Testing, 2007. **26**(8): pp. 1049-1061.

http://dx.doi.org/10.1016/j.polymertesting.2007.07.006

[5]   Fukushima, K., et al., *Biodegradation of poly(lactic acid) and its nanocomposites.* Polymer Degradation and Stability, 2009. **94**(10): pp. 1646-1655.

http://dx.doi.org/10.1016/j.polymdegradstab.2009.07.001

[6]   Lin, W.-C., W.-D. Yang, and S.-Y. Jheng, *Photocatalytic degradation of dyes in water using porous nanocrystalline titanium dioxide.* Journal of the Taiwan Institute of Chemical Engineers, 2012. **43**: pp. 269-274.

http://dx.doi.org/10.1016/j.jtice.2011.10.010

[7]   Fischer, K., et al., *Photoactive microfiltration membranes via directed synthesis of TiO$_2$ nanoparticles on the polymer surface for removal of drugs from water.* Journal of Membrane Science, 2015. **478**: pp. 49-57.

http://dx.doi.org/10.1016/j.memsci.2015.01.009

[8]   Ao, C.H., et al., *Photodegradation of volatile organic compounds (VOCs) and NO for indoor air purification using TiO$_2$: promotion versus inhibition effect of NO.* Applied Catalysis B: Environmental, 2003. **42**(2): pp. 119-129.

http://dx.doi.org/10.1016/s0926-3373(02)00219-9

[9]   Chawengkijwanich, C. and Y. Hayata, *Development of TiO$_2$ powder-coated food packaging film and its ability to inactivate Escherichia coli in vitro and in actual tests.* International Journal of Food Microbiology, 2008. **123**: pp. 288-292.

http://dx.doi.org/10.1016/j.ijfoodmicro.2007.12.017

[10]   Xu, J., et al., *Photokilling cancer cells using highly cell-specific antibody-TiO₂ bioconjugates and electroporation.* Bioelectrochemistry, 2007. **71**(2): pp. 217-22.

http://dx.doi.org/10.1016/j.bioelechem.2007.06.001

[11]   Naghibi, S., et al., *Mortality response of folate receptor-activated, PEG–functionalized TiO₂ nanoparticles for doxorubicin loading with and without ultraviolet irradiation.* Ceramics International, 2014. **40**: pp. 5481-5488.

http://dx.doi.org/10.1016/j.ceramint.2013.10.136

[12]   Wang, T., et al., *Potential application of functional porous TiO₂ nanoparticles in light-controlled drug release and targeted drug delivery.* Acta Biomaterialia, 2015. **13**: pp. 354-363.

http://dx.doi.org/10.1016/j.actbio.2014.11.010

[13]   Devanand Venkatasubbu, G., et al., *Folate targeted PEGylated titanium dioxide nanoparticles as a nanocarrier for targeted paclitaxel drug delivery.* Advanced Powder Technology, 2013. **24**(6): pp. 947-954.

http://dx.doi.org/10.1016/j.apt.2013.01.008

[14]   Zhuang, W., et al., *Preparation, characterization, and properties of TiO₂/PLA nanocomposites by in situ polymerization.* Polymer Composites, 2009. **30**(8): pp. 1074-1080.

http://dx.doi.org/10.1002/pc.20658

[15]   Ali, N.A. and F.T.M. Noori, *Gas Barrier Properties of Biodegradable Polymer Nanocomposites Films.* Chemistry and Materials Research, 2014. **6**(1).

[16]   Gupta, K.K., et al., *Hydrothermal in situ preparation of TiO₂ particles onto poly(lactic acid) electrospun nanofibres.* Applied Surface Science, 2013. **264**: pp. 375-382.

http://dx.doi.org/10.1016/j.apsusc.2012.10.029

[17]   Hong, Y., et al., *Electrospinning of multicomponent ultrathin fibrous nonwovens for semi-occlusive wound dressings.* Journal of Biomedical Materials Research Part A, 2009. **89A**(2): pp. 345-354.

http://dx.doi.org/10.1002/jbm.a.31968

[18]   Luo, Y.-B., X.-L. Wang, and Y.-Z. Wang, *Effect of TiO₂ nanoparticles on the long-term hydrolytic degradation behavior of PLA.* Polymer Degradation and Stability, 2012. **97**(5): pp. 721-728.

http://dx.doi.org/10.1016/j.polymdegradstab.2012.02.011

[19]   Sharifah Nafisah, S.I., et al., *Epoxidation of Palm Oil Catalyzed by Titanium-Grafted Silica Catalyst.* Advanced Materials Research, 2013. **812**: pp. 30-37.

http://dx.doi.org/10.4028/www.scientific.net/AMR.812.30

[20]   Taghizadeh, M.T., *Stabilizing effect of epoxidized sunflower oil as a secondary stabilizer for Ca/Hg stabilized PVC.* eXPRESS Polymer Letters, 2008. **2**(1): pp. 65-76.

http://dx.doi.org/10.3144/expresspolymlett.2008.9

25

[21]   Bouchareb, B. and M.T. Benaniba, *Effects of epoxidized sunflower oil on the mechanical and dynamical analysis of the plasticized poly(vinyl chloride).* Journal of Applied Polymer Science, 2008. **107**(6): pp. 3442-3450.

http://dx.doi.org/10.1002/app.27458

[22]   Benaniba, M.T., N. Belhaneche-Bensemra, and G. Gelbard, *Stabilization of PVC by epoxidized sunflower oil in the presence of zinc and calcium stearates.* Polymer Degradation and Stability, 2003. **82**(2): pp. 245-249.

http://dx.doi.org/10.1016/s0141-3910(03)00178-2

[23]   Guidotti, M., et al., *Epoxidation of unsaturated FAMEs obtained from vegetable source over Ti(IV)-grafted silica catalysts: A comparison between ordered and non-ordered mesoporous materials.* Journal of Molecular Catalysis A: Chemical, 2006. **250**(1-2): pp. 218-225.

http://dx.doi.org/10.1016/j.molcata.2006.01.032

[24]   Kumar, D. and A. Ali, *Ti/SiO$_2$ as a Nanosized Solid Catalyst for the Epoxidation of Fatty Acid Methyl Esters and Triglycerides.* Energy & Fuels, 2012. **26**(5): pp. 2953-2961.

http://dx.doi.org/10.1021/ef300127c

[25]   Silvestre-Alberó, J., et al., *Spectroscopic, calorimetric, and catalytic evidences of hydrophobicity on Ti-MCM-41 silylated materials for olefin epoxidations.* Applied Catalysis A: General, 2015. **507**: pp. 14-25.

http://dx.doi.org/10.1016/j.apcata.2015.09.029

[26]   Silva, K.I.M.d., et al., *Structural stability of photodegradable poly(l-lactic acid)/PE/TiO$_2$ nanocomposites through TiO$_2$ nanospheres and TiO$_2$ nanotubes incorporation.* Polymer Bulletin, 2014. **71**(5): pp. 1205-1217.

http://dx.doi.org/10.1007/s00289-014-1119-0

[27]   Pakorn, O., O. Mantana, and T. Pramaun, *Crystallization of Polylactide and Its Stereocomplex Investigated by Two-Dimensional Fourier Transform Infrared Correlation Spectroscopy Employing Carbonyl Overtones.* Society for Applied Spectroscopy, 2007. **61**(12): pp. 1352-1358.

[28]   Buzarovska, A., et al., *Effect of TiO$_2$ nanoparticle loading on Poly(l-lactic acid) porous scaffolds fabricated by TIPS.* Composites Part B: Engineering, 2015. **81**: pp. 189-195.

http://dx.doi.org/10.1016/j.compositesb.2015.07.016

[29]   Sriromreun, P., et al., *Standard methods for characterizations of structure and hydrolytic degradation of aliphatic/aromatic copolyesters.* Polymer Degradation and Stability, 2013. **98**(1): pp. 169-176.

http://dx.doi.org/10.1016/j.polymdegradstab.2012.10.014

[30]   Shimamoto, G.G., M.M.A. Favaro, and M. Tubino, *Simple Methods via Mid-IR or1H NMR Spectroscopy for the Determination of the Iodine Value of Vegetable Oils.* Journal of the Brazilian Chemical Society, 2015. **26**(7): pp. 1431-1437.

http://dx.doi.org/10.5935/0103-5053.20150111

26

| Band (cm⁻¹)	Assignment
3007	vC–H olefinic
2923	v_{as}CH₂
2853	v_sCH₂
1741	v_{as}C=O
1651	vC=C
1465	δ_sCH₂
1160	v_{as}C–O
844	CH–O–CH epoxy ring

Supplement Data 1: ATR-FTIR spectra of: (a) sunflower oil (SFO), (b) ESFO-1, (c) P-T-SFO-1, and (d) P-P-T-SFO-1, obtained from epoxidation reaction at 65°C.

27
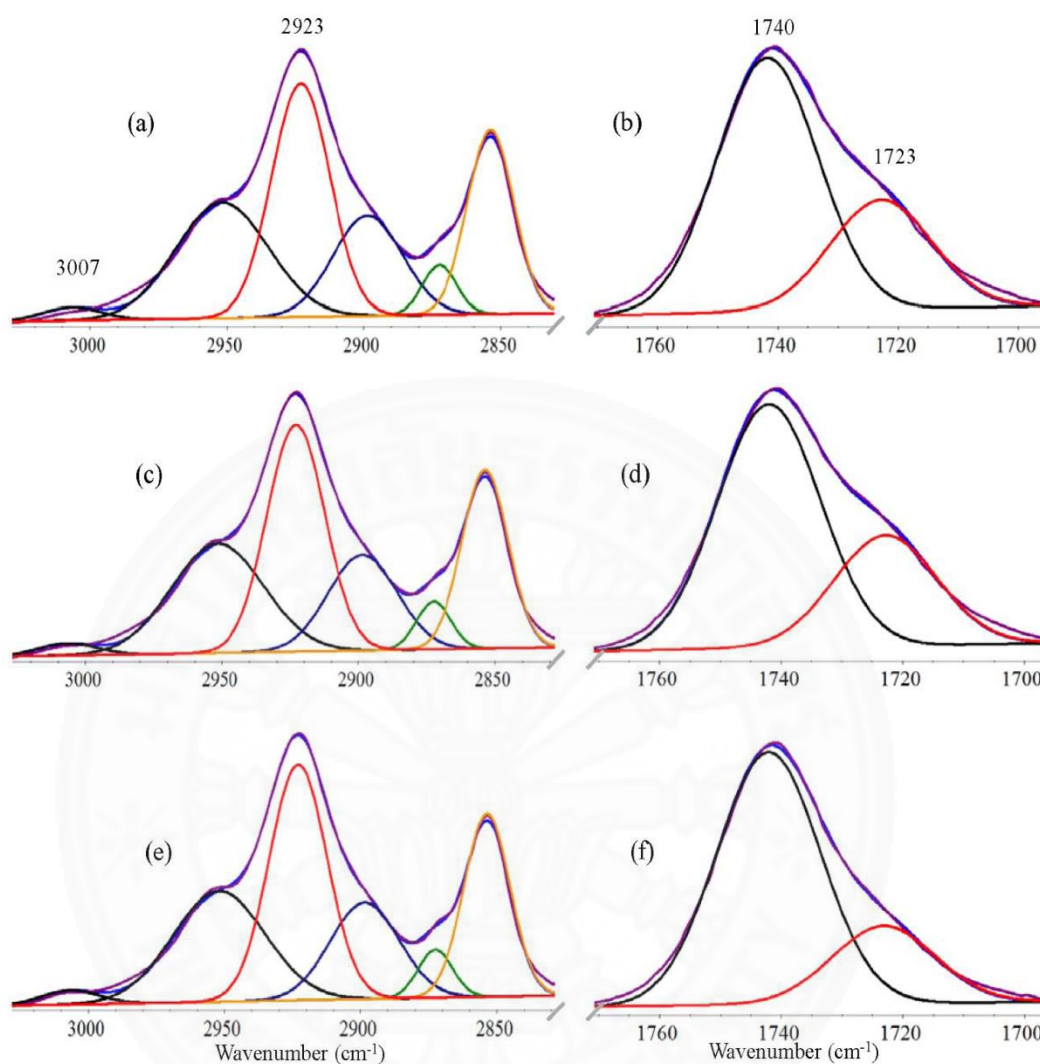
Supplement Data 2: Curve fitting results from FTIR bands of olefinic bond and FFA liberation of (a)-(b) ESFO-1, (c)-(d) P-T-ESFO-1, and (e)-(f) P-P-T-ESFO-1, obtained from epoxidation reaction at 65°C.

28
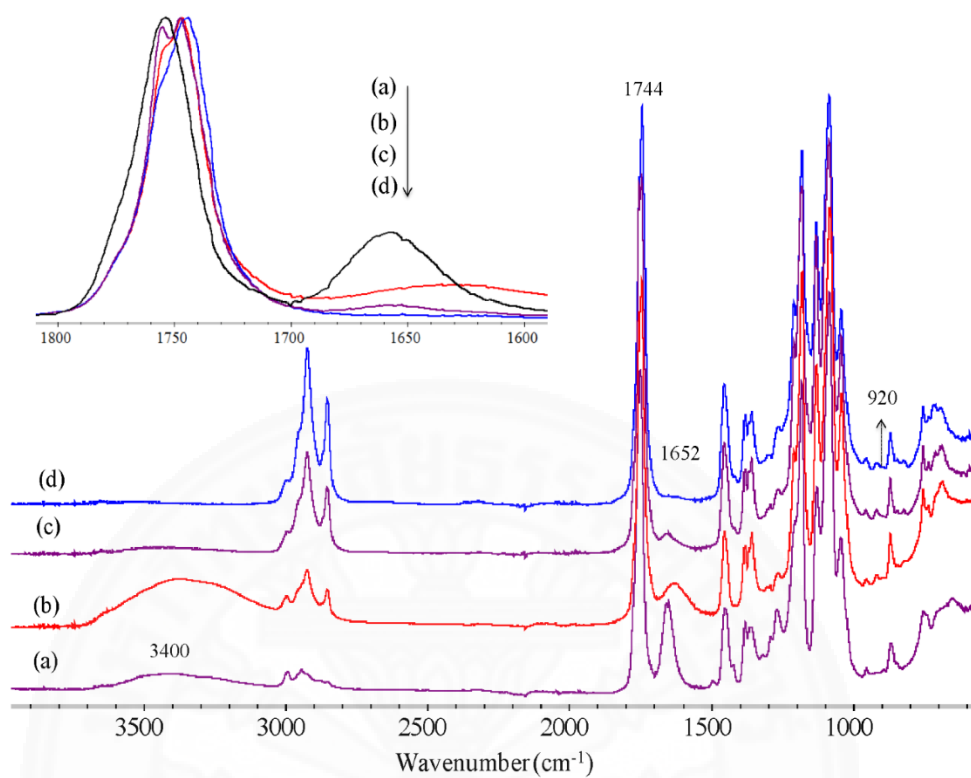
Supplement Data 3: ATR-FTIR spectra of fiber catalyst before and after epoxidation process: (a) P-P-T15 fiber, (b) P-P-T-ESFO-0.5 (65°C), (c) P-P-T-ESFO-0.5 (room temp), and (d) P-T-ESFO-0.5(room temp).

29

124